TECHNISCHE
UNIVERSITÄT
WIEN

VIENNA
UNIVERSITY OF
TECHNOLOGY

D I S S E R T A T I O N

3D Modelling and Reconstruction of Peripheral Arteries

ausgeführt
zum Zwecke der Erlangung des akademischen Grades
eines Doktors der technischen Wissenschaften

unter Anleitung von
Ao.Univ.Prof. Dipl.-Ing. Dr.techn. Eduard Gröller
Institut für Computergraphik und Algorithmen

eingereicht
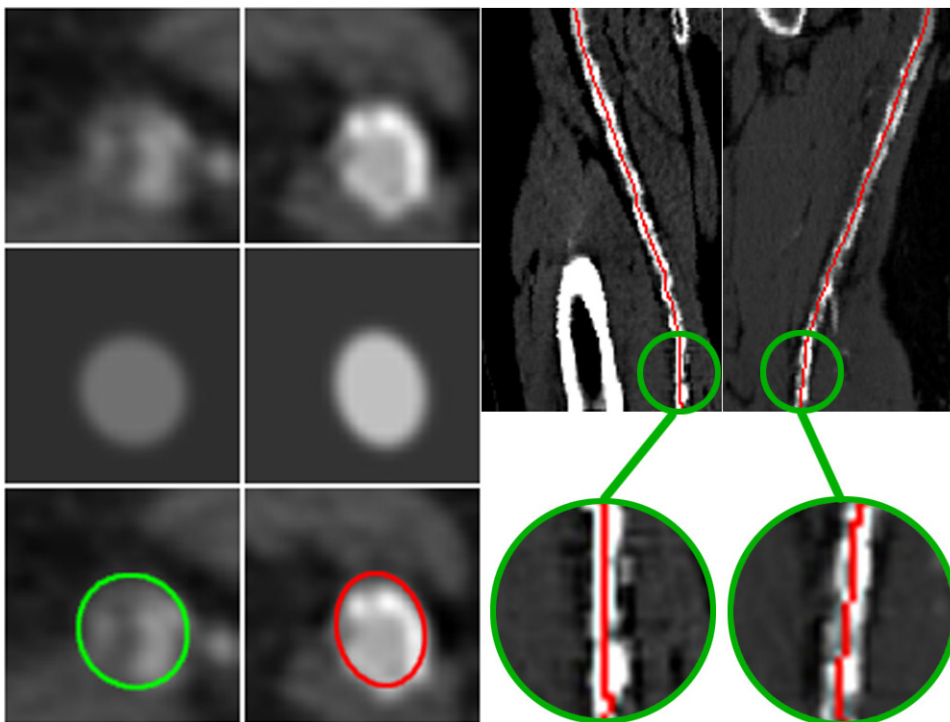an der Technischen Universität Wien,
Fakultät für Informatik

von
Alexandra La Cruz
Matrikelnummer: 0426667
Fickeystrasse 6/20
1110 Wien, Österreich
geboren am 03.09.1971
in Caracas, Venezuela

Wien, im Jänner 2006

Alexandra La Cruz

3D Modelling and Reconstruction of Peripheral Arteries

(PhD Thesis)

Institute of Computer Graphics and Algorithms
Vienna University of Technology, Austria
http://www.cg.tuwien.ac.at/research/vis/angiovis/

A mis padres Juan de Mata y Chela
a mis hermanos Juan Carlos, Wilmer, Felix, Carolay y Roso
a mis sobrinos Gabi y Carlitos,
Eduardito,
Valeria y Valentina,
Dilso, Dilma, Dany y Daniel,
a mi familia, en especial a Laya, Dilcia, Mirian, Nayipsi y
Nayibi
a mis amigos,
y por sobre todas las cosas a DIOS.

ACKNOWLEDGEMENTS

ABSTRACT

A model is a simplified representation of an object. The modeling stage could be described as shaping individual objects that are later used in the scene. For many years scientists are trying to create an appropriate model of the blood vessels. It looks quite intuitive to believe that a blood vessel can be modeled as a tubular object, and this is true, but the problems appear when you want to create an accurate model that can deal with the wide variability of shapes of diseased blood vessels. From the medical point of view it is quite important to identify, not just the center of the vessel lumen but also the center of the vessel, particularly in the presences of some anomalies, which is the case diseased blood vessels.

An accurate estimation of vessel parameters is a prerequisite for automated visualization and analysis of healthy and diseased blood vessels. We believe that a model-based technique is the most suitable one for parameterizing blood vessels. The main focus of this work is to present a new strategy to parameterize diseased blood vessels of the lower extremity arteries.

The first part presents an evaluation of different methods for approximating the centerline of the vessel in a phantom simulating the peripheral arteries. Six algorithms were used to determine the centerline of a synthetic peripheral arterial vessel. They are based on: ray casting using thresholds and a maximum gradient-like stop criterion, pixel-motion estimation between successive images called block matching, center of gravity and shape based segmentation. The Randomized Hough Transform and ellipse fitting have been used as shape based segmentation techniques. Since in the synthetic data set the centerline is known, an estimation of the error can be calculated in order to determine the accuracy achieved by a given method.

The second part describes an estimation of the dimensions of lower extremity arteries, imaged by computed tomography. The vessel is modeled using an elliptical or cylindrical structure with specific dimensions, orientation and CT attenuation values. The model separates two homogeneous regions: Its inner side represents a region of density for vessels, and its outer side a region for background. Taking into account the point spread function of a CT scanner, which is modeled using a Gaussian kernel, in order to

smooth the vessel boundary in the model. An optimization process is used to find the best model that fits with the data input. The method provides center location, diameter and orientation of the vessel as well as blood and background mean density values.

The third part presents the result of a clinical evaluation of our methods, as a prerequisite step for being used in clinical environment. To perform this evaluation, twenty cases from available patient data were selected and classified as 'mildly diseased' and 'severely diseased' datasets. Manual identification was used as our reference standard. We compared the model fitting method against a standard method, which is currently used in the clinical environment. In general, the mean distance error for every method was within the inter-operator variability. However, the non-linear model fitting technique based on a cylindrical model shows always a better center approximation in most of the cases, 'mildly diseased' as well as 'severely diseased' cases. Clinically, the non-linear model fitting technique is more robust and presented a better estimation in most of the cases. Nevertheless, the radiologists and clinical experts have the last word with respect to the use of this technique in clinical environment.

Kurzfassung

Ein Modell ist eine vereinfachte Repräsentationsform eines Objekts. Die Modellbildung kann als Formen von individuellen Objekte bezeichnet werden, die später in der Szene Verwendung finden. Seit vielen Jahren versuchen Wissenschaftler ein geeignetes Modell für die Blutgefäße zu finden. Auf den ersten Blick scheint hierfür ein tubuläres Modell am Besten geeignet zu sein, allerdings erweist sich dabei eine präzise Berücksichtigung der vielfältigen Gefäßpathologien als problematisch. Aus medizinischer Sicht ist nicht nur der Mittelpunkt eines Gefäßlumens, sondern auch der Mittelpunkt des Gefäßes selbst relevant. Dies trifft vor allem bei auftretenden Anomalien, wie zum Beispiel bei pathologischen Blutgefäßen, zu.

Eine präzise Berechnung von Gefäßparametern ist eine Grundvoraussetzung für automatisierte Visualisierung und Analyse von sowohl gesunden wie auch erkrankten Blutgefäßen. Wir sind davon überzeugt, dass sich eine modell-basierte Technik am Besten für die Parametrierung von Blutgefäßen eignet. Ziel dieser Arbeit ist die Vorstellung einer neuen Technik zur Berechnung von Parametern erkrankter Blutgefäße der unteren Extremitäten.

Der erste Teil beschreibt den Vergleich verschiedener Methoden zur Approximation der Mittellinie eines Gefäßes in einem Phantom der peripheren Arterien. Sechs verschiedene Algorithmen wurden zur Berechnung der Mittellinie einer synthetischen peripheren Arterie verwendet. Die evaluierten Methoden basieren auf folgenden Verfahren: Raycasting, bei dem das Abbruchkriterium entweder schwellwertbasiert oder auf dem maximalen Gradienten basiert ist; Block-Matching, bei dem die Pixelbewegung in aufeinander folgenden Bildern geschätzt wird und schwerpunkt- oder formbasierte Segmentierung. Für die formbasierte Segmentierung wurde sowohl die randomisierte Hough-Transformation als auch Ellipsen-Fitting verwendet. Da in dem synthetischen Datensatz die Mittellinie bekannt ist, kann die Genauigkeit der Verfahren berechnet werden.

Der zweite Teil beschreibt die Einschätzung der Abmessungen der Beinarterien, die mittels Computertomographie aufgenommen wurden. Das

Blutgefäß wird durch ein elliptisches oder zylindrisches Modell mit bestimmten Abmessungen, bestimmter Ausrichtung und einer bestimmten Dichte (CT-Schwächungswerte) beschrieben. Das Modell separiert zwei homogene Regionen: Im Inneren des Modells befindet sich eine Region mit der Dichte eines Gefäßes, außerhalb befindet sich der Hintergrund. Um die Punktbildfunktion des CT-Scanners zu modellieren, wurde ein Gauß Filter verwendet, der zu einer Verschmierung der Gefäßgrenzen führt. Ein Optimierungsvorgang dient zur Auffindung des Modells, das sich am besten mit den Eingangsdaten deckt. Die Methode bestimmt Mittelpunkt, Durchmesser, Orientierung und die durchschnittliche Dichte des Blutgefäßes, sowie die durchschnittliche Dichte des Hintergrundes.

Der dritte Teil präsentiert die Ergebnisse einer klinschen Evaluation unserer Methoden, eine Grundvoraussetzung für den klinischen Einsatz. Für diese Evaluation wurden 20 Fälle aus den vorhandenen Patientendaten ausgewählt und nach Schweregrad der Erkrankung in zwei Gruppen klassifiziert. Manuelle Identifikation diente als Referenzstandard. Wir verglichen die Model-Fitting-Methode mit einer Standard-Methode, die derzeit im klinischen Einsatz ist. Im Allgemeinen war der durschnittliche Abstandsfehler für beide Methoden innerhalb der Variabilität zwischen den einzelnen manuellen Identifikationen. Jedoch erzielte die nicht-lineare Model-Fitting-Technik basierend auf einem zylindrischen Modell in den meisten Fällen eine bessere Annäherung an die Mittellinie, sowohl in den leicht wie auch in den schwer erkrankten Fällen. Die nicht-lineare Model-Fitting-Technik ist robuster und ergab eine bessere Beurteilung der meisten Fälle. Nichtdestoweniger haben die Radiologen und die klinischen Experten das letzte Wort im Hirblick auf den Einsatz dieser Technik im klinischen Umfeld.

CONTENTS

LIST OF FIGURES

LIST OF TABLES

CHAPTER 1

INTRODUCTION

Peripheral arterial occlusive disease (PAOD) of the lower extremities is a highly prevalent disorder. Although PAOD is not a frequent primary cause of mortality, this disease is a significant cause of morbidity and an adverse prognostic indicator among the elderly [86] (about 30% at age 60 and above). Catheter-based techniques are considered to be the "gold standard" for diagnosis and treatment of PAOD. However, because of their invasive nature, these techniques inherently have some complications. On the other hand, non-invasive diagnostic techniques are high operator dependent and require a time consuming examination.

This chapter introduces the reader to the peripheral vessel investigation field. First, a description of the peripheral vasculature and its main function is presented. Then, the vascular diseases that can affect the normal blood flow through the peripheral arteries are described. Different image modalities have been already used as a radiological evaluation of peripheral vascular disease. A comparative table of the different modalities is presented. Furthermore, we point out the major motivation why we focus our investigation on datasets from computed tomography angiography for peripheral vessel investigation. Finally, three of the most recent vessel visualization techniques that are applied to the blood vessels are addressed.

1.1 Lower Extremity Arterial Tree

The main function of the lower extremity arterial tree is to supply oxygen to the muscles and other tissues of the legs and feet. The 'root' of the peripheral arterial tree is the abdominal aorta (the main artery of the body). The bilateral common iliac arteries divide into the internal iliac artery (which

supplies blood to the pelvic organs) and the external iliac artery, which conducts blood to the femoro-popliteal arteries, and then, (below the knee) to the tibial arteries ((see Figure 1.1)). Clinically speaking, the distal aorta and the iliac segment (common and external iliac) are referred to 'inflow vessels', whereas femoro-popliteal and tibial segments are referred to as 'runoff' vessels. Table 1.1 describes the range of diameters of healthy peripheral arteries [54]. Of course these diameters vary from patient to patient, particularly when sex and age are taken into consideration [21]. This table reflects the wide variation of vessel diameter that we can find on peripheral vasculature.

Artery	∼ Relative Diameter (mm)	Comment
aorta	18-20	large vessel
iliac	10-12	medium vessel
femoro-popliteal	5-9	medium vessel
tibial	1-3	small vessel

Table 1.1: Relative diameter of the main group of arteries of the peripheral vasculature

1.2   Peripheral Arterial Occlusive Disease

Peripheral Arterial Occlusive Disease (PAOD) is a manifestation of atherosclerosis. It is characterized by the slow formation of atherosclerotic plaque on the inner surface (the intima) of the vessel wall, which protrudes into the vessel lumen, causing luminal narrowing (stenoses) or complete vessel occlusion (see Figure 1.2). Epidemiological and clinical studies have shown that peripheral arterial occlusive disease increases the risk of cardio-vascular events, cerebrovascular events, and mortality [64]. The narrowing produced by PAOD, restricts blood flow through affected arteries, and, depending on the extent of disease, may resulting in what is known as limb ischemia [11]. Because the disease is initially asymptomatic, it is underdiagnosed and undertreated in the initial stage of the disease [62]. As the disease progresses, symptoms will emerge; first, patients often experience leg pain and, cramping with exercise or walking ("intermittent claudication"), due to insufficient blood flow to active muscle. Symptoms are reduced within a few minutes when the patient stops walking. At later stages of the disease the blood supply may be insufficient to meet the basic metabolic demands
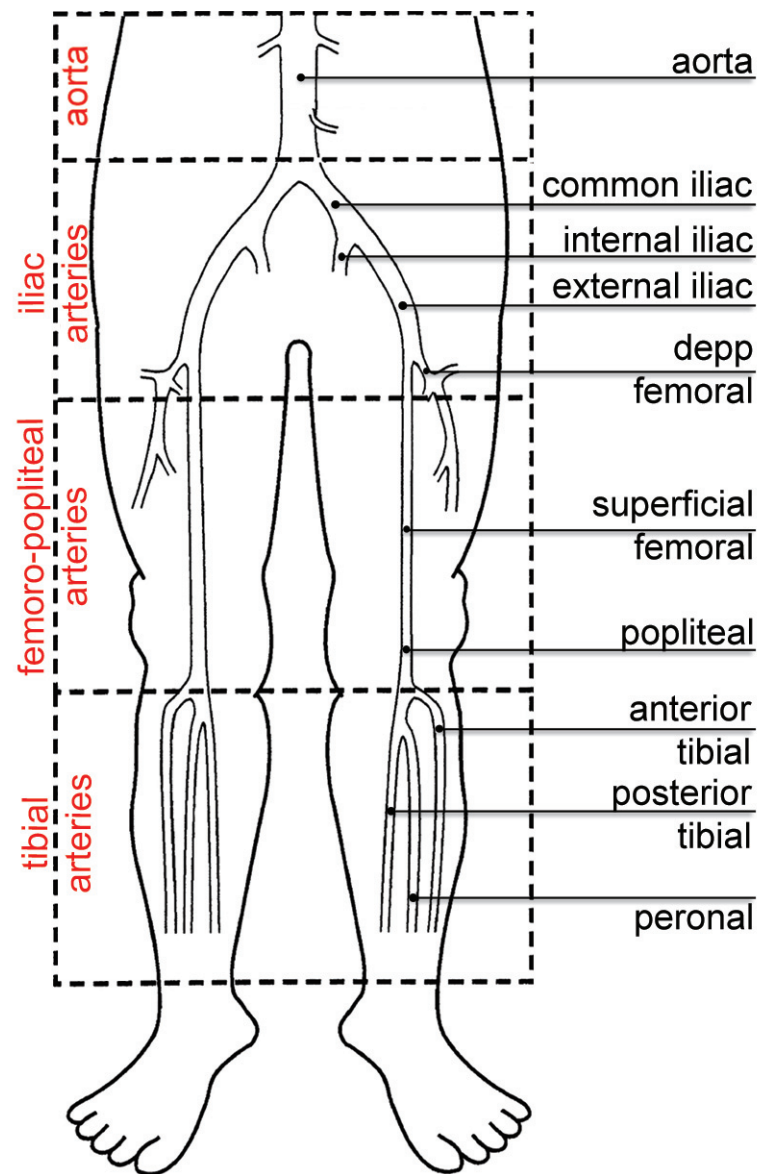
Figure 1.1: Illustrative example of the peripheral arterial tree [77].

of the dependent tissues. The corresponding clinical symptoms are rest pain and tissue loss ("critical limb ischemia"); which may eventually require amputation.

In the clinical stage of lifestyle limiting "intermittent claudication", per-

cutaneous or surgical revascularization may be indicated. The treatment decision and planning requires complete mapping of the disease process, which is often multifocal. In general, localized lesions can be treated by percutaneous balloon-catheter angioplasty [11]. For long segment occlusion, a surgical bypass is usually recommended [11]. Figure 1.3 shows an image of a patient with intermittent claudication of the left calf, caused by an occlusion of the superficial femoral artery. Note, that the slow evolution of the disease process has allowed the formation of several collateral vessel to develop.
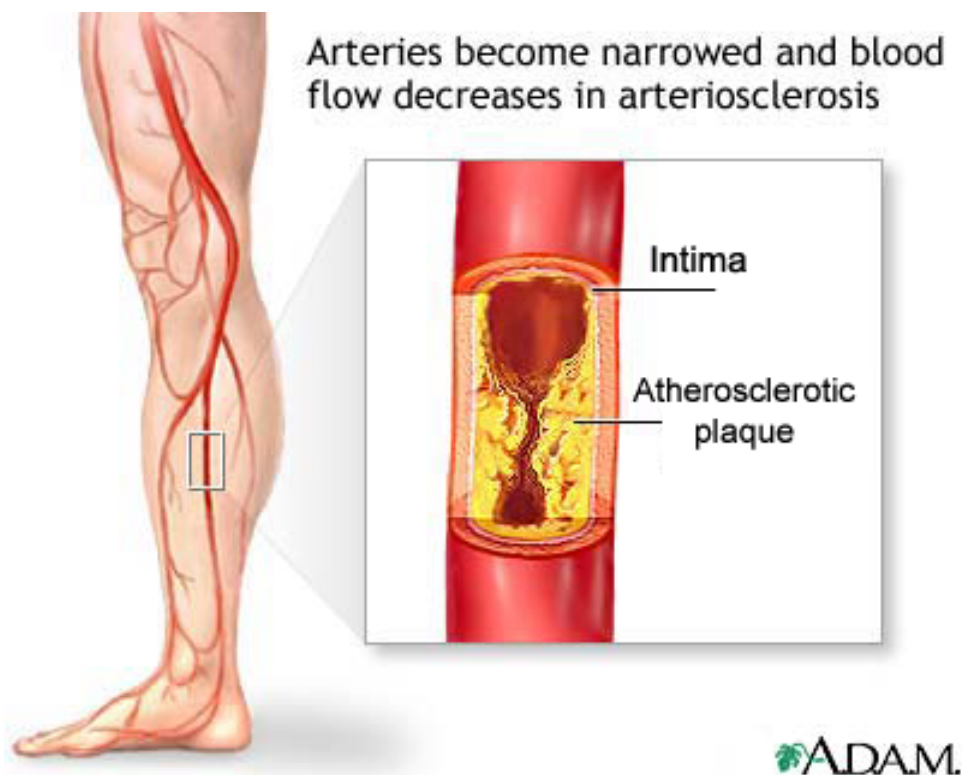
Figure 1.2: Illustration and schematic drawing of atherosclerotic plaque with luminal narrowing. This image is courtesy of Medline Plus and A.D.A.M. a Health Illustrated Encyclopedia online [56]

Vascular imaging plays a critical role for confirming the diagnosis, for staging, and treatment planning for patients with PAOD. In the next section we present an overview of different imaging modalities used for diagnosing and treating PAOD.
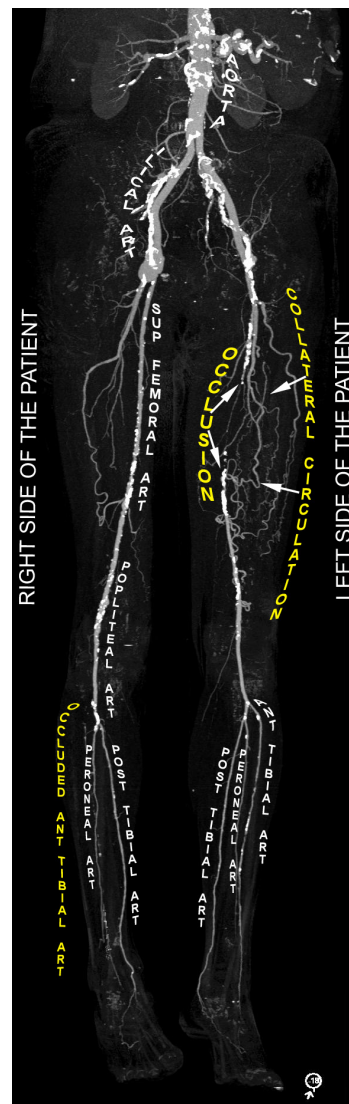
Figure 1.3: Maximum intensity projection image of a patient data with left calf claudication. Bones were removed for the purpose of better visualization of arterial vessels. Note the occlusion of the left superficial femoral artery. Several small collateral vessels fill the arteries distal to the occluded segment (image courtesy of Justus Roos from Stanford University Medical Center:justus.roos@stanford.edu)

1.3   Medical Imaging Used For Peripheral Vessel Investigation

Since the introduction of the concept of X-ray imaging by Röntgen [72] in 1895, physicians and scientists have searched for ways to enhance imaging techniques. Because the difference in tissue densities of the body is typically small, un-enhanced X-ray imaging does not allow for discrimination of individual soft tissue structures such as arteries and veins. In 1896, Haschek and Lindenthal [16] obtained the first angiogram (in vitro) in the physicochemical institute of Professor Franz Exner in Vienna. They used bismuth, lead, and barium salts to perform the first angiogram, using an amputated hand. Unfortunately, these heavy metal salts were too toxic to be administered to live human beings, and several years passed until safer and better tolerated agents were discovered, developed, and designed. In 1924, Brooks[7] performed an angiogram using sodium iodide, a more water-soluble compound, and thus initiated a slow evolution toward the creation of safer compounds through changes in the molecular structure of iodine-containing compounds. Figures in 1.4 show the first X-rays taken in December 1895 by Roentgen (left), and, the first angiogram image obtained in January 1896 by Haschek and Lindenthal (right).

| (a) | (b) |
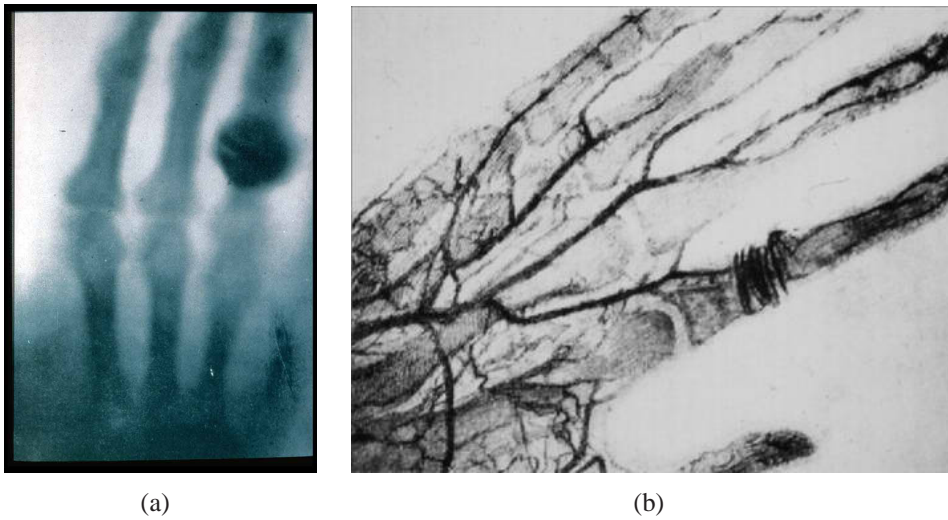
Figure 1.4: (a) The first X-rays image obtained by Röntgen in December 1895 and (b) the first angiogram image obtained by Mr. Haschek and Dr. Lindenthal in January 1896.

6

Vascular medicine has undergone a remarkable evolution in the last decades. Different image modalities have been used for peripheral vessel investigation, for diagnosis and treatment of peripheral vascular diseases. Several effective techniques are available, and continue to be improved, for the evaluation of blood vessels and blood flow. In this section we present an overview of different image modalities that have been used for radiological evaluation of peripheral arterial occlusive disease.

1.3.1   Angiography

Angiography is the name of a procedure that uses X-rays to produce a picture (the "angiogram"). This is an "invasive" procedure, because it requires the injection into the patient of a substance that is radiopaque (absorbs X-rays). This substance is commonly called a "Contrast Agent" or "Dye". Conventional angiography is considered by many to be the most accurate method of obtaining anatomic and pathologic information about the vascular anatomy and is the reference standard imaging technique prior to microsurgical reconstruction. Angiography is performed via a catheter which is inserted into a femoral artery (in the groin) and the tip is guided into the aorta. The arterial catheter is a thin, hollow, tube, which is placed into the artery. Contrast dye is then injected through the catheter and images are obtained of the desired anatomic region. Angiography is quite effective in determining arterial abnormalities such as stenosis, spasm, intimal injury and occlusion. This technique has been widely used for evaluation of potential recipient sites, particularly the lower extremity following trauma.

There are several potential complications associated with angiography, including arterial occlusion, pseudoaneurysm, renal failure and hematoma. In addition, traditional angiography requires the presence of a physician throughout the procedure, a lengthy post-procedure recovery as well as a high cost when compared with other imaging modalities.

Modern angiography units use digital substraction techniques (DSA). This technique allows showing contrast-filled vessels without any interference from the background. Using the X-rays technique, first a radiographic pre-contrast image is used as a positive copy; then a contrast agent is administered. The subtraction of the pre-contrast mask suppresses interfering structures from the 2D projection image so that the arteries become clearly defined. DSA is a new arteriography technique and it is considered the diagnostic gold standard for imaging patients with peripheral ar-

terial disease [29]. However, it is associated with a small but definite risk of complications. First, there are procedure-related complications, such as hematoma, vascular dissection, infection, etc. Second, it takes time to recover after such an invasive procedure. DSA is also a very costly procedure, and inconvenient for the patients. Thus, there is a considerable demand for a non-invasive technique to replace DSA.

1.3.2   Doppler Ultrasound

Ultrasound (US) imaging is a method of obtaining images from inside of the human body through the use of high frequency sound waves. The reflected sound waves echo are recorded and displayed as a real-time visual image. This technique does not require ionized radiation (X-rays). Ultrasound images can show movement of internal tissues and organs and enable physicians to see blood flow and heart valve functions, as it is a real-time imaging technique. It is a non-invasive method and has been used for vessel investigation using the Doppler effect. The Doppler effect is a change in the frequency of the sound wave, resulting from the motion of the reflector. Doppler US is used to detect and measure blood flow, and the major reflector are the red blood cells.

In peripheral vessel investigation this imaging technique is used to perform and provide an overview of the location, extent, and severity of vascular diseases. The ultrasound evaluation can be performed from the abdominal aorta through the tibial vessels and extended into the foot in order to facilitate clinical management decisions.

Gray-scale imaging is used to characterize the morphology of the vessel, to confirm the presence or absence of plaque, and assess plaque calcification and characteristics. Color-flow imaging is useful in evaluating subtotal obstruction of blood vessels and aneurysmal or tortuous segments, determining direction of flow, and localizing areas of stenoses.

Advantages of the US technique are that it is non-invasive, does not require contrast medium, no ionizing radiation, and provides flow information. However, it is very time consuming to examine an entire peripheral arterial tree, it is very operator dependent, and the medical documentation during examination is limited. US is ideal for screening, for characterizing short lesions, for follow-ups, but it is rarely considered an adequate technique for mapping the disease before revascularization.

1.3.3   Magnetic Resonance Imaging

Magnetic resonance imaging (MRI) is based on the principles of nuclear magnetic resonances. MRI works on the principle of the excitation of protons in body tissues and produces an image by decoding the signal received back from those same protons, following various field manipulations. Magnetic fields can be manipulated in any plane and hence images can be produced in any of the three orthogonal planes, or indeed in any oblique plane. This technique produces high quality images of the inside of the human body.

In the angiography field, magnetic resonance angiography (MRA) is a MRI study of the blood vessels. MRA provides detailed images of blood vessels without using any contrast material, although a special form of contrast material is often given to make the MRI images even clearer. Since the bones are not captured with MRA, vessels can be distinguished from bones. The procedure is painless, and the magnetic field is not known to cause any tissue damage.

This method is being widely used for evaluating blood vessels. Magnetic resonance techniques are especially useful in evaluating arterial dissection and characterizing vessel-wall morphology. Current limitations include the expense of the study, patient dissatisfaction with the technique (especially the claustrophobia experienced during a scan), difficulty with patient positioning, and it cannot be used in patients who have some kind of metal implant. However, decreased scan times and a more open design of the newer machines have lessened patient-related problems, and the cost of the procedure is likely to continue to decline, making this technique more accessible and practical.

1.3.4   Compute Tomography Angiography

Computed tomography (CT) is an X-rays based cross-sectional imaging technique, which provides transverse tomographic images through the body of a patient. The intravenous injection of radiographic contrast medium (usually into an arm vein) improves the X-rays attenuation differences (the contrast) between different tissues and vessels. In the last fifteen years, CTA has evolved dramatically. With the introduction of spiral (or helical) CT, CT has become a true volumetric modality. The technological advances of CT have also enabled the development of CT angiography. The principle of CT

angiography is the combination of a fast (within 10 - 40 seconds) high resolution CT acquisition, synchronized with good opacification of the arterial system (achieved by intravenous injection of contrast medium), followed by two- or three- dimensional image post-processing to achieve angiography-like images.

CTA has evolved together with further technical progress. The development of 4-, 8-, 16-, and now 64-channel multiple detector-row CT scanners (MDCT) has dramatically increased the scanning speed and improved spatial resolution, and CTA has evolved into a routine, non-invasive (or minimally invasive) vascular imaging tool in many vascular territories. such as pre-procedure planning and post-procedure follow-up of several endovascular procedures, including endovascular aneurysm repair, lower extremity revascularization, and renal artery revascularization. Improvements in image detail volume coverage have allowed CTA to also image the peripheral arterial tree, and early experience suggests that CTA has a good accuracy in the detection of atherosclerotic stenosis and occlusions of the extremity arteries when compared with DSA [60].

In Table 1.2, a summary of different radiological evaluations used for peripheral arterial occlusive disease is presented. Advantages and disadvantages are pointed out in this table.

1.4   CTA of Peripheral Arterial Occlusive Disease

CTA has recently evolved into a routinely applicable imaging technique to visualize the entire peripheral (lower extremity) arterial tree. Basically, our main focus is the vessel parameterization of peripheral arteries imaged by CTA. The reason is that: currently CTA is a non-invasive (less invasive) vascular imaging technique. This study tool is faster (compared to MRA), more minimally invasive (compared to DSA) than previous tools and with better spatial resolution (compared with DUS, i.e.). Detection and visualization of calcification is possible with better spatial resolution, and even when errors prone with horizontal branches are produced, this does not constitute a big problem for diagnosis [20].

A peripheral CTA dataset consists of up to 2000 transverse CT slices, and thus cannot be assessed by the radiologist or treating physician without further image post-processing. Visualization of the peripheral CTA datasets

	DUS	CTA	MRA	DSA
Anatomic detail	Not well seen. Tends to stenoses. Poor in aorto-iliac disease.	Error prone with horizontal branches, but shows eccentric stenoses well.	Good anatomic detail with use of gadolinium	Excellent
Display	2D	2D and 3D	2D and 3D	2D
Reproducibility	Operator dependent and painstaking	Good	Good	Good
Patient Comfort	No known adverse effects or contraindications, can be used at bedside	All adverse effects of contrast agent administration and radiation	Contraindicated in patients with certain prosthetic implants, pacemakers, etc. Very difficult to use in patients requiring intensive monitoring.	Adverse effects are related to contrast injection and arterial access.

Table 1.2: Summary of advantages and disadvantages of different image modalities used for the evaluation of peripheral arterial occlusive disease.

is a complex task and includes specific problems which are related to manifestations of atherosclerosis such as vessel calcifications, stenoses and occlusions. To visualize longitudinal cross sections allowing insight into the flow lumen along the vessels are very useful, especially in case of diseased vascular segments [71].

An accurate identification of the vessel centerline in CTA data sets is highly desirable, because of its crucial role in vessel visualization, automated vessel analysis, and quantification. This is not a trivial task, partic-

ularly in the presence of an atherosclerotic disease. A fairly homogenous CT density of the vessel lumen due to the contrast-medium enhanced blood characterizes healthy arteries. Blood is higher in X-rays attenuation than the surrounding soft tissues (muscles, fat), which is generally lower in attenuation than neighboring bony tissue. Diseased arterial segments, however, may have a very different X-rays attenuation. Non-calcified atherosclerotic plaque is isodense to soft tissues (see Figure 1.5), and calcified plaque has a CT density similar to bone (see Figure 1.6). The overlap in density ranges is further aggravated by the wide range of diameters observed for individual branches of the arterial tree (see Table 1.1 and Figure 1.7), as well as by the presence of image noise, scanning artifacts, limited scanner resolution with partial volume averaging, inter-individual and within-patient variability of arterial opacification.

| (a) | (b) |
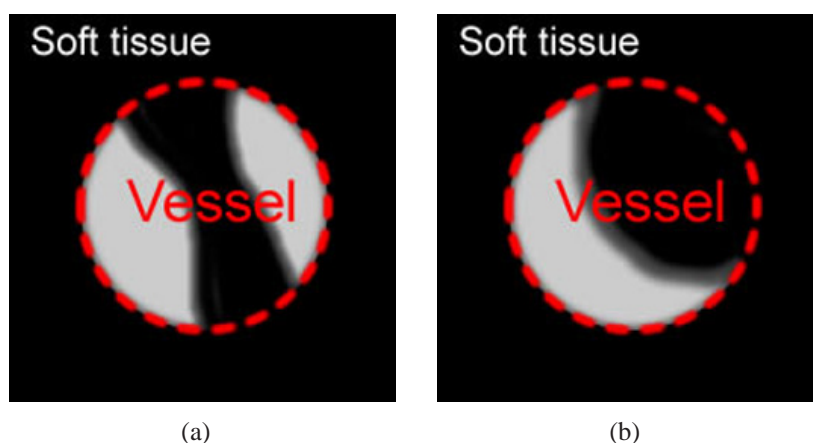
Figure 1.5: Illustrative example of a non-calcified plaque (vessel cross-section view).

Several problems from the acquisition process as mentioned before hamper the correct identification and the evaluation of peripheral arteries disease. Two of them are:

- **The partial volume effect** is the effect produced by the contribution of multiple tissues to a single pixel or voxel resulting in a blurring of intensity between boundaries. This effect makes the separation between two or more different tissues difficult. Due to this the transition between tissues is not clear; which is a big problem in small vessels.
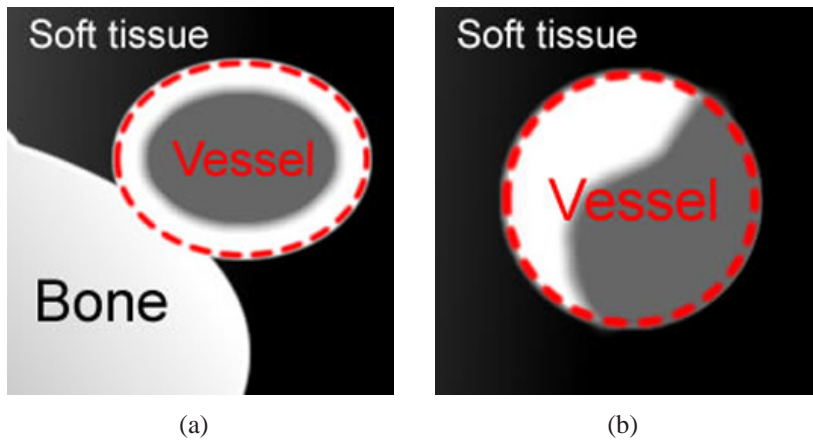
Figure 1.6: Illustrative example of a calcified plaque (vessel cross-section view), closer to bone (a), far away from bone (b).
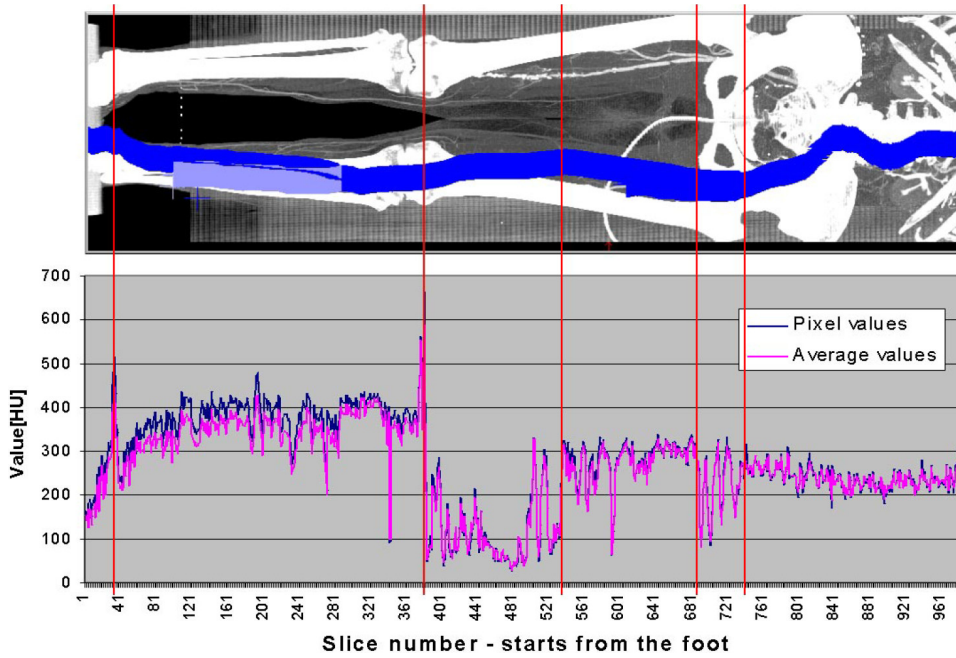
Figure 1.7: Topogram image of a PAOD dataset with a dark bold line (blue) in the place of the manually segmented left leg vessel and the voxel density values along the vessel together with the average values of density from the 3x3 surroundings of the center-path [17]

13

- **Contrast agent administration.** The contrast agent is more of a concern with the protocol followed by radiologists [73]. Poor injection of contrast agent produces images with a non-clear distinction between soft tissues and blood vessels. The poor administration of the contrast agent, added to the partial volume effect constitute a big challenge for the underlying detection of diseased blood vessels, and even healthy vessels with small diameters [22].

1.5   Visualization of PAOD in CTA datasets

Several visualization techniques have been already used for blood vessel visualization. The most known are; direct volume rendering (DVR), maximum intensity projection (MIP), iso-surface display, etc.

- **DVR** is a visualization technique that allows the whole volume dataset to be displayed. With DVR, it is possible to visualize all structures anatomically correct, but for large datasets this is time consuming. DVR depends on a transfer function definition, which allows the identification and classification of different tissues along the viewing ray. In some cases this is a challenge because it is highly dependent on the dataset.

- **MIP** displays the highest intensity value of all voxels along the corresponding viewing ray. In this case, all structures with higher intensity values are displayed in front, hiding lower intensity structures. Therefore, the bones are always in front of the vessels.

- **Iso-surface display** produces surfaces in the domain of the scalar quantity, which has the same value, the so-called isosurface value. There are different methods to generate the surfaces from a discrete set of data points. All methods use interpolation to construct a continuous function. The correctness of the generated surfaces depends on how well the constructed continuous function matches the underlying continuous function representing the discrete data set. The most used method is the marching cube algorithm [70].

We present in this section the most recent and novel visualization techniques that have been presented to the scientific community for vessel visualization, some of them have been applied for peripheral vessels.

14

1.5.1   Curved Planar Reformation

Curved planer reformation (CPR) [36] is a visualization technique that allows the representation of a whole tubular structure in a single image. The centerline of the tubular object of interest is used as input. This technique is already clinically accepted [40], and medical doctors frequently use this technique for diagnosis. Figure 1.8 is an example of CPR images generated from a patient with PAOD.
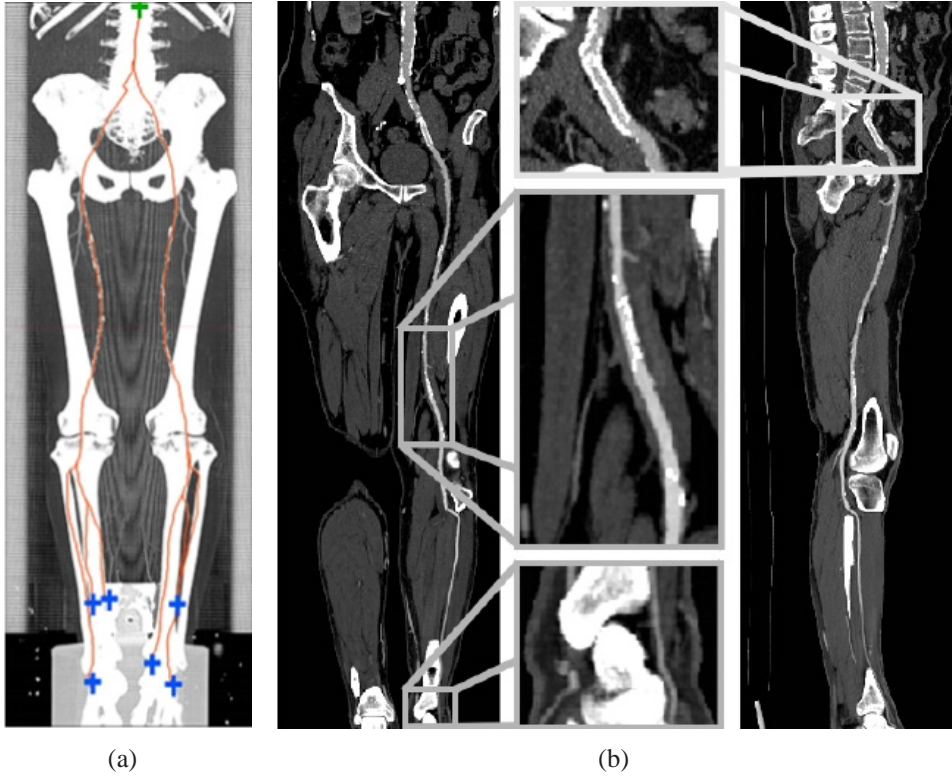
Figure 1.8: CPR example. (a) First the center path is estimated, defining starting (crosses at the top) and endpoints (cross at bottom). In (b) a coronar CPR (left) and sagittal CPR (right) from the data set in (a) [36]

The centerline determines the visualization space of the tubular structure. Depending on the geometric property of an aligned vector used for the re-sampling and the centerline, Kanitsar et al. [35], analyzed three different CPR methods (e.g., projected CPR, stretched CPR and straightened CPR). These methods were compared to each other using a phantom object. The

comparison evaluated spatial perception, isometry, and possible occlusions. The straightened CPR is preferable in many applications. Due to the fact that the surrounding tissue may be distorted in the image, it might be difficult to immediately recognize which portions of a vessel tree are actually displayed. Thus, Kanitsar et al. [35] defined three CPR enhancements that overcome this problem (more details in [35]). These CPR enhancements are; multipath CPR, rotated CPR and thick CPR. The multipath CPR allows the visualization of multiple vessels in one image without the overlapping of other tissues (e.g., bone). The rotated CPR allows rotating the projection of any CPR method. The thick CPR reduces sampling artifacts, achieving a better projection of small vessels and removing false stenoses.

1.5.2   VesselGlyph

The VesselGlyph is a novel visualization technique based on a focus & context approach [75]. This technique is designed to visualize a tubular object such as vascular structures. It is applied to contrast-medium enhanced arteries in CTA. Basically, the VesselGlyph combines direct volume rendering and curved planar reformation within a single image. It is based on a definition of separated regions where different rendering techniques are applied. Given a partially segmented data with an approximation of the centerline of the tubular structure, a region type is defined depending on the distance to the vessel centerline. The focus object is the vasculature, and the Vessel-Glyph allows the visualization of the focus object in areas where it can be obstructed by other objects in front. Images with DVR contain full anatomic information, while CPR images allow the visualization of the whole vessel structure, but the generation process can distort the anatomic information. With the VesselGlyph, the anatomic information is preserved while the vasculature is visualized as a focus object, in a single view, without any distortion. An example of four different modalities of the VesselGlyph is shown in Figure 1.9. This visualization technique has not been evaluated clinically.

1.5.3   Convolution Surface

The Convolution surface is based on the assumption that cross sections of non-pathologic vessels have a circular shape. The resulting convolution surfaces permit topology changes, seamless part joining, and an efficient implementation. This allows the construction of blended articulated models.

16
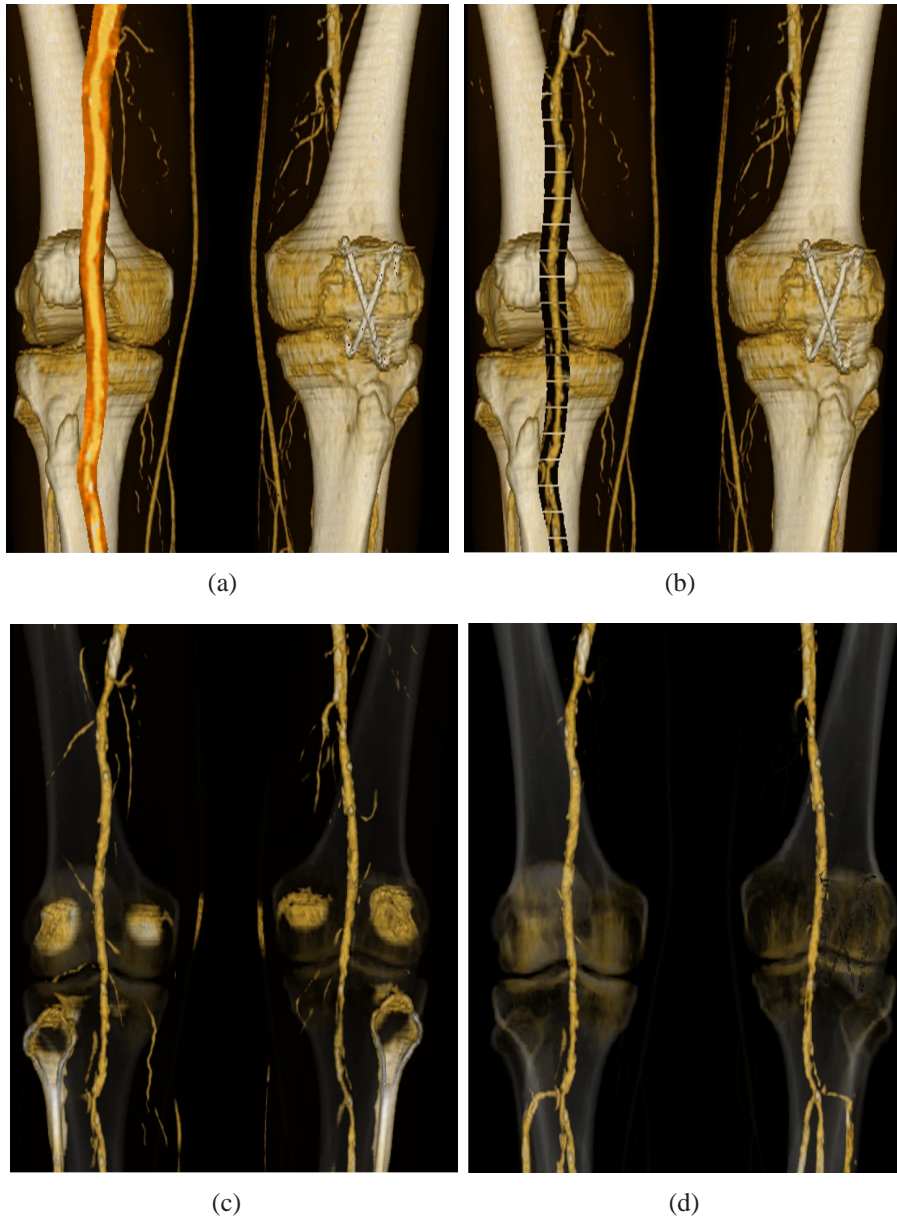
Figure 1.9: VesselGlyph examples: (a) CPR + DVR, (b) foreground-cleft in DVR with occlusion lines, (c) Thick-Slab rendering (DVR), (d) tubular rendering (DVR) [75]

The convolution surface for vessel tree visualization was explored and implemented by Oeltze and Preim [58, 59]. First, the vessel skeleton must be defined and an initial estimation of its diameter should be used as input. Then, the tubular object is defined by the convolution of the skeleton with a three-dimensional Gaussian filter. This technique is independent of the modality used for 3D imaging (e.g., MRI or CTA). An example of a cerebral vasculature imaged by MRI is shown in Figure 1.10.
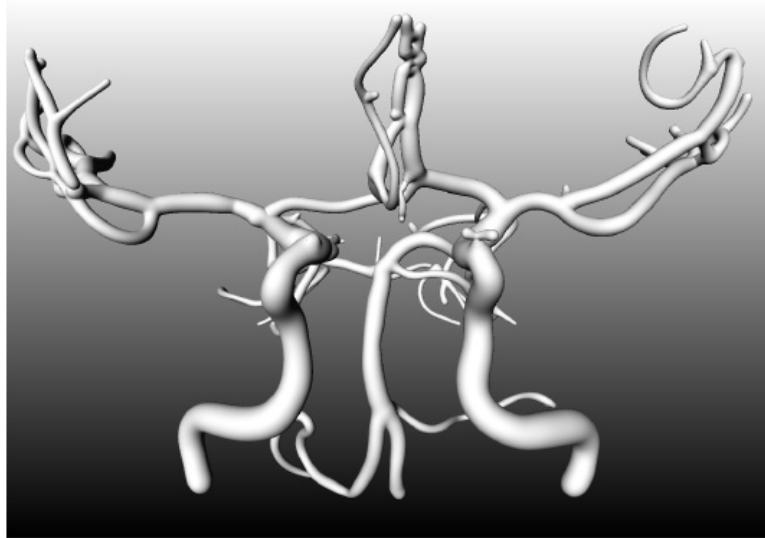
Figure 1.10: Visualization of cerebral vasculature imaged by MRI using a convolution surface [59]

The convolution surface visualization technique defines a model adequately for visualizing vascular tree structures. However, this method assumes a circular cross-section of blood vessels, it is based on an initial estimation of the skeleton and diameter estimation of the vascular tree structure. As we described, in Section 1.4, we found that with diseased blood vessels, assuming just circular cross-sections is insufficient, due to the irregularity of shape of the diseased blood vessels. The intensity image distribution of diseased blood vessel is also non-uniform.

The convolution surface was compared with other rendering techniques used for vessel visualization. Iso-surface rendering as a vessel tree visualization technique produces artifacts [27]; either vessels appear disconnected in the periphery or structures which do not belong to the vessels but exhibit similar intensity values are included in the visualization. Figure 1.11 shows

an example of comparing the convolution surface with other rendering technique including iso-surfacing.
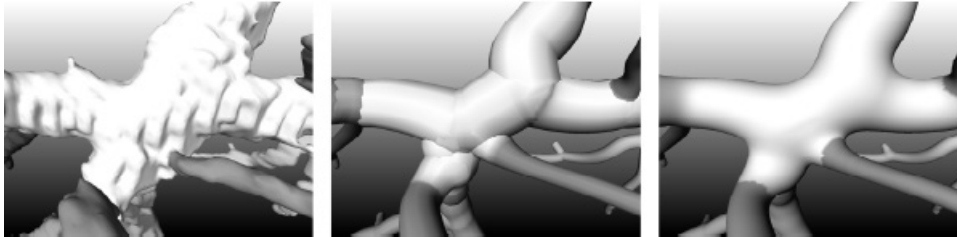
Figure 1.11: Close-up images of a vessel tree example, comparing iso-surface rendering (left) with a more refined rendering technique (middle, details in [59]) and convolution surface rendering (right) [59]

1.6 Discussion

In general, the visualization techniques presented in the previous sections assume an initial estimation of the centerline and diameter of the tubular structure. Peripheral vasculature consists of large and tiny vessel diameters, and patients with PAOD may have an irregular variability of the vessel shape. A wrong estimation of a centerline may produce wrong visualization results (e.g., using CPR), and then, the so-called pseudo-stenoses may appear. An illustrative example is shown on Figure 1.12. This may involve interactive intervention, which is time consuming.

On the other hand, peripheral vascular investigation (where the average scan length is between 110 cm and 130 cm[20]) and analysis in any image modality, require the analysis of large datasets (i.e., a CTA dataset may consist of 2000 2D slices). Which is very time consuming for radiologist without any semi-automatic or automatic segmentation algorithm that allows them identify accurately and more precisely the localization and quantification of any vascular anomaly, without wasting of time. For theses reasons, a accurate segmentation is highly required and necessary. Furthermore, the peripheral CTA has been gradually more used in clinical practice for PAOD diagnosis and posterior following treatment. Additionally, with the evolution of CT-scanner technology, high resolution imaging of the peripheral vasculature has become routinely possible. However, the density overlapping of different tissues is a major difficulty for segmentation and clear sep-

aration between different tissues from vessel tissues. A 2D visualization of the vasculature is definitely not enough, because of the superposition in 2D of bone over vessels. Besides, medical doctors and radiologists are familiar with CPR visualization, which is based on a centerline estimation in a 3D space. These are the main reasons why a segmentation of peripheral arteries is highly required and why a 3D segmentation is preferable than a 2D segmentation.
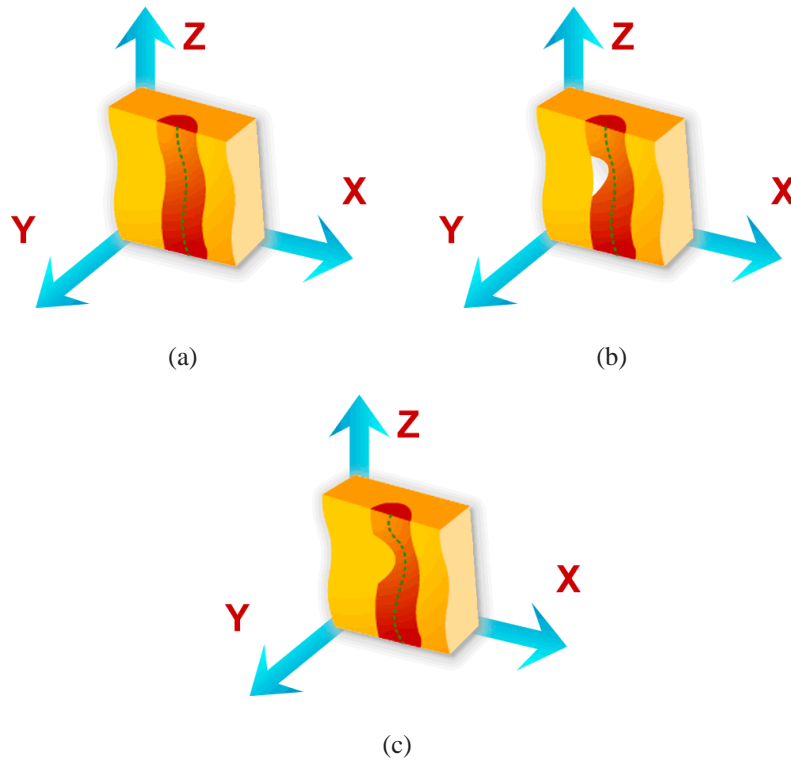
Figure 1.12: Illustrative example of a good and wrong estimation of a centerline if a CPR visualization technique is used. In this example we show (a) a good estimation on healthy data, (b) a good estimation on a diseased case, (c) a wrong estimation on a healthy or a diseased case.

1.7   Thesis Contents

The main contribution of this thesis is to present a new technique to parameterize diseased blood vessels of the peripheral vascular structures. Vi-

sualization of tubular structures such as blood vessels is quite "easy" when the blood vessel is healthy, problems appear when the vessel presents any anomaly due to the presence of some vascular disease.

This thesis presents an investigative result for blood vessel segmentation, with the focus on diseased blood vessels of peripheral arteries imaged by CTA. Medical doctors are more interested in being able to visualize and quantify vascular diseases than having just nice images. For them it is quite important to identify the center and surround area close to the vessel center. The vessel center is not defined only by the center of the lumen (which is the area where the flow goes through in the vasculature structure), but also by the calcified and occluded part of the vessel. In this case we have experienced that it is a challenge to find a simple segmentation technique that takes into account such variability. Due to this fact and the knowledge based on that, vessels conserve a tubular structure, even in the presence of calcifications and occlusions. We believe a model-based technique is the most suitable approach for showing a better or even more accurate segmentation. In this direction we present in chapter two a review of different model based techniques already applied to vessel segmentation and visualization. In this review we included the last 20 years of investigation in this area, giving the reader a good reference frame.

As we could see in the section before, most of the blood vessel visualization techniques require an accurate estimation of the centerline of the vessel. Most of them are based on an initial centerline approximation. At the beginning of our research we were more interested in the improvement of the centerline estimation than an actual centering technique used on a daily clinical basis. Therefore, we start with an evaluation of different centerline techniques that were worked on. Thus, chapter three presents an evaluation of different methods for approximating the centerline of a vessel in a phantom simulating the peripheral arteries. Six algorithms were used to determine the centerline of a synthetic peripheral arterial vessel. They are based on: ray casting using thresholds, maximum gradient-like stop criterion, pixel motion estimation between successive images called block matching, center of gravity, and shape based segmentation. The Randomized Hough Transform and ellipse fitting have been used as shape based segmentation techniques. Since in the synthetic data set the centerline is known, an estimation of the error can be calculated in order to determine the accuracy achieved by a given method. Mostly these methods work on a cross-section of the vessel from an initial vessel path tracked but not centered. Unfortunately, in this

investigation we did not find any relevant improvement for accuracy in the centerline estimation, due to the wide variability of blood vessels in patients with PAOD. However, this allowed us to conclude that it might be significant if a three dimensional space is taken into account when evaluating an ideal profile of blood vessels. In this direction we designed a new strategy for a blood vessel parameterization. This strategy is presented in Chapter four.

Chapter four describes an estimation of the dimensions of lower extremity arteries, imaged by computed tomography. The vessel is modelled using an elliptical or cylindrical structure with specific dimensions, orientation, and blood vessel density. The model separates two homogeneous regions: Its inner side represents a region of density for vessels, and its outer side a region for background. Taking into account the point spread function of a CT scanner, a function is modelled with a Gaussian kernel, in order to smooth the vessel boundary in the model. Thus, a new strategy for vessel parameter estimation is presented in this chapter. It stems from the vessel model and the model parameter optimization by a nonlinear optimization procedure, i.e., the Levenberg-Marquardt technique. The method provides center location, diameter and orientation of the vessel, as well as blood, and background mean density values.

We considered it quite important that medical doctors were involved in the development of every new approach designed to help them for diagnosis. For this reason a clinical evaluation of every new technology is crucial before it can be used in a clinical environment. Therefore, Chapter five presents a clinical evaluation of the method described in Chapter four as a first step to introduce this technique in a clinical environment. Twenty cases from available patient data were pre-selected and separated into 'minimal diseased' and 'severe diseased' vessels. Manual identification were used as our gold standard. We compared the model fitting method against a standard method, which is presently used in the clinical environment.

CHAPTER 2

MODEL BASED SEGMENTATION TECHNIQUES

Part of this chapter is based on the following publication:

Bühler K., Felkel P., and **La Cruz A.**: Geometric Methods for Vessel Visualization and Quantification - A Survey. Geometric Modelling for Scientific Visualization. G. Brunnett, B. Hammann, H. Müller, and L. Linsen, (eds), Kluwer Academic Publishers. pp 399-420. 2004.

2.1 Introduction

In medical imaging, segmentation is the process of classifying and separating different tissues. It is a prerequisite for quantification of morphological disease manifestation, for volume visualization and modeling of individual objects, for chirurgical operation planning and simulation (e.g., using virtual endoscopy).

We found that recently, two relevant works in this area were presented to the scientific community. In both of them, the authors presented an overview of different segmentation and visualization techniques designed for identifying and modeling vessels and tube-like structures. Bühler et al. [8] present a survey and discussion of different geometric techniques applied to vessel visualization and geometric model generation. Kirbas et al. [39], classified several segmentation methods according to the technique that was used. They point out that there is no single segmentation method that allows the extracting of the vasculature across different medical imaging modalities

23

(e.g., MRA, CTA, US, etc.), and not even across different vascular anatomic territories. Some methods use threshold values, or an explicit vessel model to extract contours. Other techniques require image processing (depending on the data, quality, noise, artifacts, etc.), a priori segmentation, or post-processing.

A general segmentation technique is based on the intensity level. This technique relies on the assumption that the blood vessels have a different intensity level than soft tissue or bone. This is due to the absorption and/or emission property of the object being imaged by any modality, which is different for blood, muscle, bone, air, fat, etc. Based on this fact it is possible to classify different objects according to the thresholds of intensity level defined for every tissue. Nevertheless, due to many factors (e.g., noise, partial volume effect, artifacts, etc.) this approach is not enough for an accurate segmentation. Thus, an immediate improvement is using a technique that allows an adaptive local thresholding [31], or using a statistic shape model [12, 13]. The region growing technique [5, 8, 39], which can be seen as an extension of a thresholding technique is based on a classification of pixels (voxels) that fulfill certain constrains defined previously. From an initial pixel (voxel), the neighborhood is analyzed and added to the region if it satisfies a decision rule. Normally the decision rule is defined using threshold values, the gradient operator, and/or spatial proximity. This method assumes that discontinuities are not possible between objects. The growing criteria should be sufficient to face local image variations. Due to the variations in image intensities and noise, region growing can result in holes and over-segmentation. An improvement to this method includes mathematical morphology [74], which may avoid holes and remove the connectivity between different tissues. This technique has been used for blood vessel segmentation in combination with other techniques as a post-processing step [63].

As mention in the previous chapter, our main focus is the segmentation of blood vessels imaged by CTA. The vessel lumen of healthy vessels in CTA datasets is characterized by a fairly homogenous CT density. On diseased blood vessels it is a challenge to identify the center of the vessel, due to the characteristics of non-calcified and calcified plaque, as it was described in a previous chapter. Therefore, it is not surprising that density and gradient information alone is insufficient to accurately extract the centerlines of a diseased arterial tree. The overlap in density ranges is further aggravated by the wide range of diameters observed for individual branches

24

of the arterial tree, as well as by the presence of image noise, scanning artifacts, limited scanner resolution with partial volume averaging, and finally, inter-individual and within-patient variability of arterial opacification. For this reason, we believe that a model-based technique is more suitable for the problem we are dealing with in our investigation.

Classical model based segmentation algorithms [8, 39] applied to vessel extraction are based on fitting circular, elliptical or cylindrical geometric models to the data, assuming a tubular shape. Such techniques combine thresholds with gradient information [87] or derivative estimation [42, 43, 44] in order to approximate the vessel boundary. Then, this initial boundary estimation is fitted to a geometrical model (e.g., circular or elliptical cross-section or cylindrical structure).

This chapter contains an overview of the most recent works related to model based segmentation techniques applied to blood vessels. We present a list of the most important model based segmentation techniques that we considered and which have been used in the last two decades. Various research has been already done in this area. However, an accurate vessel segmentation and visualization continues to be an open problem. Most of the recent works have been motivated to provide more confidence and faster techniques.

2.2 Deformable Models

The deformable model approach is described in more detail as a geometric model used for blood vessel segmentation and visualization by Bühler [8]. Kirbas et al. [39], also classified it as a model based approach.

Deformable models [53] appear to be one of the most promising segmentation techniques. This approach is powerful and widely used for segmentation and geometric model generation in 2D and 3D data [8], and it can be used for any modality [39]. These techniques are based on a minimization process of an energy function. This energy function involves internal and external forces. The internal forces allow smoothness of the contour and the external forces move the deformable structure towards the edges of the underlying data. Depending on the definition of the energy function, the deformable model inflates or shrinks towards the object. Normally, the energy function involves the gradient information or derivative values around the deformable object.

Depending on the parameterization used for the model and the definition

of the energy function, in the literature [8] three more common deformable models are found. They are: the snakes or active contours, level-sets, and probabilistic snakes.

2.2.1 Snakes

The snake approach uses a parameterized curve which evolves over time. This technique has been applied in many areas of medical segmentation. Gong et al. [26] define a deformable super-ellipse for prostate segmentation. Hernandez et al. [28] use this approach for three-dimensional segmentation of brain aneurysms in CTA. Lorigo et al. [49] present a deformable model based on active contours for segmentation of brain vasculature. The main goal of the snake is to minimize a weighted sum of influences from various energy forces. Conventionally, this parametric model usually relies on a set of basis functions. Depending on the shape of the object it may require a re-parameterization that is heuristically or interactively controlled [85]. A new generation of deformable models was designed to avoid such problems, which is the well-known level-set approach [61].

2.2.2 Level-sets

A level-set is based on an implicit model to represent surface shapes. This approach is topologically flexible and can split and join as necessary in the deformation process [53], without a re-parameterization [85].

The level-set approach has been widely used for vascular segmentation [8] in general, aortic aneurysm segmentation [48, 76], and centerline detection of colon CT data [15]. Wang et al. [83] used this approach as an experimental result to segment a case of lower extremity occlusive diseases.

2.2.3 Probabilistic Snakes

Another way to define an energy function in a deformable model approach is using statistic information. This approach is called the probabilistic snake. A probabilistic shape model generally assumes that image features are random variables with shape dependence on probability distributions [52]. This approach searches the probability of an image of a given model, using a Bayesian framework. Pujol et al. [68] applied this approach for segmentation of intravascular features of coronary arteries imaged by US.

26

Yim et al. [90, 91, 92] present a deformable model for reconstructing the vessel surface of a carotid artery. The deformable model is based on a cylindrical coordinate system of curvilinear axes [92]. The model consists of a mesh, where vertices are evenly spaced in the axial and in the circumferential directions. In this mesh the vertices deform only in the radial direction and their position is described by their radial location. The method allows for curves in the vessel axis, variability in the vessel diameter, and variability in cross sectional shape. Internal and external forces produce the deformation. The internal forces push the vertices to minimize discontinuities in the radial location between adjacent vertices. The external forces push the vertices towards peaks in the gradient magnitude images. In this approach it is possible that adjacent radial meshes intersect each other. In this case a warping process is used to solve this problem (more details in [92]). Here, the axes are selected manually. Later on, Yim et al. [91] present an improvement of the location of the vessel axes by a skeletonisation technique. This skeletonisation technique is based on the ordered region-growing algorithm (ORG). The ORG represents the image as an acyclic graph, which can be reduced to a skeleton by specifying starting and ending point. This may construct paths, which are not part of the vessel. A pruning process solves this error. This pruning process is based upon branch lengths. Branches without a minimal length are removed.

Feng et al. [18] present a 3D geometric deformable model for tubular structure segmentation. Based on internal and external forces, Feng et al. introduced a new energy term which incorporates the information of the spatial relationship between tubular branches. The results were shown only with experimental data [18].

2.3 Multi-scale Methods

Multi-scale methods are based on the extraction of large structures at low-resolution images and fine structures at high-resolution images. Multi-scale methods [44] as well as deformable models have been used more recently for blood vessel segmentation. In fact, Whitaker et al. [85] point out that the combination of the level-set method with a multi-scale approach allows the model to start on a coarse grid and progress on finer grids until a solution is reached. This reduces computation time and controls the relative importance of differently sized structures in the model. A similar combination of level-set and multi-scale approaches was used by Boldak et al. [6].

The multi-scale approach uses the Hessian matrix, which contains the second derivatives of the data. This method is based on the fact that the smallest Eigen value of the Hessian matrix is close to zero at the center of tubular structures, and the other two Eigen values are high and close to equal, assuming a circular cross-section.

Krissian et al. [42, 43, 44] presented a new approach to segment vessels of 3D angiography data of the brain using the multi-scale technique.

Frangi et al. [25] introduce a multi-scale vessel enhancement approach applied to segment and analyze the vasculature on cardiac images. Frangi [23, 24, 25] worked in his PhD thesis on the application of a three-dimension model for vascular and cardiac images based on a multi-scale method for vessel enhancement. Many other authors have used this approach to model geometric flows of cerebral vasculature imaged by MRI [78].

Joshi et al. [32, 33] present a Bayesian multi-scale three-dimensional deformable template approaches based on a medial representation for the segmentation and shape characterization of anatomical objects in medical imagery. Via the construction of templates, information about the geometry and shape of the anatomical objects under study should be given, beforehand. Defining probabilistic transformations on these templates pursues the anatomical variability. The multi-scale deformable template is based on the medial axis representation of objects proposed by Blum [4]. This technique was applied for the automatic extraction and analysis of the shape of anatomical objects from brain and abdomen, imaged by MRI and CT respectively.

2.4 Geometry Based Segmentation

Geometry based segmentation is based on a parametric model, which defines a tubular model. This tubular model with elliptical or cylindrical cross-section has been applied on 2D and 3D datasets. Mostly this approach is combined with a deformable model or a multi-scale approach. Given a parametric model of a tubular object (e.g., generalized cylinder) and using the deformable model approach it can be deformed to get the most appropriate model. On the other hand, using the properties of the Hessian matrix and the medialness approach [25] a cylindrical model can be extracted. Medialness or core is defined in terms of convolution kernels at many positions and scales (in scale space), with scales, i.e., kernel widths, that are a signif-

icant fraction of the radial width of a tubular object. Basically a medialness function measure the degree of belonging to the medial axis of the object.

2.4.1   Geometry Based Segmentation Combined with a Deformable Model Approach

Boldak et al. [5, 6] proposed a segmentation of three-dimensional vessels imaged by CTA using geometrical moments, assuming that segments can be considered as tube-like structures. A 3D geometrical moment-based method is used to localize the center of the vessel and its local direction, by using a local approximation by a cylinder. This ideal cylinder separates two homogeneous regions. The area inside the cylinder (the vessel) is defined with a higher intensity level and the area outside (background) with a lower intensity. Filtering ideally smoothes the transition between both regions. This approach uses several adaptive controls that allow dealing with pathological patterns such as dense and scattered calcifications. The disadvantage of this method is that it allows an underestimation of the diameter for better tracking in a defined window size. It makes a compromise to avoid including other structures in the window, like: bones, distinct vessels, highly curved vessel parts, etc. This window size can be adjusted by applying an adaptive control. This is performed by means of an exponential weighting of the current and previous vessel diameter values in order to avoid window size oscillations. Using a heuristic approach to handle calcifications and stenoses, the algorithm removes calcifications using a region growing approach, allowing also the removal of vessel tissues, and this introduce slight changes of the vessel shape. The advantage with this heuristic rule is that it also removes bones that appear closer to the vessel. Then, the level set approach [6] is used in order to refine the segmentation process allowing improvement of the delineation accuracy of contours and calcifications. This approach has been applied to segmentation of the lower limb vessels.

Baun et al. [3] presented a method for 3D surface modelling of the cerebral vasculature of 3D medical images using active contours. In this work Baun et al. used the generalized cylinder to represent the active contour. The generalized cylinder allows the modelling of an elongated tubular object with cylindrical or elliptical cross section. In this case it is necessary to reach a global minimum in order to minimize the energy function used by the active contour. This global minimum is reached using dynamic programming for energy minimization. The energy function defines an internal and

external force. The external force is based on the gradient, stopping the contour when an edge is reached, which is defined by the highest gradient value. The internal forces model the rigid and tension of the object, which allow a bending behavior and prevent clustering of neighbor points on the axes. The initial forces also include a radius constraint, which is used to minimize the differences of radiuses in a same vessel segment defined between bifurcation points. In this case, the basic idea of using dynamic programming is to treat the minimization as a path-planning problem of finding the optimal path between multiple paths at multiple decision states. Each transition between the points on the spine, and between the different radiuses, is equal to a transition in the decision stage. Each decision stage contains information of the previous stage, reducing the complexity problem considerably. This work presented encouraging results on CTA and MRA datasets applied for segmentation of cerebral vasculature.

2.4.2 Geometry Based Segmentation Combined with a Multi-scale Approach

Aylward et al. [1] map image intensity to height. This is based on the fact that a 3D image can be viewed as a 3D surface in 4D space, and a 2D image can be viewed as a 3D surface, with peaks in areas of height intensity. It is assumed that tubular objects generally appear brighter than background, and the centerline follows a ridgeline. The segmentation technique is used in combination with a multi-scale approach that allows the extraction of a tubular model using the properties of the Hessian matrix and the medialness approach [25]. As we said before the medialness functions measure at a given point the degree of belonging to the medial axis of the object. Furthermore, the multiscale medial axis can be defined by applying the medialness function at multiple scales. Aylward et al. [1] illustrate the capabilities of the method for medical applications that involve a variety of tubular structures in clinical data of different organs, patients, and image modalities.

2.5 Model Fitting

A model fitting is a segmentation method that typically tries to fit a simple geometric shape, such as an ellipse or curve to the locations of extracted images features in an image [65]. A more general approach, in this direction, is to fit a spline or surface [65] to different features. Huang et al. [30] used

a tubular model to recognize 3D elongated objects from 2D images using a minimization process to fit a model.

Recently, Wörz and Rohr [88] presented a 3D parametric intensity model for accurate segmentation and quantification of human vessels. This approach is based on a 3D cylindrical parametric intensity model, which is fitted to the image through an incremental process based on a Kalman filter. The Kalman filter [34] is a recursive technique, based on a set of mathematical equations that provides an efficient computation to estimate the stage of a process, minimizing the mean squared error. Kalman pointed out that the filter supports estimations of past, present, and future stages, even when the precise nature of the modeled system is unknown. The model applied by Wörz and Rohr have been applied to segment vessels of 3D MRA images. Bifurcations are not handled automatically; instead an intervention from the user is necessary to indicate the starting and ending point between bifurcations. Figure 2.1 shows different profile examples of 2D slices of three different vessel sizes imaged by MR. The real appearance of the blood vessel profile indicates that a Gaussian model alone is not enough to model a vessel. Figure 2.2 shows some segmentation results for the pelvis arteries and the coronary arteries by Wörz and Rohr.
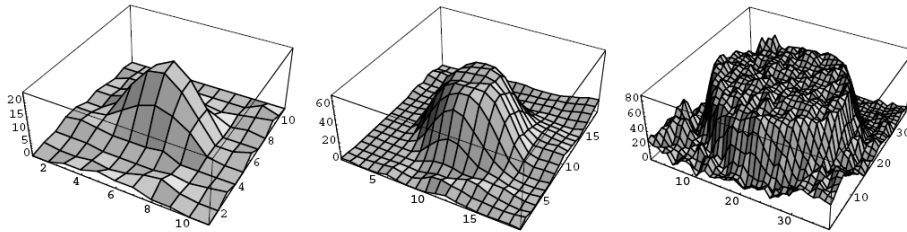
Figure 2.1: Intensity profiles of 2D slices of a thin vessel in the pelvis (left), the iliac artery of the pelvis (middle), and the aorta (right) in 3D MR images [88].

2.6 Hybrid Segmentation

A hybrid segmentation approach involves a combination of different approaches in order to take benefit of their advantages while minimizing their potential drawbacks. Bartz et al. [2] present a hybrid segmentation tech-
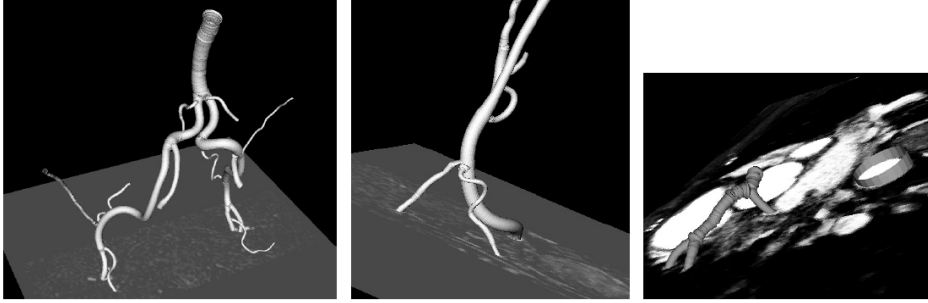
Figure 2.2: Segmentation results of applying the cylindrical model to arteries of the pelvis (left and middle) as well as to coronary arteries and the aorta (right) [88].

nique based on three main steps that are executed iteratively. The different approaches used in the respective order are: region growing, 2D wave propagation, and 2D template matching. This approach is used to segment a trachea-bronchial tree. The region growing is used as a pre-segmentation process. Then, the 2D wave propagation tries to reconstruct bronchi walls in 2D slices. In areas of small bronchi diameters, the wave propagation does not work properly. Therefore, a 2D template is defined and matched with a small window of the image, in order to correctly segment small bronchi diameters. This technique was not used for blood vessel segmentation, but should be suitable for it, because it assumes tubular shapes and different diameter dimensions.

Nain et al. [55] combine image statistics and shape information to derive a region-based active contour that segments tubular structures and penalizes leakages. Kretowski et al. [41] present a model-based approach to medical imaging analysis. The approach is aimed at understanding the influence of the physiological (related to tissue) and physical (related to image modality) processes underlying the image content. The methodology is exemplified by modeling first, the liver and its vascular network, and second, the standard CT scan acquisition process. This solution is proposed in order to avoid intersections among vessels belonging to arterial and/or venous trees, which are physiologically connected.

2.7   Discussion

All algorithms and techniques presented in this chapter have been designed, used, or are suitable for blood vessel segmentation. In general intensity-based approaches are not sufficiently powerful for being applied to PAOD patients. This is mainly because of the intensity overlap between blood vessels and bone tissues in CTA data. An additional challenge is that the partial volume effect has a high influence in areas where a bone is close to vessel tissues, making the separation between these tissues more difficult. The choice of a threshold level is quite subjective and highly depending on the data set. Using intensity-based approaches alone to deform a model for vascular segmentation often results in leakages in areas where the image information is ambiguous.

Deformable models are strongly dependent on the initialization and the data. It may be difficult to define the stopping criteria to be used during the deformation process. A trade off between freedom of deformation, performance, and accuracy of the extracted model should be defined beforehand. Interactive control may be required in the deformation process or for the re-parameterization of the model. However, a higher level of precision may involve a more time consuming process.

On the other hand, multi-scale approaches allow the enhancement of vessel structures. In the case of a CTA dataset, we may have the risk of enhancing the bones more than the vessel [17]. Furthermore, this approach is based on the properties of the Hessian matrix, which contains second derivatives. This may not work properly on a vessel with tiny diameter.

Our experimental results on synthetic and real clinical data [45] suggest that even the gradient information and derivatives are not sufficient to accurately extract the centerlines of peripheral arteries. This is due to the overlapping of density ranges between vascular and non-vascular structures, the variability in opacification between patients and from aorta to pedal vessels, image noise, and partial volume averaging.

In general all authors who presented a review or a survey of different segmentation techniques of medical images in general or blood vessels, agree that future research in the segmentation of medical images should strive towards improving the accuracy, precision, and computational speed of segmentation methods, as well as reducing the amount of manual interaction. But the most important focus should be on the design of a clinically applicable method. It is unlikely that automated segmentation will ever re-

place medical doctors, but it will likely become a crucial element of analyzing medical images. In computer integrated surgery the visualization of anatomy is a critical component [65].

CHAPTER 3

CENTERLINE APPROXIMATIONS OF BLOOD VESSELS

3.1 Introduction

The vessel centerline is widely used for 3D reconstruction and modelling of vessel structures. It has been used as a basis for several vessel segmentation techniques [39], and as starting point for a geometric model definition of vascular structures [8]. The skeletonization of a vascular structure is a

35

method widely used for centerline detection [67]. Several methods based on the skeletonization use thresholds and object connectivity [57], distance field calculation [67], and mathematical morphology based on dilation, erosion, opening and closing operators [79]. These approaches have been applied on different image modalities (e.g., MRI, CTA) and vascular structures. Many of them have been applied on a specific part of the vessel structure, for example, cerebrovascular structures [67], coronary arteries from biplane angiograms [10] or the aorta [87]. These techniques and methods have not been applied to the centerline detection of peripheral vessels, where the level of intensity decreases from top to bottom, from aorta to pedal (tibial and fibular arteries). For peripheral arteries, an accurate detection of the centerline is very difficult, specifically where the diameter can be between only two to four voxels. The partial volume effect also makes the correct identification of small vessels (e.g. tibial and fibular arteries) difficult.

In this chapter, an accuracy evaluation of six techniques for approximating the vessel centerline in peripheral arteries is presented. They are based on: ray casting using thresholds, maximum gradient-like stop criterion, pixel motion estimation between successive images called block matching, center of gravity, and shape based segmentation. The Randomized Hough Transform and ellipse fitting have been used as shape based segmentation techniques. This chapter has the following structure. Section 3.2 describes each method which has been evaluated. Section 3.3 presents the evaluation and the results. Finally, Section 3.6 presents the conclusions.

3.2 Centerline Approximation Methods

Starting from an initial path of the vessel, six different techniques to approximate the vessel centerline have been used in order to evaluate accuracy and quality. The initial path is estimated using the vessel tracking technique developed by Kanitsar et al. [36]. This technique consists of finding the path with the minimum cost. The cost is defined by a cost function which depends on a value associated to the density for vessels *vs* other tissues, the Laplacian filter, and the gradient magnitude between two adjacent voxels along the path.

The path generated by vessel tracking is, with high probability, inside the vessel structure and is taken as basis to apply the different centerline approximation methods. Along this path, a perpendicular cross-section is estimated for each point. Each center approximation technique presented in

the following sections is applied to each perpendicular cross-section (on a 2D plane). The vessel centerline is defined as a 3D curve smoothed using B-splines.

3.2.1 Ray Casting

Ray casting methods trace several rays from one point inside the object to the outside. The idea is to trace several rays $\overrightarrow{r_i}$ from one initial point inside the object until a boundary is detected (see Figure 3.1). Wink et al. [87] and Kanitsar et al. [36] use this technique to approximate the vessel centerline.

Wink et al. [87] use gradient information to detect the border of the vessel. First, they calculate the gradient via convolution of the original image with a normalized Gaussian derivative, in order to reduce noise and other irregularities in the image. Then, they define the border as the position where the gradient magnitude in the direction of the ray reaches a first maximum above some threshold. The threshold has to be significantly higher than the typical noise level in the data set. This threshold depends on the image quality (e.g., contrast, noise and resolution), and is therefore modality-dependent. On the other hand, Kanitsar et al. [36] apply the ray casting technique based on a valid density interval for vessels, and stop a ray when a density value along the ray is outside this interval. This valid interval for a vessel was defined empirically between t_{lower} and t_{upper} densities.

Two techniques based on ray casting were implemented. One is denoted as ray casting with thresholds (RCT) and the other as ray casting with maximum gradient (RCMG). RCT is the same ray casting technique as used by Kanitsar [36]. RCMG uses the maximum gradient along the ray as stopping criterion. Furthermore, the RCMG method uses also the lower threshold value t_{lower} to validate that tissues with lower density than this threshold value are not considered.

After several border points are estimated, the true center is calculated by:

$$[x_c, y_c] = \left[\frac{\sum_{i=1}^{n} x_i (d_{i-1} + d_{(i)mod(n)})}{2\sum_{i=1}^{n} d_i}, \frac{\sum_{i=1}^{n} y_i (d_{i-1} + d_{(i)mod(n)})}{2\sum_{i=1}^{n} d_i} \right] \quad (3.1)$$

Here, x_c and y_c are the coordinates of the center calculated, n is the number of border points detected, x_i and y_i are the coordinates of the *i-th* border point, and d_i is the distance between two adjacent border points x_i
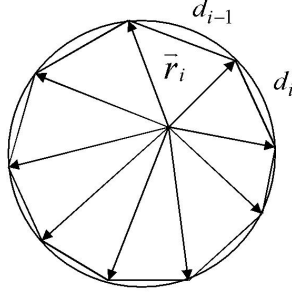
Figure 3.1: Example of the ray casting method

and x_{i+1}. The function *mod* is used due to the circular connection between successive border points.

3.2.2 Block Matching

The Block Matching (BM) technique is used for motion estimation between successive frames in video compression. More details are described in [14]. We assume that two 2D images are related by a simple shift determined by x_d and y_d. These values are estimated by minimizing the magnitude of the difference between shifted states of the two images as:

$$[x_d, y_d] = min_{x'_d, y'_d} \sum_{i,j} \left[f_{2D}(i + x'_d, j + y'_d, 1) - f_{2D}(i, j, 0) \right]^2, \qquad (3.2)$$

where x'_d and y'_d are the displacements of pixels in image space. Then, the new center would be:

$$[x_c, y_c] = [x'_c + x_d, y'_c + y_d] \qquad (3.3)$$

where x'_c and y'_c are the initial center location of the vessel cross-section.

This method is applied incrementally for pairs of successive cross-sections of the initial vessel path. It looks for the best matching between two vessel cross-sections by applying a shift on the original cross-section. The consecutive cross-section is shifted to several new positions and matched with the previous cross-section. The best match result is selected as center of the vessel in consecutive cross-sections.

3.2.3   Center Of Gravity

The weighted center of gravity (CoG) has been used widely for estimation of object centers in gray level images with sub-pixel precision [81]. The center of gravity can be defined as the equilibrium point where the entire weight of the object is concentrated. For a $2D$ gray level image the center of gravity is defined in [81] as:

$$[x_c, y_c] = \left(\frac{\sum_{x,y \in \Omega} x w(x,y)}{\sum_{x,y \in \Omega} w(x,y)}, \frac{\sum_{x,y \in \Omega} y w(x,y)}{\sum_{x,y \in \Omega} w(x,y)} \right), \tag{3.4}$$

where Ω defines the area containing pixels that belong to the vessel. $w(x,y)$ is the weight for each coordinate in the Ω space, and can be defined as:

$$w(x,y) = f_{2D}(x,y) - m \tag{3.5}$$

and,

$$m = min_{x,y \in \Omega}(f_{2D}(x,y)) \tag{3.6}$$

The function $f_{2D}(x,y)$ corresponds to the density value of a pixel (x,y) in the perpendicular 2D cross-section.

The threshold values t_{lower} and t_{upper} defined for the RCT technique, were used also in this method to determine those points which belong with high probability to the blood vessel. Considering only those pixels whose density value are between those lower and upper threshold values.

3.2.4   Ellipse Fitting

Blood vessels have a tubular structure, which can be defined by a set of elliptical shapes along its axis. Therefore, an approximation of the center-line of the vessel can be estimated as the center of an elliptical shape moved along its axis. This technique is denoted as ellipse fitting (EF). Starting from the initial path obtained via vessel tracking, the Canny edge detector [9] is applied in order to get a set of points around the vessel boundary. Then, these points are approximated with an ellipse using the Lagrange multiplier technique. The problem can be described as:

Given:

- A set of 2D Points $P = \{\mathbf{x}_i\}_{i=1}^n$, where $\mathbf{x}_i = (x_i, y_i)$

39

- A curve $C(\mathbf{a})$ characterized by the vector $\mathbf{a}$. Where $C(\mathbf{a}) = \{\mathbf{x}|F(\mathbf{a},\mathbf{x}) = 0\}$, in our case $F(\mathbf{a},\mathbf{x})$ is the representation of general conic curves which is given by:

$$
\begin{aligned}
F(\mathbf{a},\mathbf{x}_i) &= ax_i^2 + bx_iy_i + cy_i^2 + dx_i + ey_i + f \\
&= \left[x_i^2, x_iy_i, y_i^2, x_i, y_i, 1\right]\left[a,b,c,d,e,f\right]^T,
\end{aligned}
\tag{3.7}
$$

with $\mathbf{a} = [a,b,c,d,e,f]$ and $\mathbf{x}_i = [x_i^2, x_iy_i, y_i^2, x_i, y_i, 1]$

- A distance metric $\delta(C(\mathbf{a}),\mathbf{x})$ as a measure of the distance from a point $\mathbf{x}$ to the curve $C(\mathbf{a})$, which is defined by $F(\mathbf{a},\mathbf{x}_i)^2$.

The problem consists of minimizing the sum of squared algebraic distances $\sum_{i=1}^{n} F(\mathbf{a},\mathbf{x}_i)^2$ that fit an ellipse. For ellipse they must satisfy $b^2 - 4ac < 0$. After this optimization problem is solved [19], the ellipse center and axis can be extracted using Equation (3.7).

3.2.5   Randomized Hough Transform

The randomized Hough Transform (RHT) technique introduced by Xu et al. [89] consists of randomly selecting a subset of points from an image and fitting a parameterized curve to them.

First, the Canny edge detector is applied [9] in order to get a binary edge image. Then, parametric ellipses are extracted using the technique defined by MacLaughlin [50]. He describes a method to accelerate the ellipse detection in an image using the RHT. This technique consists of randomly selecting three points (P_1, P_2, P_3) from the binary edge image, and defining the ellipse that passes through these points (see Figure 3.2). For each point P_i the tangent to the curve is estimated, selecting a neighborhood around this point and finding the line of best least-squares fitting to the curve in this neighborhood. The mid point m between P_1 and P_2 is calculated, and connected with the intersection point t between the tangents of these points (see Figure 3.2(a)). The possible center of the ellipse will lie in the line defined by $\overrightarrow{tm}$. The process is repeated with the points P_2 and P_3, which define a second line. The intersection of these two lines will be the center of the ellipse.

With the center c of the detected ellipse (see Figure 3.2(b)) whose coordinates are (x_c, y_c), and the three points $P_1 = (x_1, y_1)$, $P_2 = (x_2, y_2)$, and $P_3 = (x_3, y_3)$ a possible ellipse is estimated as:

- The ellipse equation (derived from Equation (3.7)) is defined as:

$$a(x-p)^2 + 2b(x-p)(y-q) + c(y-q)^2 = 1 \qquad (3.8)$$

  With the restriction $b^2 - 4ac < 0$, where p and q are the center of the ellipse.

- Translating the center to the origin, Equation (3.8) is reduced to:

$$ax^2 + 2bxy + cy^2 = 1 \qquad (3.9)$$

- If the coordinates from P_1, P_2, and P_3 are substituted in Equation (3.9), the following equation system is derived:

$$\begin{bmatrix} x_1^2 & 2x_1y_1 & y_1^2 \\ x_2^2 & 2x_2y_2 & y_2^2 \\ x_3^2 & 2x_3y_3 & y_3^2 \end{bmatrix} \begin{bmatrix} a \\ b \\ c \end{bmatrix} = \begin{bmatrix} 1 \\ 1 \\ 1 \end{bmatrix} \qquad (3.10)$$

- Solving the equation system from (3.10) for a, b, and c gives the remaining ellipse parameters.

- Then we check the restriction $b^2 - 4ac < 0$. If it is true, the parameters represent a valid ellipse. If this restriction is not true, it means that the selected points do not lie in the same ellipse, or the tangent estimation were inaccurate. In this case, this parameters are discarded and we choose new three points randomly.

- The parameters (p, q, a, b, c) must be converted into polar coordinates (p, q, r_1, r_2, θ), where r_1 and r_2 are the radii of the major and minor axis of the ellipse respectively, and θ is the angle of rotation for the major axis. In this way the parameter of the ellipse are calculated.

Each found ellipse must be validated [50]. This process is done by drawing the ellipse into the image and looking for all the possible points that exist in the data image and are part of the border of this ellipse. For each point on the detected ellipse, a 5-D accumulator is used to aggregate the number

of valid ellipses found. Each dimension in the accumulator represents one parameter of the ellipse. After a predefined number of iterations, the cell with the maximum value in the 5-D accumulator determines the parameters for the best ellipse found in the image.
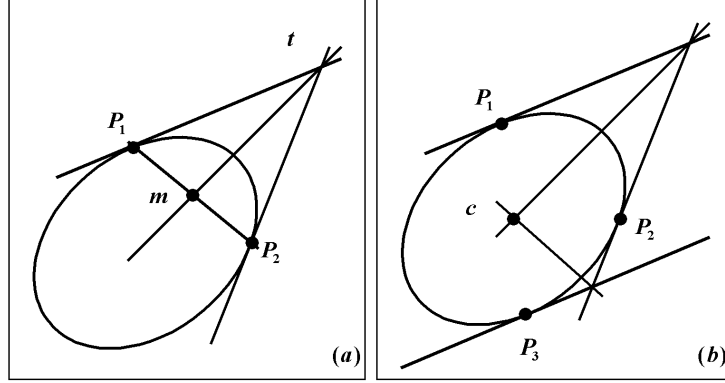
Figure 3.2: Ellipse Approximation. (a) Estimation of the line where the ellipse center should pass. (b) Estimation of the ellipse center.

3.3   Evaluation

Three different synthetic data sets have been used to evaluate the accuracy of each method described in Section 3.2. Each data set consists of 3D data of 256x256x768 voxels of 0.5^3mm, and it simulates a vessel structure of the peripheral arterial tree, from aorta to pedal. The diameter of the vessel varies along the z-axis from about 0.7 to about 23mm, from the slice 767 to the slice 0. The density for a vessel is defined between 1130 and 1350 and the background density between 1080 and 1100. The curvature of the vessel is simulated by a helix with an angle of 32.14^o and radius 76.8 voxels. Each data set includes Gaussian noise, which has been added with a σ of 0, 5 and 10 respectively. An example of the synthetic data is shown in Figure 3.3.

For the evaluation of the centerline estimation several graphs have been generated, describing the error as the distance between the center in the synthetic data, which is known, and the center estimated by the respective method. The RCT, RCMG, EF and RHT methods estimate the vessel centerline and its diameter in individual slices. The CoG and BM estimate just the vessel centerline. Therefore, two types of graphs were generated. The

Figure 3.3: Maximum Intensity Projection of the synthetic data.

first shows the distance error between the real and the estimated centerline.
The second shows graphically the difference between the real and the esti-
mated diameter of the vessel. Both graphs are plotted along the synthetic
vessel.

Method	Mean error (mm)	Comments
RCT	$\approx 1.11 \pm 0.4$	- Good center approximation along different diameters - Overestimates the diameter - Threshold dependent
RCMG	$\approx 1.82 \pm 0.9$	- Good center approximation along different diameters - Overestimates the diameter - Threshold dependent
BM	$\approx 0.99 \pm 0.63$ for vessel with diameter $< 5mm$	- Time consuming - Requires an optimization process - Better for small vessels ($< 5mm$ of diameter) than large vessels
CoG	$\approx 0.8 \pm 0.4$	- Best center approximation along different diameters
EF	$\approx 0.56 \pm 0.22$	- Edge detector dependent - Not robust enough
RHT	$\approx 5.23 \pm 6.89$	- Fails many times especially for small vessels - In general there are not enough points in a vessel cross-section (vessel diameter $< 5mm$) available to get significant results - Not robust enough - Computationally expensive

Table 3.1: Comparison of the evaluated methods.

3.4   Discussion

Table 3.1 describes concisely the result of several experiments carried out for each method. The RCT, RCMG and CoG use threshold values to consider vessel pixels. These values were determined empirically based on the density distribution analysis of vessels on CTA data done by Kanitsar et al. [36]. For the evaluation these values were varied according with the data set. The selection of a good threshold interval to identify vessel pixels results in a better approximation of the center. Figures 3.4(a, b and c) show the distance error achieved with these methods. These graphs show how CoG exhibits better results than RCT and RCMG. The BM method starts with a good center approximation for the first three or five cross-sections. The problem with this technique is that it accumulate an error for every estimation. This error is quite difficult to measure and it is accumulative. Furthermore, the distance error (shown in Figure3.4) is relative to the vessel diameter. For large vessel diameter the distance error is bigger than for small vessel diameter. Even when this behavior is general for all the others

technique, with this technique the distance error is higher.

The EF and RHT use the Canny edge detector. This detector uses two threshold values for the "hysteresis process" involved in the method, which classifies the pixels resulting from the previous Gaussian filtering, gradient information, and non-maximum suppression steps [9]. The threshold values used for the Canny edge detector were modified empirically, but were not able to achieve better results for small vessels. Peaks in Figures 3.4(e,f) show where the methods fail because of the Canny edge detector or not enough points to extract the parameters of the ellipse using the EF or the RHT techniques. The method from MacLaughlin [50] was used to extract possible candidates to ellipses from the point clouds data resulted from the Canny edge detector by the RHT. For this method, many parameters and threshold values must be handle in a precise way. This makes an accurate evaluation of this method difficult. In general, RCT, RCMG, EF and RHT overestimate the diameter of the vessels (see Figure 3.5).

Timings are giving in Table 3.2. While BM and RHT clearly have the longest execution times, RCT, RCMG, and CoG are fast and do no exhibit significant performance differences. EF is slower than the latter three methods, but still tolerable.

The main goal of this study was the accuracy evaluation of several vessel centering techniques using a synthetic data. Basically, because we can evaluate the precision of each technique, knowing in advance what should be the result. As we can see in Figures 3.4(a, b and c), and in Table 3.1, the RCT, RCMG and CoG methods showed better center approximation using synthetic data set. It would have been interesting to simulate mildly and severe pathologic forms in our simulated data, but the point was that if our centering methods does not work well on a regular simulated data (without abrupt changes), it is not expected to work better on more sophisticated simulated data. This was the main reason why we use this synthetic dataset, described before for the evaluation. As an experiment we applied these techniques using real patient data set. For this experiment we selected the anterotibial artery, which is a small vessel with a diameter between 4, and 1 mm. This patient data present some calcifications. We can observed in Figures 3.6 an example. In this Figure, the best approximation was shown by the RCMG (every rotation of the CPR images shows a good centering estimation).

3.5   Improvements

The RCT, RCMG and CoG can be improved using an adaptive threshold estimation during the centerline process. The BM requires to optimize the search process for the best matching, and could be implemented using sub-pixel precision for a best approximation. For EF and RHT it is important to use a very good edge detector or refine the threshold values used by the Canny edge detector. The RHT technique that has been used in this work requires a refining process of all parameters involved in the method, which is out of our focus.

RCT	RCMG	EF	CoG	BM	RHT
1.797	1.594	3.969	1.531	174,000	104,000

Table 3.2: Execution times in seconds for each evaluated method.

3.6   Conclusion

In this chapter an evaluation of different techniques to approximate the center of the vessel in the peripheral arterial tree was done. Synthetic data sets were used in order to evaluate the accuracy of each method. In general all methods are sensitive to noise. The CoG method exhibits less sensitivity to noise than the other techniques. The RCT, RCMG and CoG methods provide the best approximation to the center. The BM technique requires an optimization process for better results. The EF technique depends on the parameters of the Canny edge detector. The RHT technique also depends on the parameters of the Canny edge detector, and is computationally expensive.

The methods analyzed were selected as a result of an exploration of different methods used to determine elliptical shapes and detect the objects center. In this study, the RCT method is the only one used for centerline detection of vessel structures in our clinical environment. The other methods are not yet used in this area, but they were considered because of simplicity, novelty in the area, and low sensitivity to noise. The centerline estimation of the peripheral arteries is a difficult task, because of the partial volume effect, the diameter of small vessels (tibial and fibular arteries), the overlapping of density values between vessels, bones and soft tissues.

As a result of this study, the RCMG technique was quite well accepted
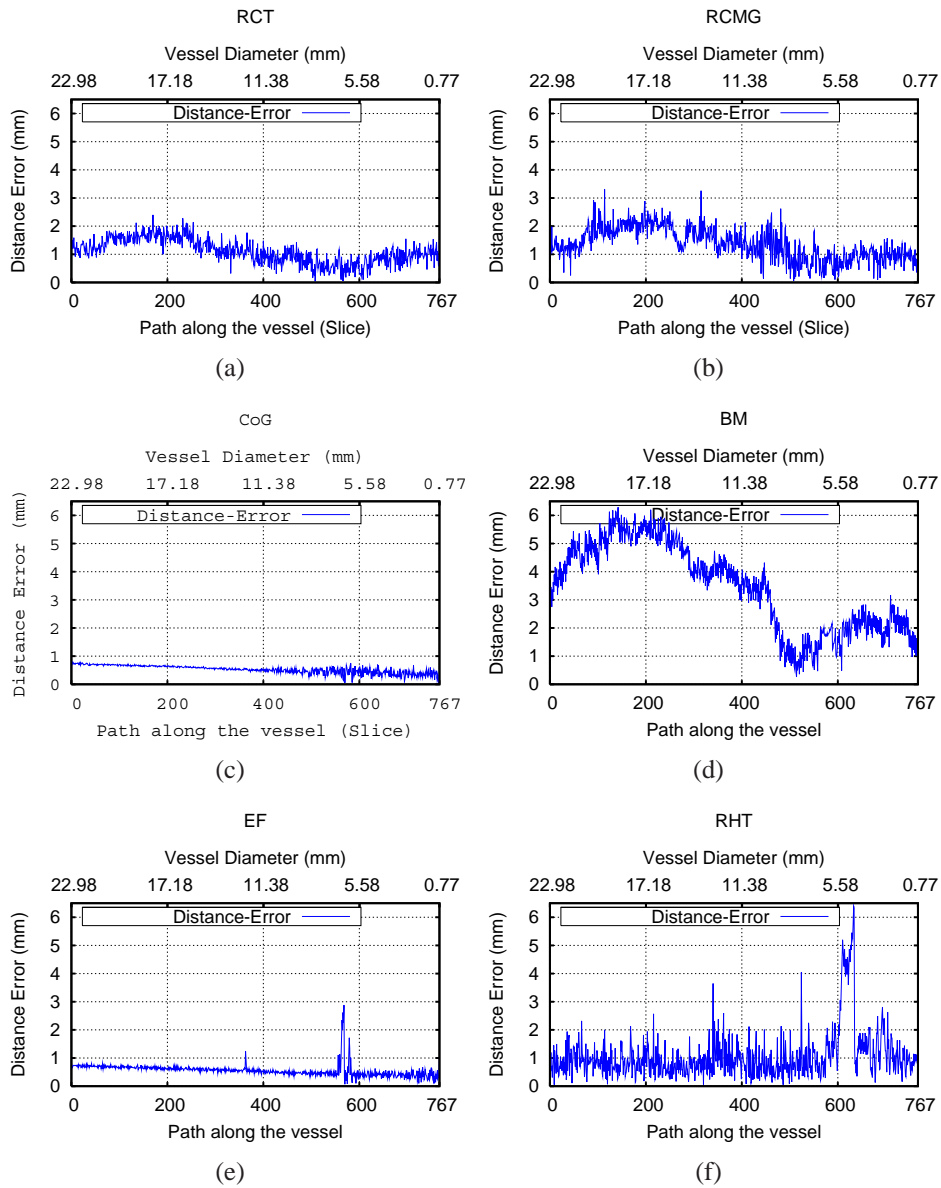
Figure 3.4: Distance error graphs of the center estimated by the (a) RCT, (b) RCMG, (c) CoG, (d) BM, (e) EF, and (f) RHT method

by radiologist from our clinical environment. Actually, they are using this method for daily diagnosis and evaluation (in the Central Hospital of Vienna) and for research (in the Medical Center of Stanford University). This
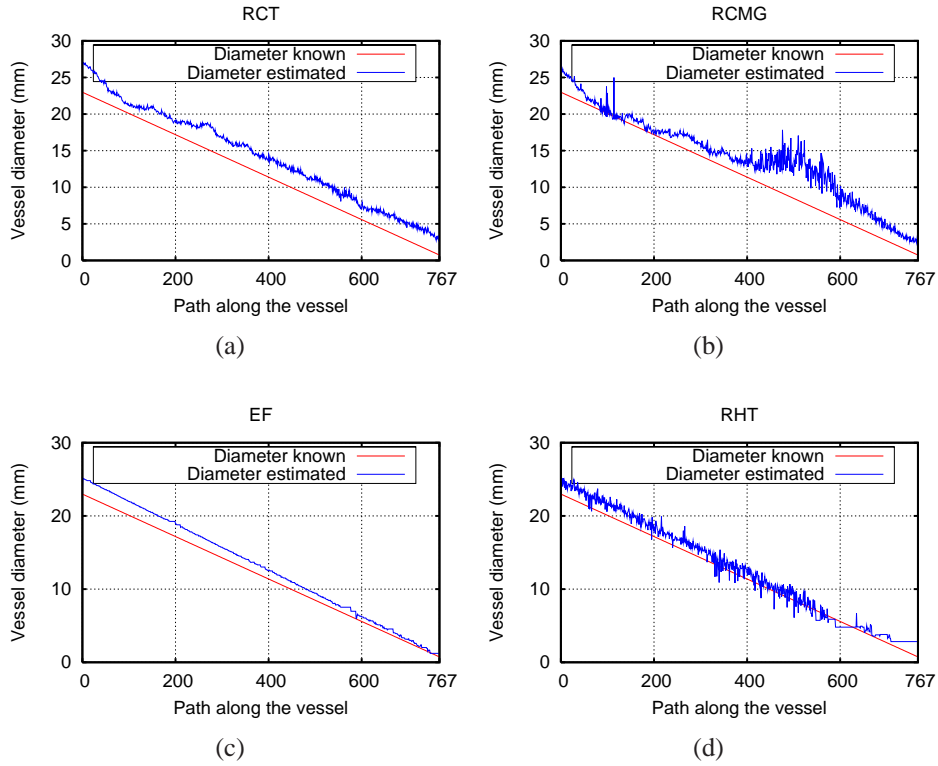
Figure 3.5: Diameter estimated by the (a) RCT, (b) RCMG, (c) EF, and (d) RHT method

method is mainly used for center approximation of the aorta and superficial femoral arteries.
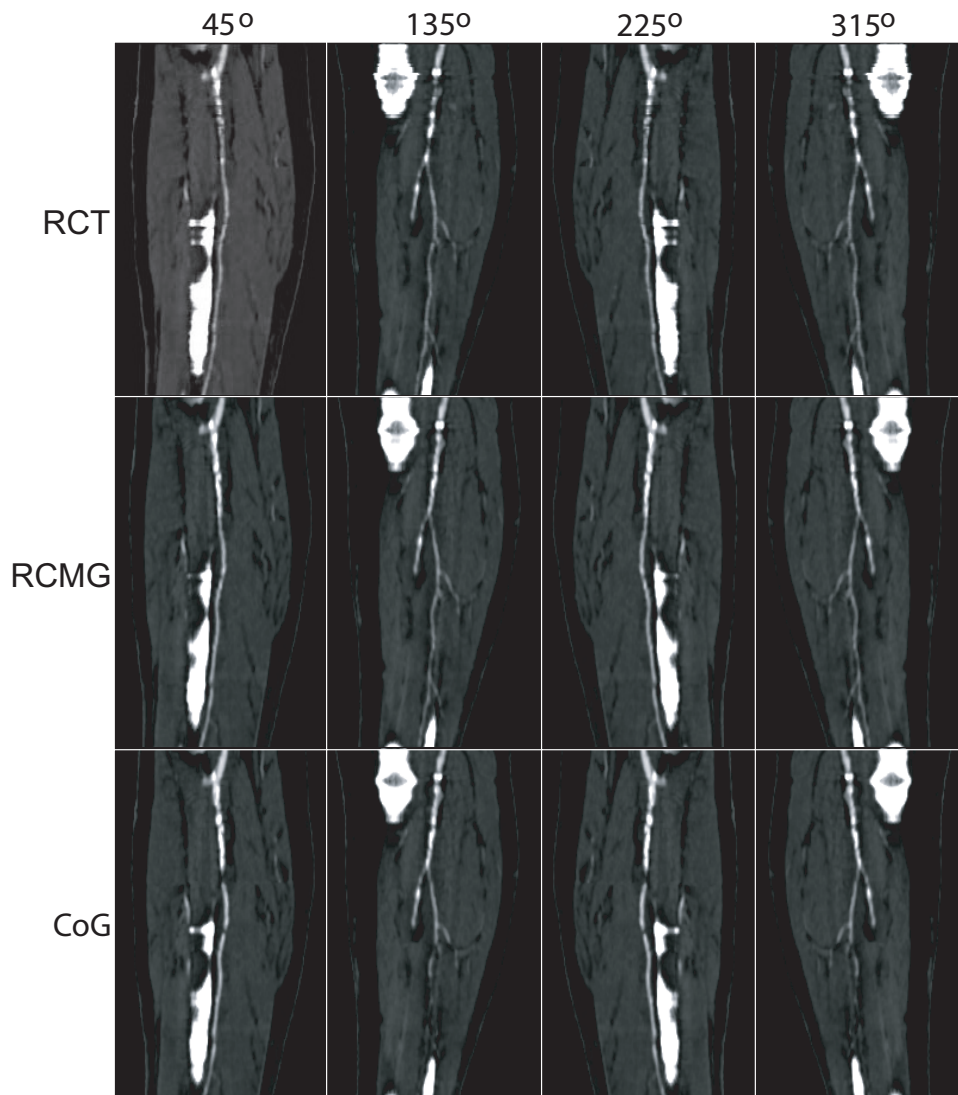
Figure 3.6: From left to right rotating CPR with 45, 135, 225 and 315 degrees. From top to bottom centerline detected with RCT, RCMG, and CoG. This data corresponds to a femoral with a diameter between 2mm and 4mm, and present calcifications and bifurcations. Brighter objects correspond to bone structures. For this data the best approximation center in different rotations of the CPR is exhibited by the RCMG method.
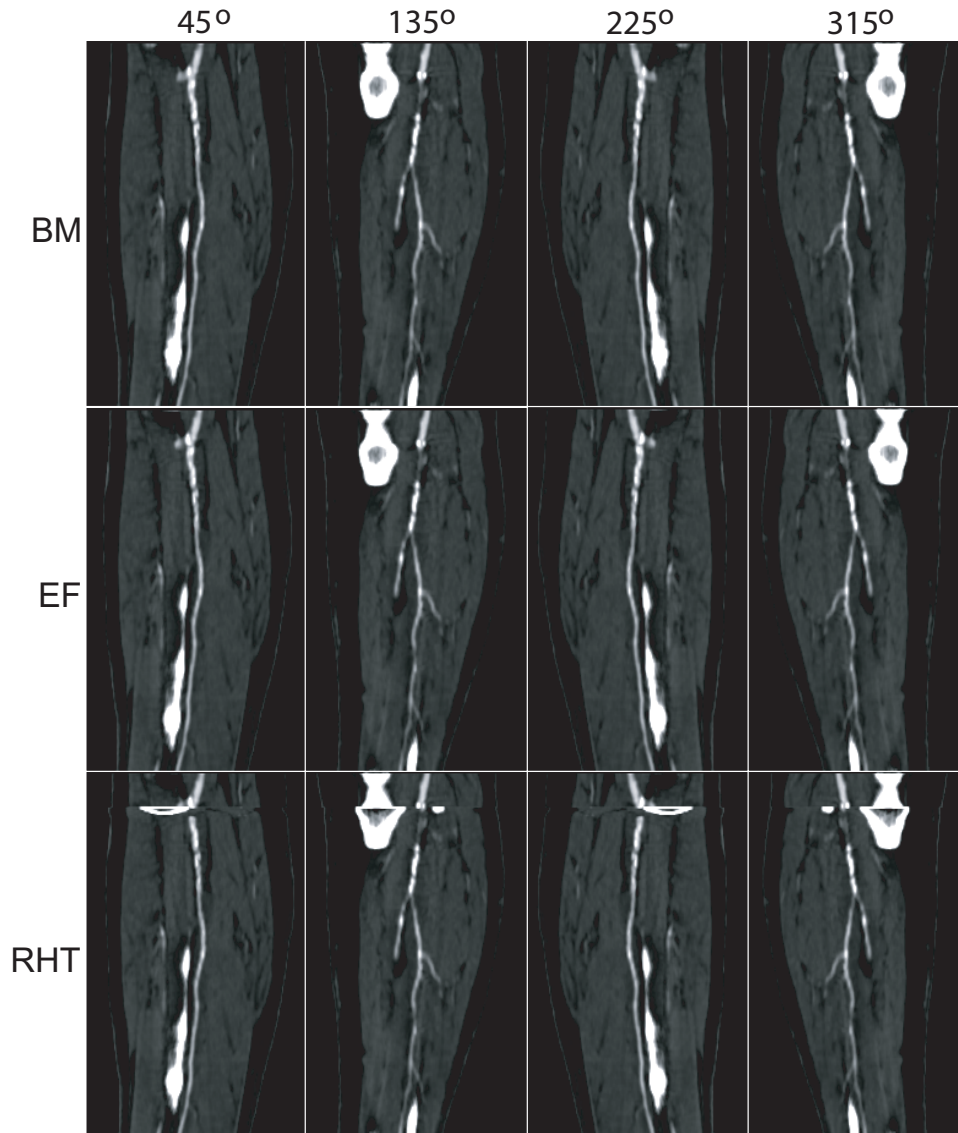
Figure 3.7: From left to right rotating CPR with 45, 135, 225 and 315 degrees. From top to bottom centerline detected with BM, EF, and RHT. This data corresponds to a femoral with a diameter between 2mm and 4mm, and present calcifications and bifurcations. Brighter objects correspond to bone structures. This is without consider bifurcations, and corresponds to the CoG method. For this sample the best result is exhibited by the EF method.

Chapter 4

Vessel Model Fitting

4.1 Introduction

The most characteristic feature of an artery (healthy or diseased) is its cylindrical or tubular shape. A cylindrical or tubular shape can be modeled as elliptical or circular cross-sections along its medial axis, and can then be fitted to a candidate vascular structure. As a result of the estimated vessel diameter and density, a more robust extraction of the vessel centerline is expected, even in the presence of atherosclerotic disease. We are particularly interested in finding a model that best fits the data concerning tubular shape and mean density value.

In this chapter, we present two new strategies to estimate vessel parameters from an initial vessel model using a non-linear minimization process. The first strategy attempts to fit an elliptical cross-section model to the ves-

sel. The second strategy uses a 3D cylindrical model of the vessel to fit it to the data. This approach was presented to the visualization community in 2004 [46], and this chapter is based mainly on this publication.

This chapter is divided into five sections. Section 4.2 describes the main motivation of this work and the importance of extracting a better parameterization of diseased blood vessels. Section 4.3 presents the non-linear model fitting technique using an elliptical cross-section (in 2D) and a cylindrical shape (in 3D). In Section 4.4 we present and discuss our results and finally, in Section 4.5 draw the conclusions of this work.

4.2   Motivation

Automatic segmentation and accurate centerline identification of diseased arteries certainly is a challenge. We are currently using a density and gradient based vessel tracking and centering technique to process clinical cases of patients with PAOD [37]. In patients with extensive disease, substantial expert user interaction and manual corrections are necessary to bridge the segments where standard segmentation fails. Figure 4.1 is an illustration of extensively diseased vessel territories where expert user interaction was required to generate images of adequate diagnostic quality. In this case, a technique capable of identifying the vessel by its cylindrical or tubular shape might have produced a similar or better result in determining the centerline. This would improve the visualization technique actually used in the clinical environment, which is mostly Curved Planar Reformation (CPR) and its extensions [37].

4.3   Non-Linear Model Fitting

In this chapter, we present two different vessel models. An elliptical model in 2D (M2D) and a cylindrical model in 3D (M3D). Each model has a set of unknown parameters, which are estimated by minimization of a χ^2-based merit function. Both methods require an initial estimation of the parameters. They can either be obtained from the initial path defined by vessel tracking, or from the previous slices, which requires only an initial seed point.

We represent the vessel by a 2D (ellipse in a slice) or 3D (cylinder) implicit model f. The CT-scanner, due to finite dimensions of its detectors, blurs the data, which leads to partial volume effects (PVE) [82]. This can be modeled by a non ideal point spread function (PSF) of the scanner, which we

Figure 4.1: MIP image (left) of a clinical peripheral CTA dataset obtained from a patient with advanced peripheral arterial disease with superimposed tree of vessel-centerlines. The encircled areas indicate vessel regions, where automated centerline calculations failed due to excessive disease and vessel calcifications, and thus required manual placement of center points by a radiologist, to achieve the resulting Curved Planar Reformation (right).

can approximate with a Gaussian G_σ. Then we model the PSF by estimating the distance to the surface (Equation 4.1) and by calculating the density (Equation 4.2):

First, a distance to the geometrical object is estimated for an implicit function by

$$dist = \frac{f}{\|\nabla f\|}, \tag{4.1}$$

where f is the implicit function of the geometrical object. The PSF from the CT-scanner can be modeled by a Gaussian with variance σ applied to the distance to the geometrical object. Finally, the mean density is computed by

$$density = b + V \bigotimes G_\sigma(dist), \tag{4.2}$$

where b is the mean density value for non-vessel tissue or background and V is the mean density value for vessels.

The *erfc* function (see Figure 4.2) is defined as the complementary error function encountered in integrating the Gaussian distribution [84]. For simplicity and in order to avoid the convolution operation, *erfc* can be used as an approximation of G_σ, since a convolution of a unit step with a Gaussian results in the *erfc* function. Therefore for the estimation of the PSF we substitute $G_\sigma(dist)$ by $erfc(dist/\sigma)$.
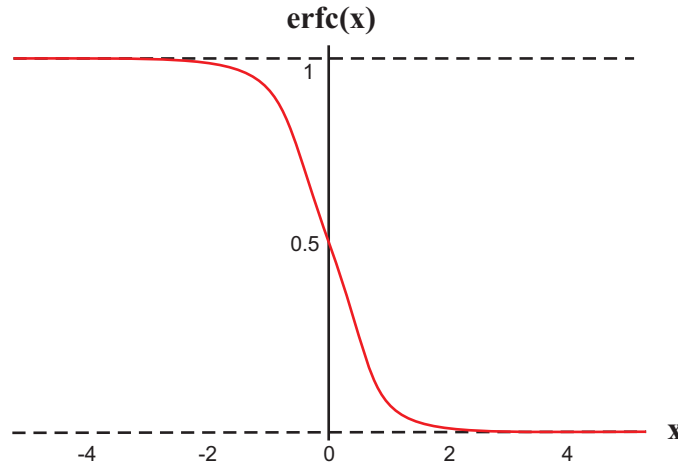
Figure 4.2: *erfc* function

4.3.1   Elliptical Cross-section Model of a Vessel

An elliptical cross-section of a vessel is modeled using the following parameters:

- Center of the ellipse, given by (x_0, y_0)

- Radius dimensions, given by (r_x, r_y)

- Rotation angle, given by α

- Gaussian filter with parameter σ to model the PSF from the CT-scanner using the *erfc* function

- Mean density value V for a vessel structure

- Mean density value b for background

For a general ellipse with a rotation parameter α, its implicit function is given by:

$$
\begin{aligned}
f(x,y) \quad = \quad & \frac{[(x - x_0)\cos(\alpha) - (y - y_0)\sin(\alpha)]^2}{r_x^2} + \\
& \frac{[(x - x_0)\sin(\alpha) + (y - y_0)\cos(\alpha)]^2}{r_y^2} - 1 \qquad (4.3)
\end{aligned}
$$

4.3.2   Cylindrical 3D Model of a Vessel

The cylindrical 3D model is created using the following parameters:

- Center of the cylinder, given by (x_0, y_0, z_0)

- Radius dimensions of the cross-section for the cylinder, given by (r_x, r_y)

- Rotation angles around the x and y axes, given by α and β

- Gaussian filter with parameter σ to model the PSF from the CT-scanner using the *erfc* function

- Mean density value V for a vessel structure

- Mean density value b for background

We assume a cylinder along the z-axis rotated with respect to the x axis by α, and with respect to the y axis by β. The cylinder is centered at (x_0, y_0, z_0) (see Figure 4.3). A general elliptic cylinder can be modeled by the implicit function as given by Equation (4.4):

$$
\begin{aligned}
f(x,y,z) \;=\; & \frac{[(x-x_0)\cos(\beta)+(y-y_0)\sin(\alpha)\sin(\beta)+(z-z_0)\cos(\alpha)\sin(\beta)]^2}{r_x^2} + \\
& \frac{[(y-y_0)\cos(\alpha)-(z-z_0)\sin(\alpha)]^2}{r_y^2} - 1 \qquad (4.4)
\end{aligned}
$$

Figure 4.4 illustrates the data generated by a cylindrical 3D model. We create a set of slices with elliptical cross-sections along the z-axis. This model is modulated by its parameters until it fits the data.

4.3.3 Levenberg-Marquardt Method

The Levenberg-Marquardt method [47, 51] is a nonlinear minimization technique. This technique can be used to fit a model to data when it depends nonlinearly on a set of M unknown parameters a_k, $k = 1, 2, ..., M$. The idea of the Levenberg-Marquardt algorithm is to minimize a merit function χ^2 and iteratively determine the best fitting parameters by minimization. The merit function measures the agreement between the model and the given data. In a fitting process, the parameters of the model are adjusted to achieve a minimum in the merit function. The process is repeated while χ^2 decreases and is stopped when a change in the parameters changes χ^2 by an amount $<< 1$, which is not considered statistically significant any more.

Let us assume that we are fitting N data points (x_i, y_i) $i = 1, ..., N$, to a model $f(x; \mathbf{a})$ that has M adjustable parameters a_k. The model predicts a functional relationship between the measured independent and dependent variables.

$$
y = f(x; \mathbf{a}) \qquad (4.5)
$$

The idea is to minimize the merit function χ^2 given by:

$$
\chi^2(\mathbf{a}) = \sum_{i=1}^{N} \left[\frac{y_i - f(x_i; \mathbf{a})}{\sigma_i} \right]^2 \qquad (4.6)
$$

(a)

(b)
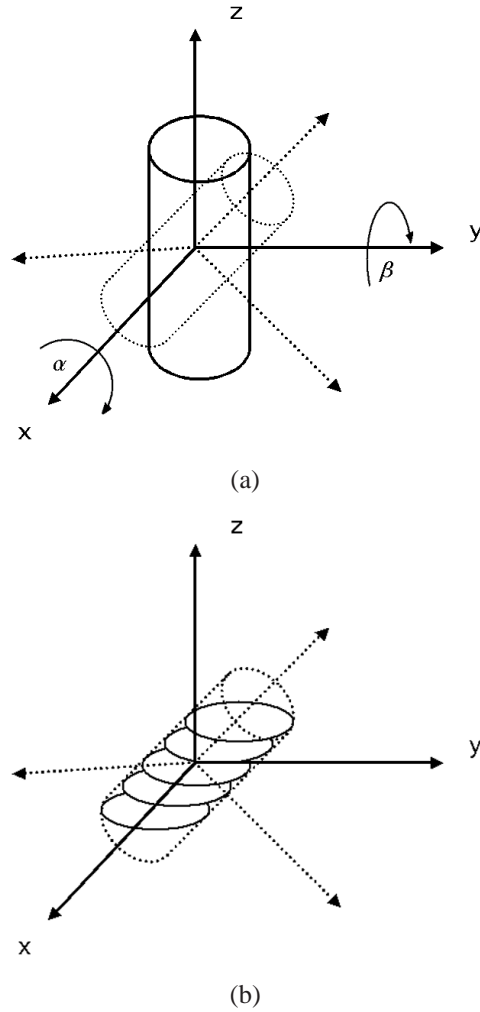
Figure 4.3: (a) Cylinder along the z-axis rotated with angles α and β around the x-axis and y-axis respectively. (b) Elliptical cross section along the z-axis of the rotated cylinder

where y_i is an n-dimensional data point, and with the same dimension $f(x_i; \mathbf{a})$ is a value from the model evaluated with parameters $\mathbf{a}$. In our case we used 2 - dimensional data for the elliptical cross-section model, and 3 - dimensional data for the cylindrical model. σ_i is the measurement error (standard deviation) of the $i - th$ data point, presumed to be known. In our case we do not know this value, and we set all of them to the constant value

57
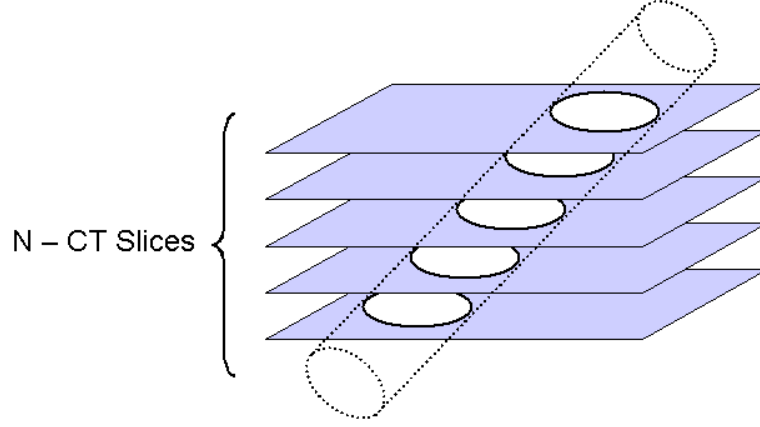
Figure 4.4: Illustrative example of a cylindrical model

$\sigma_i = 1$ as is suggested in [66].

   Given an initial estimation of parameters $\mathbf{a}$, the Levenberg-Marquardt process consists of [66]:

(1) Compute $\chi^2(\mathbf{a})$

(2) Set an initial value for λ, say $\lambda = 0.001$.

(3) Solve the linear equation $\sum_{l=1}^{M} \alpha'_{kl} \delta a_l = \beta_k$ for $\delta \mathbf{a}$ and evaluate $\chi^2(\mathbf{a} + \delta \mathbf{a})$

(4) if $\chi^2(\mathbf{a} + \delta \mathbf{a}) \geq \chi^2(\mathbf{a})$, increase λ by a factor (for simplicity, in our implementation we use a factor of 10) and go to (3)

(5) if $\chi^2(\mathbf{a} + \delta \mathbf{a}) < \chi^2(\mathbf{a})$, decrease λ by the same factor as in (4), update the trial solution $\mathbf{a}$ by $\mathbf{a} + \delta \mathbf{a}$ and go back to (3)

where

$$
\begin{aligned}
\alpha'_{ll} &\equiv \alpha_{ll}(1+\lambda) \\
\alpha'_{lk} &\equiv \alpha_{lk} \qquad (k \neq l)
\end{aligned}
\tag{4.7}
$$

and $\delta \mathbf{a}$ represents the steepest descent, and

58

$$\beta_k = -\frac{1}{2}\frac{\delta\chi^2}{\delta a_k} = \sum_{i=1}^{N} \frac{[y_i - f(x_i;\mathbf{a})]}{\sigma_i^2}\frac{\partial f(x_i;\mathbf{a})}{\partial a_k} \qquad (4.8)$$

and

$$\alpha_{kl} = \sum_{i=1}^{N} \frac{1}{\sigma_i^2}\left[\frac{\partial f(x_i;\mathbf{a})}{\partial a_i}\frac{\partial f(x_k;\mathbf{a})}{\partial a_l}\right] \qquad (4.9)$$

4.4   Results

As first result, we apply both model fitting to a synthetic data set. This should illustrate that both methods produce quite similar results concerning the curvature (see Figure 4.5).

The synthetic data set consists of 3D data of 256x256x768 voxels with size 0.5^3mm. The diameter varies along the z-axis from about 0.7 to about 23 voxels, simulating the size-range of arterial vessels imaged with CT. The vessel density is defined between 1130 and 1350 and the background density between 1080 and 1100 (which corresponds to CT attenuation values of 130 to 350, and 80 to 100 Hounsfield Units, respectively). The curvature of the vessel is simulated by a helix with an angle of 32.14 degrees and a radius of 76.8 voxels.

We apply the cylindrical model fitting to a real patient dataset in a region of interest where manual segmentation by experts is required (see Figure 4.1). Figures 4.6 and 4.7 show the results of fitting an initial model to a set of ten slices of volumetric data, starting from an initial seed point. In the Figures, the first and last columns of images correspond to the first and the last slice of a sub-volumetric region defined by a set of 10 slices (as an example). The center column of images correspond to the slice in the middle of the dataset. The upper row of images corresponds to a partially occluded or calcified vessel. The second row of images corresponds to the fitted model. Finally, the third row is a superposition of the cylinder enclosing the vessel. In Figure 4.6, we can see that there is not a clear distinction between the vessel boundary and soft tissue or vessel background. It looks like a bifurcation, but it is not. This is certainly a difficult case where any other preprocessing step using derivative estimation, gradient information or thresholds are likely to fail. However the cylindrical vessel model fits quite well to the sub-volumetric data of the vessel. Figure 4.7 shows the result on a calcified vessel. This is also a difficult case to segment. From

59
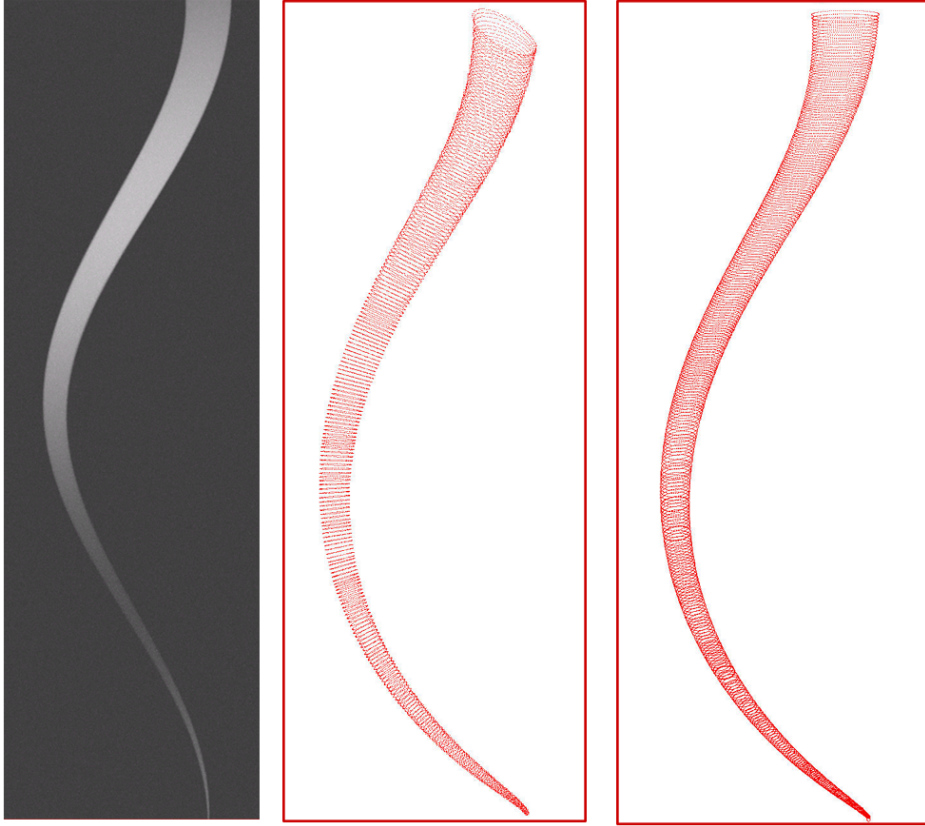
Figure 4.5: Result on synthetic data. Left, MIP image of the synthetic data, followed by elliptical cross-section model fitted along the vessel path, and finally a parameterized vessel by cylindrical model fitting

a medical point of view it is quite important to extract the entire vessel dimensions, rather than the lumen only, because it allows an estimation of the relative degree of a stenosis. In both cases (Figures 4.6 and 4.7) the density of the fitted model corresponds to the mean density of the data. This would help to combine this technique with an adaptive process to correct for inter- and intra-individual variation of the degree of vascular opacification, and to distinguish vessels from other structures, such as bone.

Finally, we present a comparison of the cylindrical model with a clinical application. It is based on the ray casting with threshold (RCT) developed by Kanitsar et al. [37] and evaluated in [45] as a good approximation of the vessel centerline. Figure 4.8 presents the center path generated
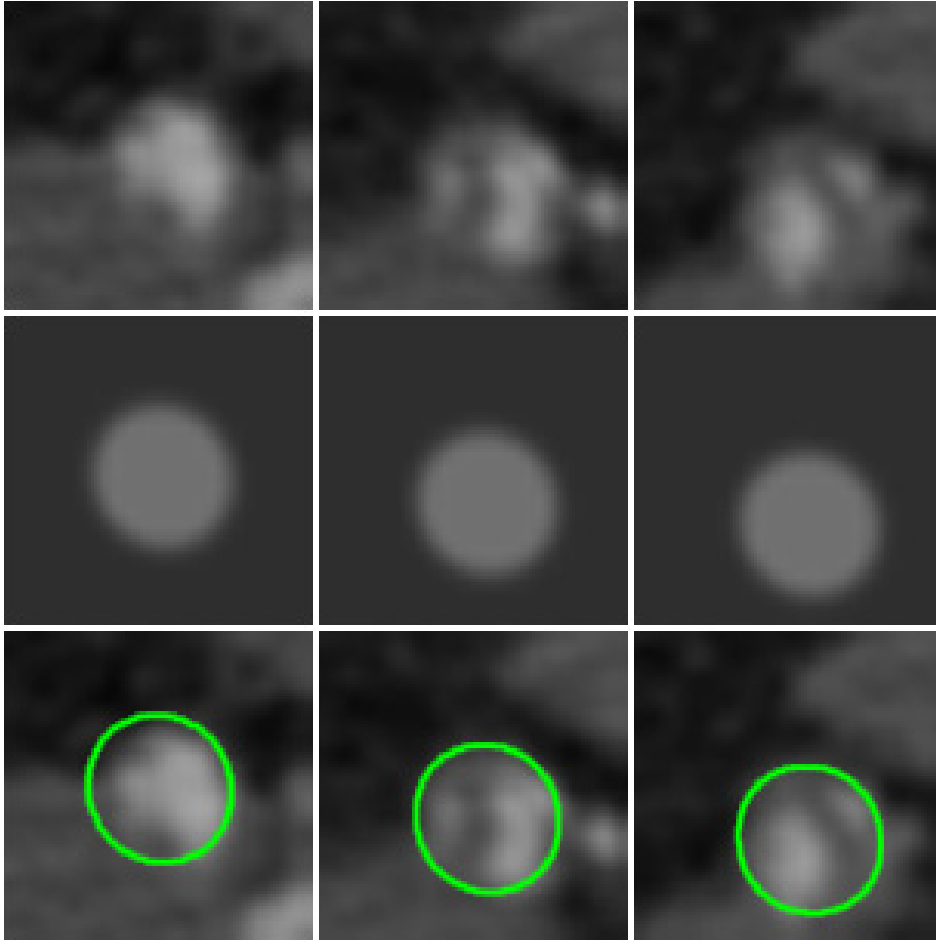
Figure 4.6: Result of fitting to a vessel with a partial occlusion

by the RCT technique (see Figure 4.8(a)) and the cylindrical model fitting (see Figure 4.8 (b)). Here, we can see how the centerline generated by the RCT technique is not actually in the center. The centerline extracted from the cylindrical model fitting looks more centered (see zoomed circular area, showed in Figures 4.9(a) and (b)).

In Figures 4.9(a) and (b)), zoomed images illustrate the improved approximation of the central path with the cylindrical model fitting technique. Note the artificial high-grade stenosis in the 45° view in Figures 4.9(a), which is caused by the eccentric course of the centerline path. Figures 4.9 (a) and (b), are particularly relevant because they show one of the limita-
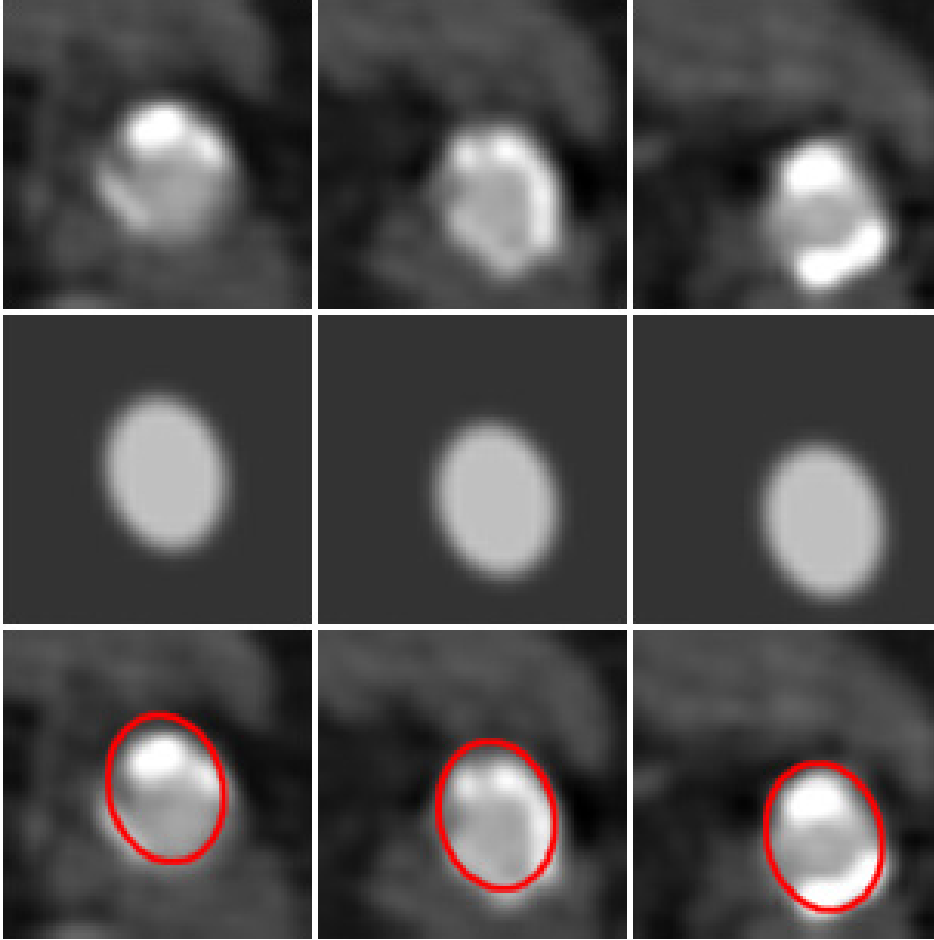
Figure 4.7: Result of fitting to a vessel with calcifications

tions of the CPR [37] visualization technique, which is its dependence on an accurate centerline estimation. An off-axis reformatting surface for the CPRs causes artificial vessel narrowing or 'pseudo-stenoses' in the resulting image (see zoomed circular window in Figure 4.9). Figure 4.9 also allows us to visually determine that the cylindrical model fitting gives a better center approximation and avoids the generation of artificial stenoses in the CPR images. The vessel segmented in Figure 4.10 is characterized by a complex pattern of densities within the diffusely diseased left femoral artery. There are pockets of residual lumen (light grey), irregular areas of non-calcified plaque (dark grey), and areas of calcified atherosclerotic plaque (white).

The centerlines and CPR images from the cylindrical model fitting are more accurate than the RCT based results, and compare favorably to those based on expert user interactions.

Concerning the performance, for a dataset of 512x512x224 voxels, the process took about 210 seconds, that means 0.9 seconds per slice. Table 4.1 summarizes the advantages and limitations using non-linear model fitting.

Advantages	Limitations
- It does not use density and any operator estimation such as gradients or derivatives. - It does not require preprocessecing steps. - It produces very good results on diseased vessels.	- Requires a definition of initial parameters close to the data. This s done only for the first slice, the following estimations are based on previous slices. - It does not work on bifurcations. - Performance (~ 0.9 sec/slice).

Table 4.1: Advantages and limitations using the non-linear vessel model fitting

4.5   Conclusion

This chapter describes a strategy to parameterize a vascular structure from a vessel model by a non-linear fitting process. The Levenberg-Marquardt method is used as a non-linear minimization process, which allows to extract optimal parameters from a model that best fits the data.

In this chapter, we present a segmentation solution for visualization and analysis purposes in cases where classical segmentation methods based on boundary detection often fail. Diseased vessels show a wide variability of density values, which is a challenge because calcifications appear as bones and partial occlusion or soft plaque appear as soft tissue. This makes it difficult to detect the vessel boundaries. The cylindrical 3D model fitting requires neither a preprocessing step nor any operator estimation, such as, gradients, derivatives, etc.

Results were evaluated just in a qualitative way instead of using also a quantitative analysis. For these reason, a clinical evaluation is required in order to present a quantitative comparison with the second best centering technique we evaluated in previous chapter. This is the concerning to the next chapter, where we present a clinical evaluation of the non-linear model

(a)

(b)
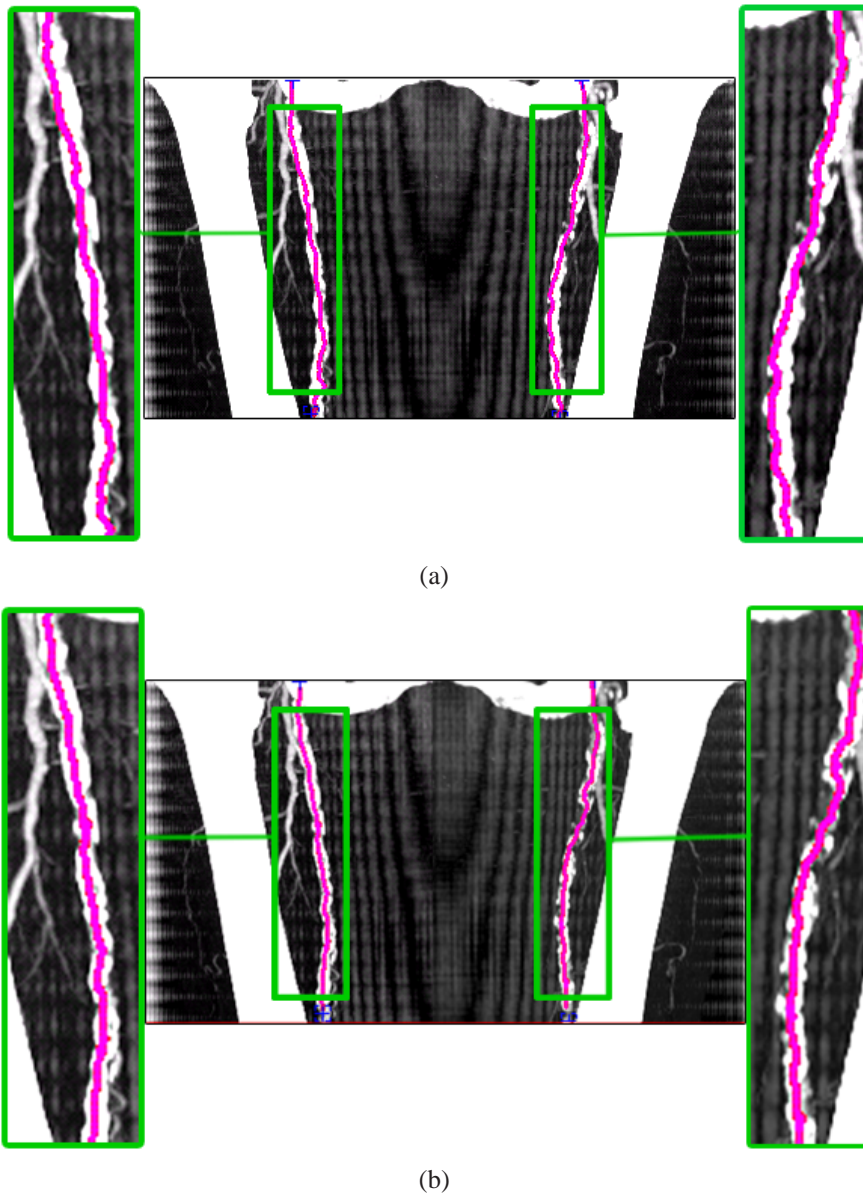
Figure 4.8: MIP images with superimposed centerline generated by (a) the RCT technique and (b) the cylindrical model fitting. Note, that patient images are shown as if viewed from the front of the patient. The right femoral artery is thus on the left side of the image.

(a)

(b)
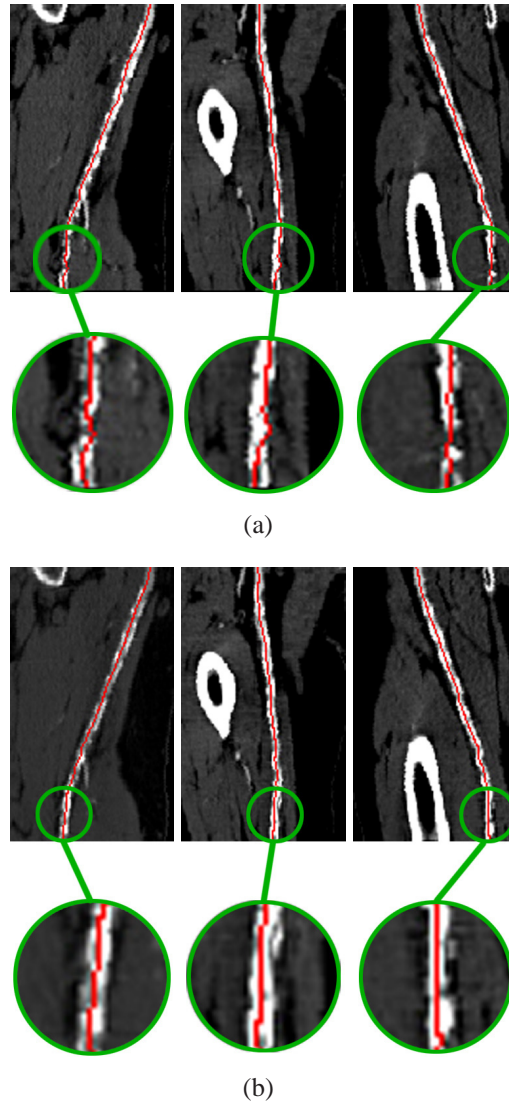
Figure 4.9: CPR images of the right femoral artery from the same dataset as Figure 4.8, viewed from three different angles (-90° [as if viewed from the right side of the patient], 0° [viewed from the front of the patient], and 45° [as if viewed from an oblique left standpoint relative to the patient]), with superimposed center-paths. Images in panel (a) were created from the RCT centerline approximation. Images in panel (b) were created with the cylindrical 3D model fitting.

fitting technique compared to a centering approximation technique actually used in a clinical environment for daily patient evaluation.

The cylindrical model fitting can be considered as initial step to implement an automatic segmentation of vascular structures. Future work should address the following issues: performance, handling of vessel bifurcations, and inclusion of further anatomical knowledge.

(a)

(b)
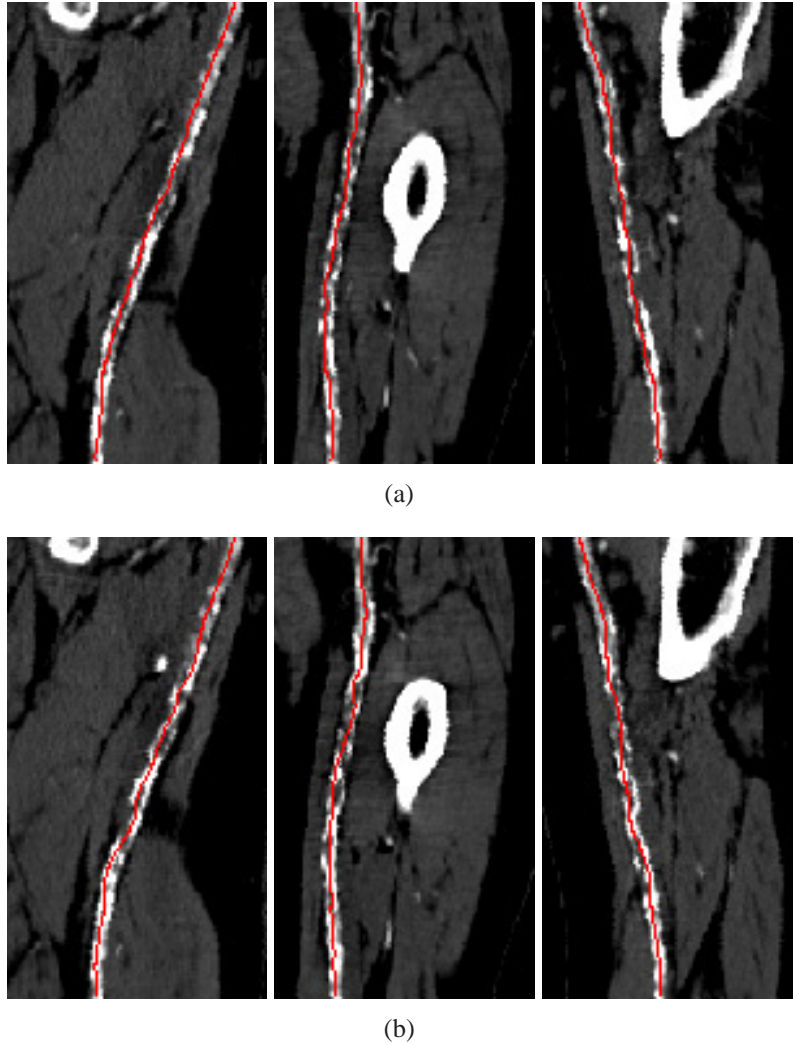
Figure 4.10: CPR images of the left femoral artery from the same dataset as Figure 4.8, viewed from three different angles (-90° [as if viewed from the right side of the patient], 0° [viewed from the front of the patient], and 45° [as if viewed from an oblique left standpoint relative to the patient]), with superimposed center-paths. Images in panel (a) were created from the RCT centerline approximation. Images in panel (b) were created with cylindrical model fitting. Note the improved course of the centerline in (b) in this example of complex attenuation of the diseased blood vessel, caused by residual lumen, hypodense (non-calcified) plaque, and hyperdense calcified plaque.

67

CHAPTER 5

CLINICAL EVALUATION OF A NON-LINEAR MODEL FITTING TECHNIQUE

5.1 Introduction

Automated and semi-automated centerline extraction techniques have been successfully employed in the past with excellent results in normal or minimally diseased vascular segments. But these semi-automatic techniques, which rely on density properties in the data, tend to fail in significantly diseased vascular segments. In these cases the density ranges differ substantially from normally perfused vessels and overlap widely with neighboring non-vascular structures such as soft tissues and bone. Newer algorithms have been investigated and seem to further increase the accuracy of centerline estimations. Among them, a frequently integrated method is the ray casting with threshold technique (RCT) [35]. The RCT technique was evaluated and compared against other centering methods (see Chapter three). This technique shows a better approximation on synthetic data sets. The RCT technique is based on threshold values and gradient estimation by tracing rays from the vessel center to the vessel border. In the previous chapter (Chapter four), we presented a new approach of an automated centerline extraction that uses a non-linear fitting process [46]. The preliminary results were very promising, but thorough evaluation needs to be executed before putting the proposed technique to clinical usage. The crucial step is therefore validation and comparison of the proposed technique for a potential clinical application. The task of a comprehensive validation is rather diffi-

cult in clinical datasets. A major obstacle is the lack of an objective gold standard. Furthermore, the situation is intricate because of anatomical variability of diseased vessels, the presence of image noise, motion artifacts, metallic implants (i.e. intravascular stents) and possible poor opacification in "real life" data sets. The accuracy of a segmentation algorithm is most commonly evaluated by comparison with a manual segmentation, as there is no true gold standard. Ideally, all methods should be evaluated for performance on data from a realistic phantoms or cadaver studies, but this is not practical given the wide spectrum clinical disease manifestations.

Thus, the expert manual segmentation is compared with the output of the centering method. The main purpose of the study presented in this Chapter, is to present an evaluation of three automatic centerline extraction techniques compared to manually derived centerlines from three expert operators in order to evaluate each algorithm for precision and robustness in real peripheral CT-angiography datasets. One of these techniques is actually used in daily clinical routine, which is the ray casting with threshold technique (RCT). This technique is described in detail in Chapter three. The other two techniques are based on non-linear model fitting, already presented in the previous chapter (Chapter four). They are: the elliptical model in 2D (M2D) and the cylindrical model in 3D (M3D). We are interesting in a comparison of these non-linear techniques using clinical datasets. First, in Section 5.2, we describe the methodology used for the evaluation. In Section 5.3 we explain how the distances between centerlines are estimated. In Section 5.5 we present results and finally in Sections 5.6 the conclusions for this chapter are presented.

5.2 Materials and Methods

5.2.1 Vessel Segments

Twenty CT angiography data sets of the lower extremities were identified by an expert. Ten of these datasets focused on the iliac vessels and ten on the femoro-popliteal arterial segments. Figure 5.1 shows an example dataset of peripheral vasculature and the anatomical area of the iliac and femoro-popliteal segments, respectively. Datasets within every group of data (femoro-popliteal and iliac), they were categorized into five 'mildly diseased' and five 'severely diseased' segments per group, respectively. Thus a total of five 'minimal diseased' and five 'severely diseased' iliac arter-
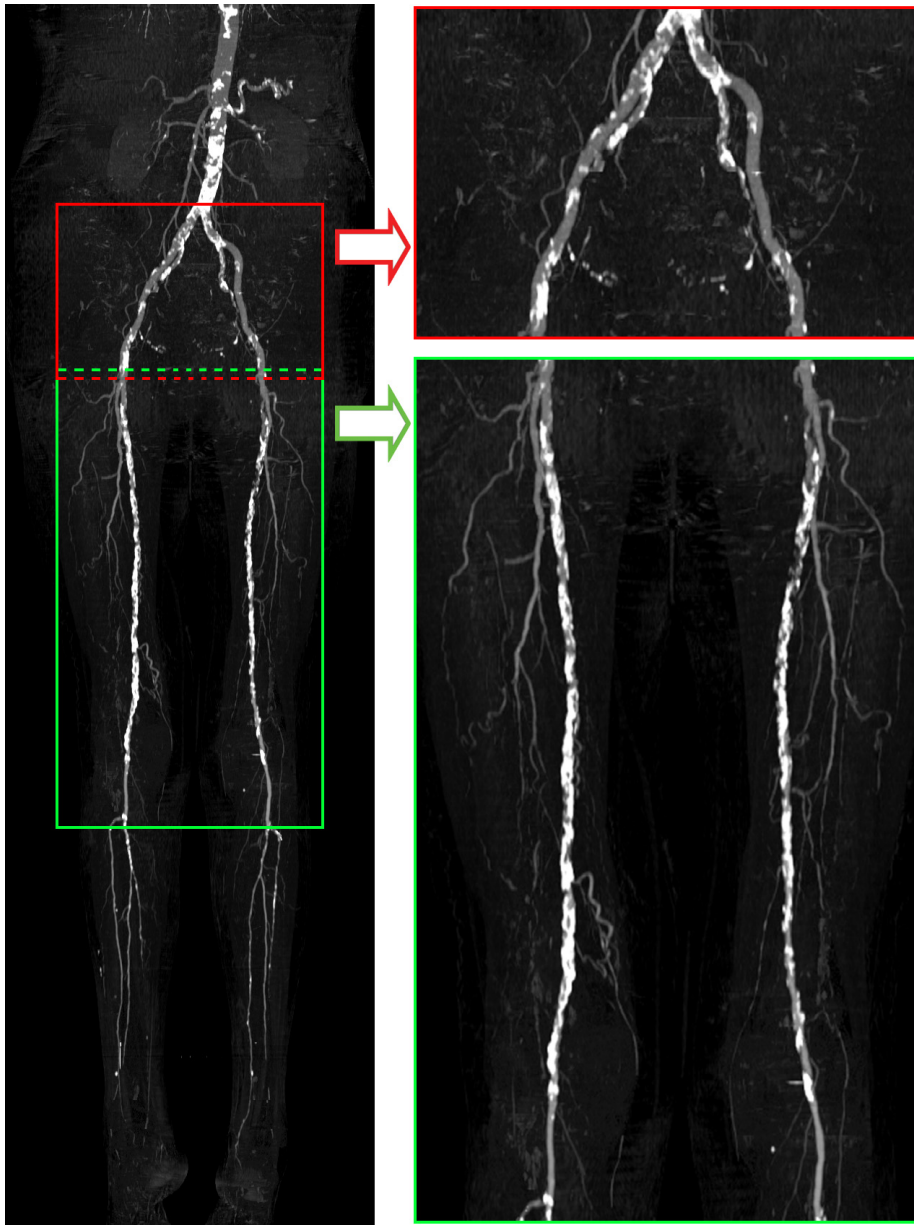
Figure 5.1: Maximum intensity projection image of a full patient data (left). The bone was removed manually for better vessel visualization. These images show the two arterial segments we are using in this work for evaluation, the iliac (top-right) and femoro-popliteal (bottom-right) arteries.

ial segments as well as five 'minimal diseased' and five 'severely diseased' femoro-popliteal arterial segments were examined. Bifurcations were not considered, in this analysis.

5.2.2   Reference Standard Centerlines

Manually Defined Centerlines

In order to gain a subjective standard of reference regarding the course of the centerlines, three experts (two radiologists and one radiological technologist all experienced in CTA of the lower extremities and its post processing) manually defined centerlines in the preselected vascular segments. This process was carried out on the same workstation on which later the automated centerline extraction was performed. This workstation simultaneously displays transverse images, Maximum Intensity Projection (MIP) as well as CPR's. To extract a manual centerline, the experts manually placed a series of connected points on transverse images in the center of the vessel of interest. The distance between the points along the course of the vessel was chosen by each expert individually, in order to get the best path in the center of the vessels according to each expert's subjective appreciation. The experts were free to choose the window center/level settings as well as the magnification of the transverse image. After placing every point, the experts controlled the produced path on the simultaneously displayed CPR image (see Figure 5.2(a),(b), and (c)) and corrected the points if they were not satisfied with the result. Thus, every manual segmentation corresponds with a 3D centerline considered, by every specialist, sufficiently precise for diagnosis.

To achieve information regarding the variability within each observer (intra-operator variability) and the variability between observers (inter-operator variability), every manual identification was done twice by all operators for all vascular segments. A time interval of 8 weeks was chosen between each reading to reduce a possible recall bias.

Analysis of Manual Centerlines

The manual centerline is a meaningful reference standard in the absence of a true gold standard. Furthermore, the quantitative comparison of manual centerlines from different experts provides information on acceptable range

71
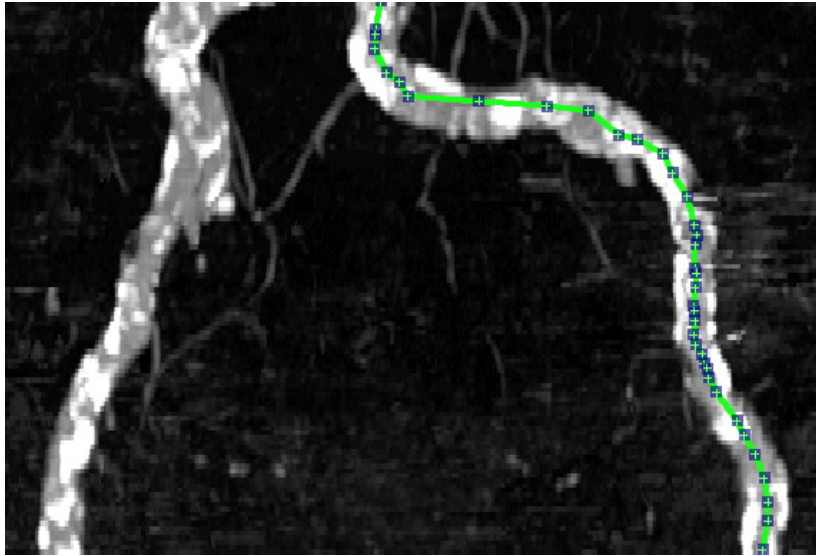
(a)
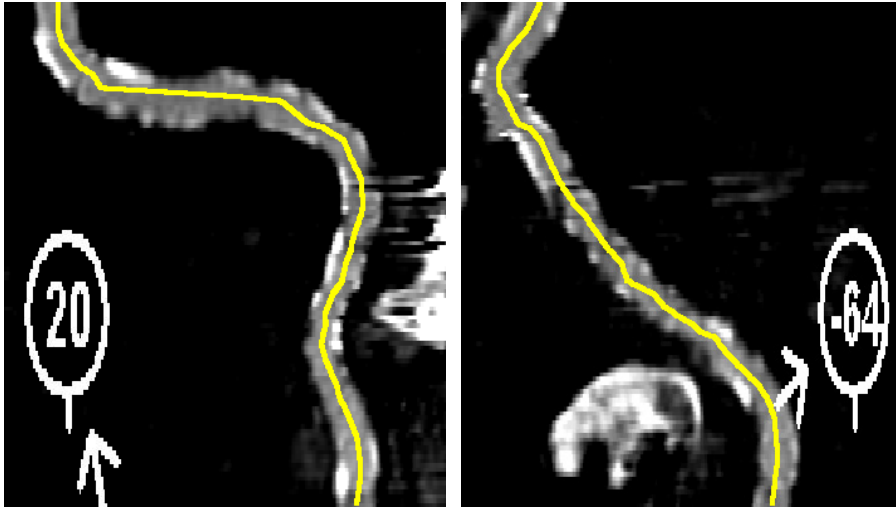
(b)   (c)

Figure 5.2: Example of a manual centerline (a) and its corresponding CPR image for validation. As an example, CPR views with 20° (a) and -64° (b) of rotation [viewed from the front of the patient] are shown. The user can rotate the CPR view and visualize any angle of rotation.

72

of precision that is desired (as a goal) for every automatic centering technique.

The acceptable range of precision is estimated by analyzing the intra-operator and inter-operator variability. The analysis was done as follows: the centering paths from the operators were compared to each other in order to evaluate the inter-operator and intra-operator variability. The way how we compared these centerlines is described in details in Section 5.3. The evaluation is carried out by comparing distances between manual centerlines. The result is used as a reference of an acceptable range of precision for analyzing how far the centerlines are estimated by the automated methods from the reference standard, which is the manual centering.

5.2.3 Automated Centerline Extraction

We used three centerline techniques already described in Chapters three and four. The first is the ray casting with threshold technique (RCT), which was evaluated against five others techniques (see Chapter three), and resulted as one of the most accurate technique. However, our experience has shown that this technique is not optimal enough and requires, in diseased datasets, a difficult tuning process, which makes it a tedious work for radiologists and technologists. The second and third technique are the non-linear model fitting with two modalities, two-dimensional (M2D) and three-dimensional modality (M3D) (see Chapter four for details).

Evaluation of the automatically extracted centerlines

To evaluate the quality of automatically extracted centerlines, they need to be compared to the reference standard. The comparison process first needs to find correspondences between identified center-points and then measure differences (see Section 5.3). As a result, we get information about the mean and the maximum difference between the reference standard and the automatically extracted centerlines. This process is executed for all three automatic techniques (RCT, M2D, M3D) and mutual comparison is provided to get insight on the quality of the individual techniques.

5.3   Distance Error Estimation Measures

The comparison was done evaluating the distances between two centerlines, acquired by automatic techniques (estimated centerlines), and the manual centerlines (reference centerlines) as follows:

- **Definition of common arterial segment.** In this study, for the same patient we have more than one centerline extracted. Due to some freedom while manually identifying the centerlines, from different centerlines there are arterial segment regions, which do not correspond with the same arterial segment length (the beginning or end of the arterial segment) of another centerline. In order to avoid the effect of the exact start and end point, we compare arterial segments that correspond to a common arterial segment extension for every centerline (reference and estimated centerlines). Thereby, we manually extract common arterial segment extensions, which are those arterial segment whose centerline are in the region defined by the first common slice and the last common slice for the same arterial segment (see Figure 5.3).
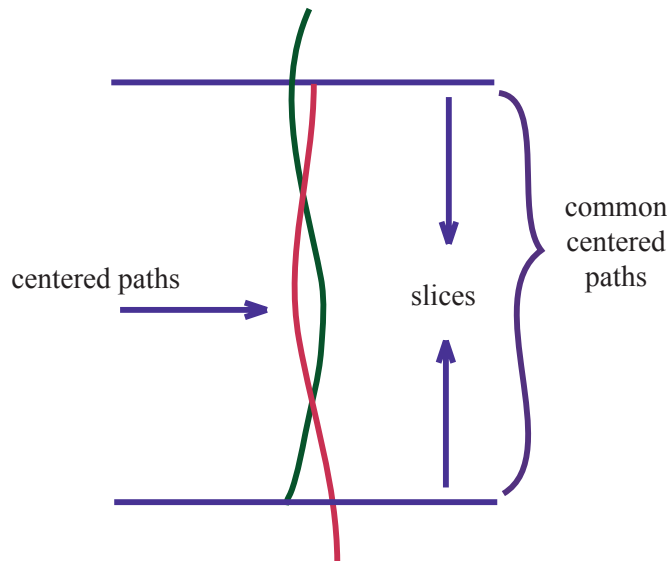
Figure 5.3: Example that illustrates a common segment part extraction for two centered paths.

- **Finding an optimal match between centerlines.** The estimated centerline and reference centerline need to correspond to the same arterial

segment. For the error measurement process it is important to find the correspondence between points on centerlines to be compared. First, every centerline (estimated or reference centerline) is resampled to an equidistant set of points. Then, for quantifying the distance between two centerlines we use the Dynamic Time Warp technique (DTW), as described Rabiner et al. in [69], which is a sequence alignment method that allows to find an optimal match between two given curves that overall have a similar shape (see Figure 5.4). The DTW can efficiently find a sequence alignment between two curves that allows a better distance measure to be calculated. This method is very well known in the area of signal processing and it is used to evaluate differences between two signals along time. This DTW technique was also used to clinically evaluate a path centering technique for virtual colonoscopy [80].

- **Dynamic Time Warping.** The DTW method consist on: Given two series Q and C, of length n and m respectively, where: $Q = q1, q2, , qi, , qn$ and $C = c1, c2, , cj, , cm$. To align two sequences using DTW we construct an n-by-m matrix where the (i^{th}, j^{th}) element of the matrix contains the distance $d(q_i, c_j)$ between the two points q_i and c_j (With Euclidean distance, $d(q_i, c_j) = (q_i - c_j)^2$). Each matrix element (i, j) corresponds to the alignment between the points q_i and c_j. This is illustrated in Figure 5.4. A warping path, is a contiguous set of matrix elements that defines a mapping between Q and C. The warping path is typically subject to several constraints, the main idea is to define a path with minimum cost from one corner of the matrix to the other corner. The corner points correspond with the starting and ending points of each series. The cost function is based on an accumulated distance along the warping path (see Figure 5.4(c)), details in [69]. In case of identical curves, the warping path would be exactly the diagonal of the distance matrix and the accumulated cost (along the warping path) would be equal to zero.

- **Euclidean distance estimation between corresponding points.** Once we have sequentially aligned the centerlines, the Euclidean distances between corresponding points (q_i, c_j) are calculated, which is the element (i^{th}, j^{th}) of the distance matrix between centerlines.
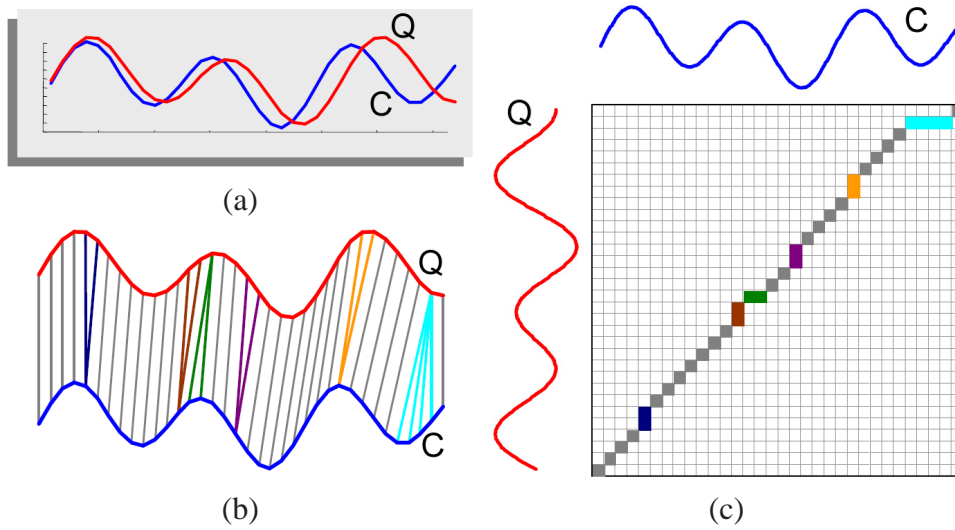
Figure 5.4: The DTW technique, in (a) two curves for comparison, (c) the warping path, and (b) the optimal sequence aligned between these curves [38].

5.4 Statistical Analysis used for Evaluation

The intra-operator and inter-operator evaluation of distances between manual centerlines was based on a Student t-test analysis. We use the t-test as a statistical tool to assess whether the mean error distance of different groups (see Table 5.1) are statistically different from each other. The evaluation of different centering techniques was done by using the analysis of variance (ANOVA). We use ANOVA, in order to compare significant differences between three groups, which are the error distances from each centering technique (M2D, M3D, and RCT) compared with our reference standard. A p-value of less than 0.05, was considered a statistically significant difference. A p-value less than 0.001 was considered a highly significant difference.

5.5 Evaluation Results

In the following sections, we present the evaluation results of the operator variability and the comparative analysis from every method. The main reason for doing the variability evaluation between operators is the lack of a true gold standard. Furthermore the comparison of different operators pro-

vides information of the required level of precision.

5.5.1   Evaluation of Operator Variability

Quantitative Analysis

We have four sets of vessel segments, two sets of femoro-popliteal artery, and two sets of the iliac artery, categorized by 'mildly diseased' and 'severely diseased' groups, respectively. We have two kinds of measurements for every group. They are the distance error variability within each operator (intra-operator) and the distance error variability between operators (inter-operator).

The result (see Table 5.1) shows a significant difference ($p = 0.01$) between intra- and inter-operator variability. The intra-operator error distance (1.0 mm) was significantly smaller ($p < 0.05$) than inter-operator error distance (1.2 mm), which is not surprising. Then, we considered it is important to evaluate independent groups separately. The intra-operator and inter-operator measurements were ordered into separated groups (iliac and femoro-popliteal segments), in order to evaluate the variability separately on different arterial segments, and in both cases we found:

- A significant difference ($p < 0.05$) between femoro-popliteal and iliac arterial segment groups. The operator error distance for femoro-popliteal segments was significantly smaller (0.9 mm and 1.0 mm) than iliac segments (1.2 mm and 1.4 mm), corresponding with the intra- and inter-operator variability, respectively.

- No significant difference were identified between 'mildly diseased' and 'severely diseased' cases for expert operators.

Considering theses findings and evaluating the mean values from each group, we conclude that the variability is more significant if we consider the artery segment (femoro-popliteal and iliac) than the state of the patient ('mildly diseased' and 'severely diseased'). For this reason we also made a separate analysis of separated groups of the femoro-popliteal and the iliac cases, and we found:

- For the femoral cases: It was observed a very high significant difference ($p < 0.001$) between 'mildly diseased' (0.8 mm) and 'severely

Groups	Mean Error Distance (mm)	Maximum Error Distance (mm)	t-Test (p value)
Operator variability			
Intra- *vs* Inter-operator	$1,047$ *vs* $1,195$	$2,318$ *vs* $2,737$	0.014
Intra-operator			
Femoro-popliteal *vs* Iliac	$0,942$ *vs* $1,152$	$1,529$ *vs* $2,318$	0.041
'Middle Diseased' *vs* 'Severe Diseased'	$1,027$ *vs* $1,067$	$2,318$ *vs* $1,889$	0.706
Inter-operator			
Femoro-popliteal *vs* Iliac	$0,984$ *vs* $1,405$	$1,702$ *vs* $2,737$	$0.71x10^{-13}$
'Mildly Diseased' *vs* 'Severe Diseased'	$1,145$ *vs* $1,244$	$2,401$ *vs* $2,737$	0.092
Femoro-popliteal			
'Mildly Diseased' *vs* 'Severely Diseased'	$0,812$ *vs* $1,140$	$1,430$ *vs* $1,702$	$0.26x10^{-12}$
Intra- *vs* Inter-operator	$0,942$ *vs* $0,984$	$1,529$ *vs* $1,702$	0.493
Iliac			
'Mildly Diseased' *vs* 'Severely Diseased'	$1,431$ *vs* $1,277$	$2,401$ *vs* $2,737$	0.053
Intra- *vs* Inter-operator	$1,152$ *vs* $1,405$	$2,318$ *vs* $2,737$	0.010

Table 5.1:   Intra- and inter-operator variability shows significant differences between groups of patients with a probability *p* from the Student t-test analysis. The mean and maximum of the distances are also compared in this table.

diseased' (1.1 mm) cases. No significant difference between intra- and inter-operator variability was found.

- For the iliac cases: No significant difference ($p = 0.05$) was observed between 'mildly diseased'(1.4 mm) and 'severely diseased' (1.3 mm) cases. The inter-operator variability (1.4 mm) was significantly larger ($p < 0.05$) than the intra-operator variability (1.2 mm). We assume that in these cases the operators could be more 'tolerant' or 'forgiving', may be due to the diameter of the vessels (between 12 mm and 10 mm), and the CPR's images obtained from the segmentation were

for them enough clear for diagnosis.

Qualitative Analysis

We could observe that the wide variability between operators is mainly due to the grade of disease and the curvature of the arterial segment. Figure 5.5 shows an example of intra-operator variability (see Figure 5.5(a)) and inter-operator variability (see Figure 5.5(b)) for a 'severely diseased' iliac arterial segment. These plots correspond to the data set in Figure 5.6. Overall two peaks are observed (see Figure 5.5(b)). These peaks correspond to the arterial segment in Figure 5.6, image 1, which has a high curvature. Figure 5.6 shows a case of variability inter-operator we found in this study, below is the graph corresponding to the plotting of distance error between three readings for this case.

5.5.2 Evaluation of Automatic Methods

Due to the operator variability, we consider the average path of all operators as our reference standard for the evaluation. The average path was defined as the center of gravity of 6 points from all 6 readings (three experts, twice readings each one) defined in every cross-section perpendicular to the vessel path. We compared every centerline from the methods (RCT, M2D, and M3D) with the average path and we extracted the distances error between them.

Quantitative Analysis

Primarily, we evaluate the mean and maximum distance between two centerlines (average path from manual editing and automated centered path from methods). In these cases, we did not find significant differences between methods. Even when in most of the cases, the M3D method produced better approximations; the statistical analysis shows no significant difference between them.

We analyze the distance error along the vessel patient per patient, in order to see significant difference per patient. The result is summarized in Table 5.2.3. Only three cases presented no significant difference between methods, which represent 15% of the cases. In 5% of the cases a significant difference between methods was detected, and in 80% of the cases a very

79

(a)

(b)
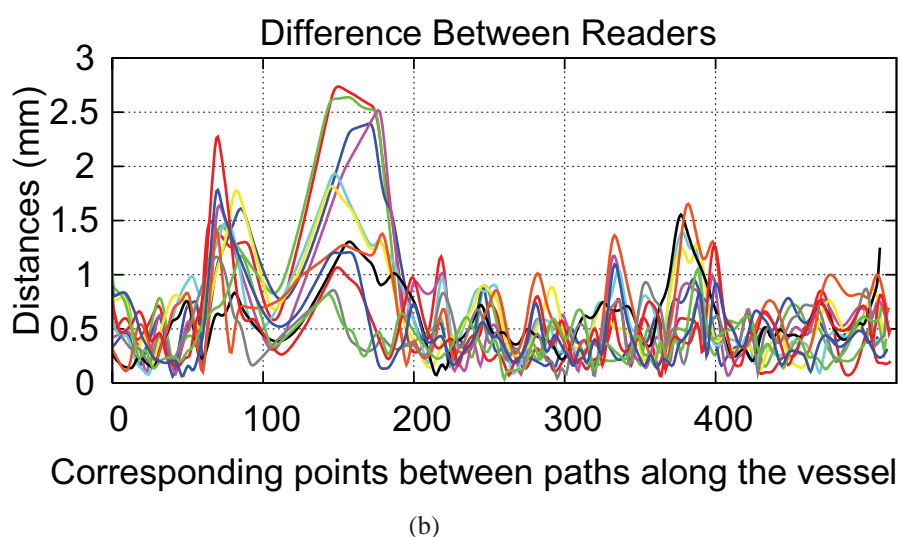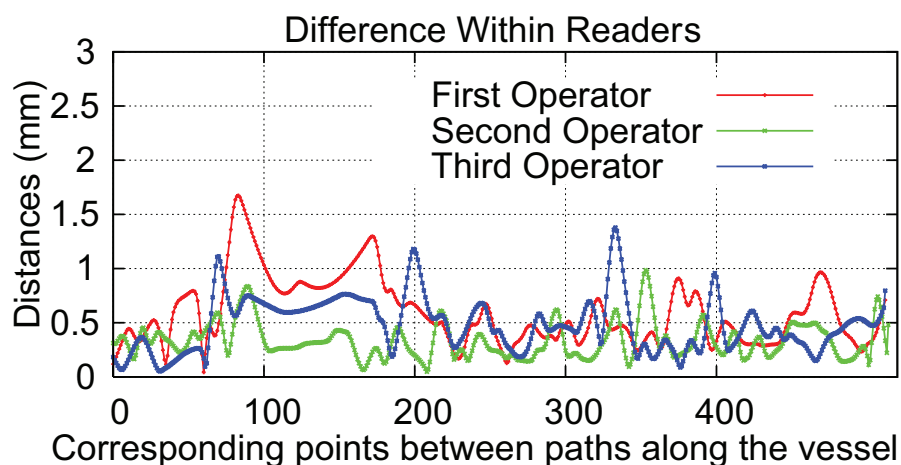
Figure 5.5: Intra-operator (a) and inter-operator (b) variability. These plots correspond to an iliac arterial segment of a 'severely diseased' case. In (b) we can only appreciate the variability inter-operator, which is quite wide. 12 combinations of distance error graphs between operators (3 operators, every one made two manual editing of centerlines) are plotted in (b).

highly significant difference between methods was detected. Thus, 85% of the cases showed a significant and important difference between methods.
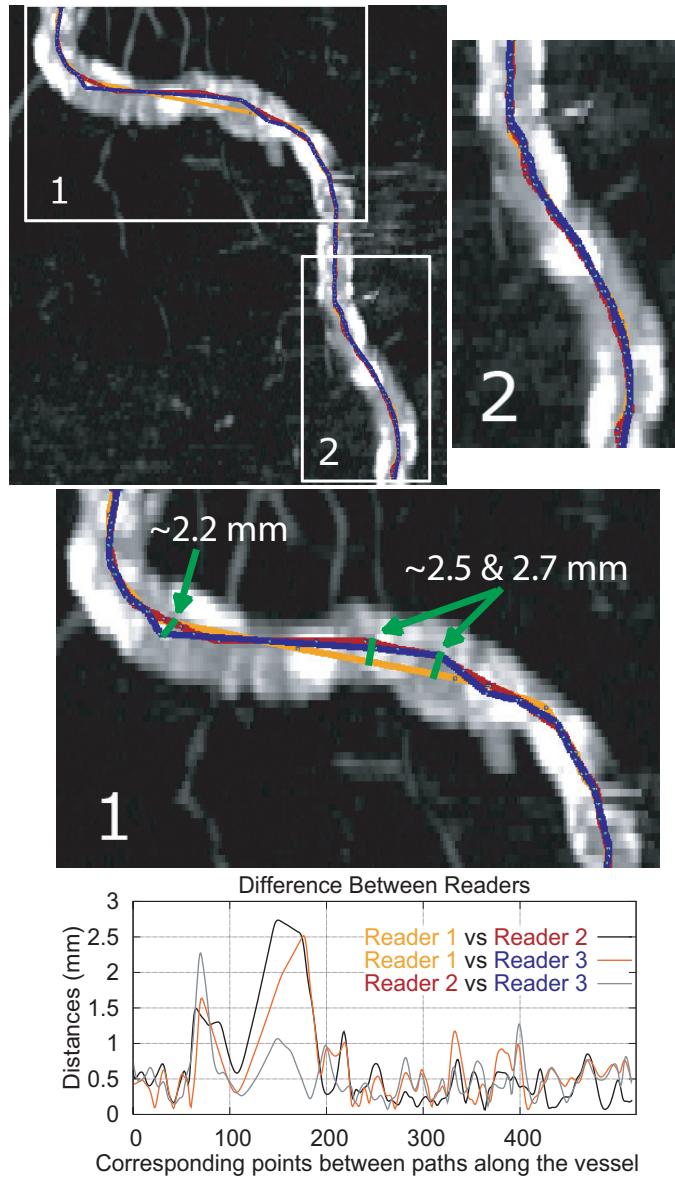
Figure 5.6: A case of inter-operator variability. Three manual centerlines are drawn [with different colors (orange, red and blue)]. Every centerline corresponds to a manual segmentation from a different operator. The plot shows the variability between them. Two remarkable peaks correspond to the area pointed it out in image 1.

From these 85%, 58.82% showed a better approximation using the M3D method, and the remaining using the RCT and M2D. Considering only diseased cases, which are the cases we are more interested, 50% of the cases presented better results with the non-linear model fitting (M2D and M3D) technique, 20% with the RCT method and the other 30% did not show a significant difference between methods.

	Mean & Maximum Error Distance (mm)			
Patient	RCT	M2D	M3D	ANOVA (p value)
Femoro-popliteal				
'Mildly Diseased'				
Pat 1	0.27 & 0.68	0.31 & 1.20	0.23 & 0.56	$p < 0.001$
Pat 2	0.20 & 0.47	0.26 & 0.51	0.21 & 0.52	$p < 0.001$
Pat 3	0.39 & 0.84	0.52 & 1.12	0.23 & 0.58	$p < 0.001$
Pat 4	0.43 & 3.08	0.40 & 1.15	0.33 & 0.89	$p < 0.001$
Pat 5	0.38 & 1.15	0.36 & 1.08	0.31 & 0.81	$p < 0.001$
Femoro-popliteal				
'Severely Diseased'				
Pat 6	0.44 & 1.49	0.47 & 1.34	0.48 & 1.51	$p < 0.001$
Pat 7	0.56 & 2.14	0.58 & 1.97	0.50 & 1.59	$p < 0.001$
Pat 8	0.32 & 1.20	0.31 & 0.99	0.30 & 0.86	$p = 0.0579$
Pat 9	0.42 & 1.09	0.76 & 3.84	0.38 & 1.20	$p < 0.001$
Pat 10	0.39 & 1.67	0.42 & 1.94	0.41 & 1.96	$p = 0.0503$
Iliac				
'Mildly Diseased'				
Pat 1	0.43 & 1.12	0.48 & 0.98	0.60 & 1.14	$p < 0.001$
Pat 2	0.41 & 0.88	0.59 & 1.12	0.41 & 0.68	$p < 0.001$
Pat 3	0.49 & 1.00	0.56 & 1.04	0.45 & 1.03	$p < 0.001$
Pat 4	0.31 & 0.62	0.35 & 0.68	0.38 & 0.73	$p < 0.001$
Pat 5	0.47 & 0.94	0.59 & 0.97	0.27 & 0.93	$p < 0.001$
Iliac				
'Severely Diseased'				
Pat 6	0.72 & 2.08	0.75 & 2.05	0.68 & 1.62	$p = 0.477$
Pat 7	0.77 & 2.17	0.73 & 2.18	0.64 & 1.64	$p = 0.013$
Pat 8	0.89 & 2.91	0.52 & 1.36	0.70 & 1.16	$p < 0.001$
Pat 9	0.30 & 0.52	0.31 & 0.60	0.36 & 0.50	$p < 0.001$
Pat 10	0.74 & 1.85	0.92 & 2.31	0.71 & 1.40	$p < 0.001$

Table 5.2: Table of significant difference between groups M2D, M3D and RCT per patient. Mean and maximum distance error between centerlines estimated by the automated methods (RCT, M2D, and M3D) and the average path of six readings.

Percentage (%) of cases within operator variability

Groups	RCT	M2F	M3F
In General (All)	60	60	70
Femoro-popliteal 'Mildly Diseased'	100	100	100
Femoro-popliteal 'Severely Diseased'	80	100	100
Iliac 'Mildly Diseased'	20	20	40
Iliac 'Severely Diseased'	40	20	40

Table 5.3: This table shows the percentage of cases whose mean and maximum distance error from every method is within the inter-operator variability.

Considering the mean from the intra- and inter-operator variability, we analyze the mean and maximum distance error per patient from different methods (see Table 5.3). In general, the mean distance error from every method was always within the inter-operator variability in 100% of the cases. The maximum distance errors of the centerlines derived by using the M3D, the M2D, and the RCT techniques were within the inter-operator variability in 70%, 60%, and 60% of cases, respectively. Separated by groups, we found that the M3F has the higher percentage of cases within the inter-operator variability, as it is shown in the Table 5.3.

Qualitative Analysis

We denoted 'mildly disease' cases as patients 1, 2, 3, 4, and 5, and 'severely disease' cases as patients 6, 7, 8, 9 and 10. We plot the maximum distance between the average path from the operators and the centered path from each method. From Figures 5.7(a) and 5.7(b), which correspond to the 'mildly diseased' cases of femoro-popliteal and iliac segments respectively. We observed that there is not a big difference between the maximum distance error from centerlines extracted automatically and the average path (< 1 mm), except for one case (patient 4 from Figure 5.7(a)), where the RCT technique showed a higher difference. In this case, the data contains poor opacification, which required a difficult tuning process of the parameter setting for the RCT technique. As we mention in Section 5.2.3, the RCT technique
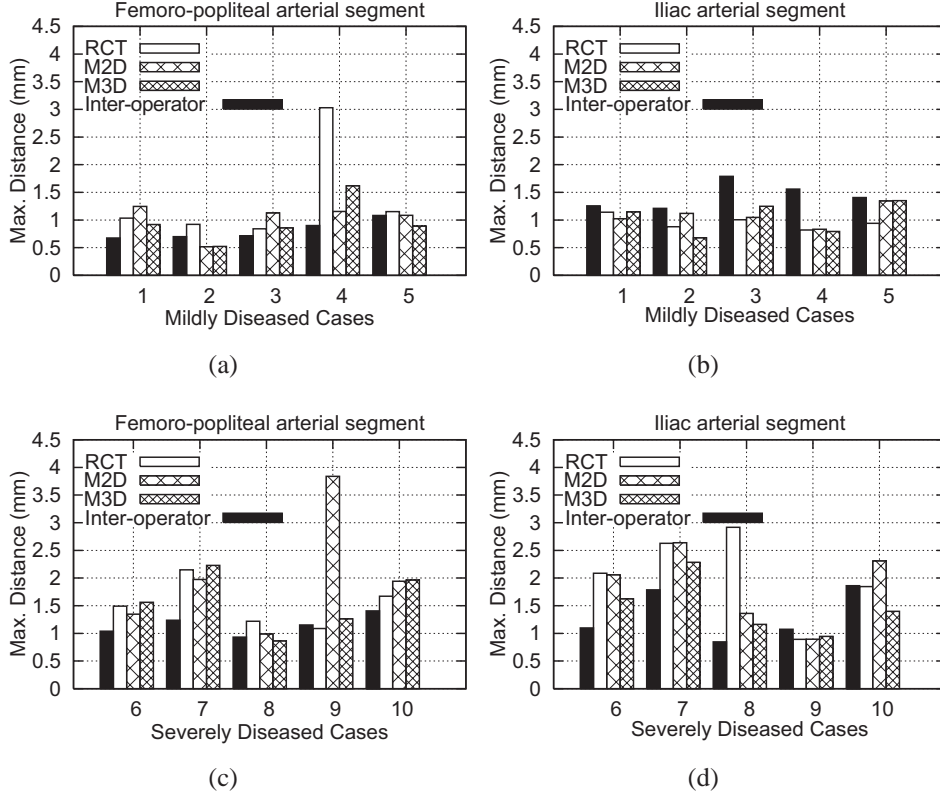
Figure 5.7: Comparison between automatic methods vs average path of manual segmentations from three expert operators. The data set corresponds with the femoro-popliteal artery segment of 'mildly diseased' (a) and 'severely diseased' (c) cases, as well as the iliac artery segment of 'mildly diseased' (b) and 'severely diseased' (d) cases, respectively. The mean distance between operator (inter-operator) for every patient was plotted as a reference (black boxes).

is based on threshold values, while the model fitting automatically adapts its initial parameters after each fitting process from the previous centering estimation. Our experience has shown that on peripheral arteries, enhanced vessels present a wide variability of its attenuation value and its diameter, from the aorta to the feet. Therefore, we cannot expect that the same threshold parameter assigned to the RCT technique works in the whole vasculature. This is one of the advantages of the model fitting technique, as we can see in Figure 5.8. In this data set, a tuning process of the RCT parameters

would improve the result, but what we want to show here is an example of a case where shows that the model fitting technique did not require any tuning process at all.

Normally, the femoro-popliteal artery is given as a rather straight shape; it does not exhibit higher curvature along the vessel, which make centerline estimation 'easy'. The M2D method produced a wrong estimation of a centerline in one of the 'severely diseased' cases (patient 9 from Figure 5.7(c)). The reason is that the M2D tries to fit an ellipse. In the case of a calcified vessel, the M2D will approximate the calcified part than the vessel itself, which is the case of patient 9 from Figure 5.7(c). On 'severely diseased' iliac arterial segments (see Figure 5.7(d)), the M3D shows always a better approximation to the center than the other techniques. Even when only the 40% of the cases of this group ('severely diseased' iliac arterial segments), the maximum distance error were under the inter-operator variability (see Table 5.3), overall, the M3D method presented a better center estimation than the others, considering, of course, the maximum distance error with respect to the average path from all readings.

5.6 Conclusion

Results show that the M3D technique is more robust than the M2D and RCT methods. However, the performance of the M3D method is the major disadvantage of this method. The model fitting technique is more intuitive than the RCT method. The RCT method requires an expert user that can set the initial parameters on complicated datasets (e.g., opacified data). The model fitting technique, in this sense, is more intuitive, as it only requires setting the initial radius of the segment. The other parameters are set automatically.

The model fitting technique is computationally slower. This makes the RCT method more attractive, which requires just some minutes for the centering estimation. However, our experience tells us that the RCT method does not work optimally on severely diseased cases as well as in some minimally diseased cases, as it is described in the previous section.

In this chapter, the results of a clinical validation of centering paths from manual specification and three automatic techniques are presented. Our main goal was to clinically evaluate a centering method recently presented to the medical visualization community [46]. Often, segmentations or vessel centering techniques present results on 'easy' datasets, which do not show the real strength or limitations of a new method. We consider this an impor-
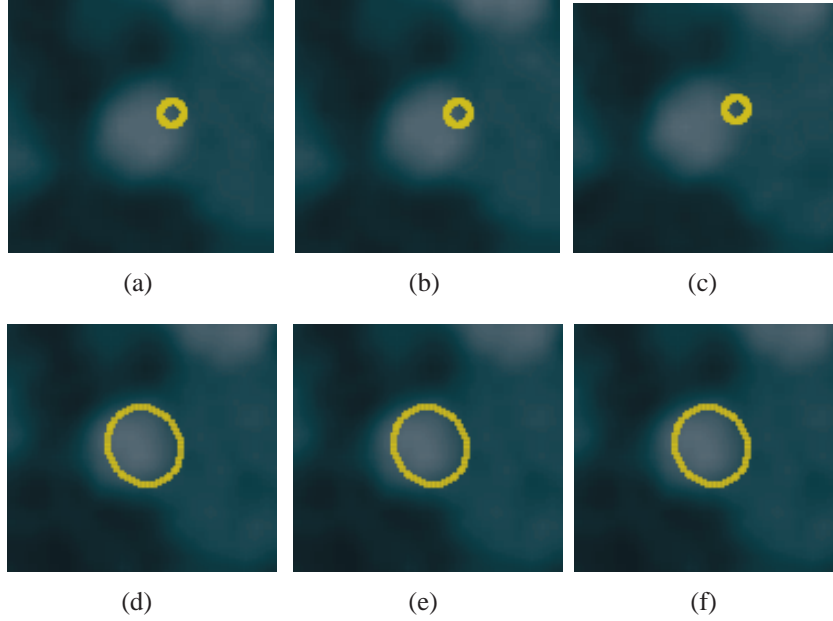
Figure 5.8: Comparison of the M3D method vs the RCT method. Images were captured for three consecutive cross-sections. (a) (b), (c) show a result produced by the RCT method, and (d), (e), (f) show a result produced by the M3D method. Figures (a), (b), (c), (d) are produced by a wrong estimation of initial parameters.

tant task to perform a clinical evaluation before implementing the method in clinical environments.

For this evaluation one practical difficulty was to find a good reference standard centerline, which can be used to measure the accuracy of different methods. As an alternative to a true gold standard we used the intra-operator and inter-operator variability, which allowed us to make an evaluation of this variability and identify the reason for this. We found two reasons why such variability intra-, inter-operator is present, which are the vessel curvature and the extent of the diseased vessel. Therefore, we use as our reference standard the resulting path from averaging all 6 readings, in every patient.

In general, the mean distance error for every method was within the inter-operator variability. However, the M3D method shows always a better center approximation in most of the cases, 'mildly diseased' as well as 'severely diseased' cases. Clinically, the M3D is more robust and presented a better estimation in most of the cases. Nevertheless, the radiologists and

clinical experts have the last word with respect to the use of this technique in clinical environment. Overall, the model fitting technique presented better results, but also require of the improvement of performance. The idea of using a model based segmentation on this kind of vessels, with higher variability of appearance, due to the diameter, opacification and level of diseased, is the most suitable way to determine the centerline along the vessel.

CHAPTER 6

SUMMARY AND CONCLUSIONS

An accuracy estimation of the centerline for blood vessels is a pre-requisite for different visualization techniques. This thesis is divided in three parts:

The first part is addressed to improve a current centerline segmentation used for daily clinical evaluation and diagnosis of peripheral arterial occlusive diseases. The ray casting technique (RCT) is investigated, which is the standard semi-automatic method actually used in a clinical environment in the central hospital of Vienna. The RCT technique is based on threshold values defined to identify the vessel boundary once a vessel tracking process has approximated a vessel path. This technique has several limitations to detect the boundary of diseased blood vessels. This is due to the high variability that diseased blood vessels may show concerning the density distribution of non-calcified and calcified plaques, and concerning the diameter from aorta to pedal arteries. Some improvements to the RCT were implemented that allowed to deal with calcified vessels whose location is far away from bones. They use the maximum gradient information along rays defined by the RCT method to detect the vessel boundary. However, on vessels with partial occlusion (non-calcified plaque) this method has some difficulties to properly identify the centerline.

We implemented and investigated different centering techniques. All of them were evaluated using a phantom simulating the density and diameter of peripheral arteries. Because the center of the vessel in the synthetic data is known an accuracy evaluation of different centering techniques could be done. These centering techniques are: the RCT, the improved RCT using a maximum gradient like stop criterion (RCMG), pixel motion estimation between successive images called block matching (BM), center of gravity (CoG), the Randomized Hough Transform (RHT), and ellipse fitting (EF).

The last two techniques have been used as shape based segmentation techniques. Results show that the RCT and RCMG were the most accurate methods.

In the second part we implemented a new parameterization technique for diseased blood vessels, which takes 3D spatial information into account for a best parameterization. This technique is based on a non-linear optimization process, which estimates the center, diameter, and mean density values for blood vessel and surrounding area or background. The method requires an initial estimation of a cylindrical (in 3D) or elliptical model (in 2D). A non-linear optimization process is used to find the 2D or the 3D model that best fits the data (M2D and M3D, respectively). This technique can be used as a semi-automatic or automatic technique; hence it does not require an initial estimation of a vessel path. The Levenberg-Marquardt method was used as a non-linear minimization process, which allows extracting optimal parameters from a model that best fits the data.

In the third part we proceeded with the clinical evaluation of our method. Results showed that the cylindrical model fitting method (M3D) is more robust than the elliptical model fitting (M2D) and the RCT method. The major disadvantage of the model fitting technique is the performance. However, it works very well on diseased blood vessels where the previous method may fail. The model fitting method can be used for the centering of localized parts when other techniques fail and one gains performance on healthy blood vessels, which do not require such a sophisticated algorithm.

The main contribution of this investigation is the implementation of a segmentation solution for visualization and analysis purposes in cases where classical segmentation methods based on boundary detection often fail. Diseased vessels show a wide variability of density values, which is a challenge because calcifications appear as bones and partial occlusion or soft plaques appear as soft tissues. This makes it difficult to detect the vessel boundaries. The cylindrical 3D model (M3D) fitting requires neither a pre-processing step nor any operator estimation, such as, gradient, derivative, etc.

The cylindrical model fitting can be considered as initial step to implement an automatic segmentation of diseased vascular structures. Future work should address the following issues: performance, handling of vessel bifurcations, and inclusion of further anatomical knowledge.

BIBLIOGRAPHY

[1] S.R. Aylward and E. Bullitt. Initialization, Noise, Singularities, and Scale in Height Ridge Traversal for Tubular Object Centerline Extraction. *IEEE Transactions on Medical Imaging*, 21(2):61–75, February 2002. 30

[2] D. Bartz, D. Mayer, J. Fischer, S. Ley, A. del Rio, S. Thust, C.P. Heussel, H.-U. Kauczor, and W. Strasser. Hybrid Segmentation and Exploration of the Human Lungs. In *IEEE Visualization 2003*, pages 177–184, October 2003. 31

[3] T. Baun, J.J. Flaaris, M. Volden, J. Haase, O.V. Larsen, and L.R. Ostergaard. Surface Modeling of Blood Vessels Based on 3D Medical Images. In *International Federation for Medical & Biological Engineering, IFMBE, IX Mediterranean Conference on Medical and Biological Engineering and Computing, Medicon 2001*, pages 969–973. Magjarevic,R., Tonkovic,S., Bilas,V. and Lackovic,I. (eds.). Zagreb: Faculty of Electrical Engineering and Computing, University of Zagreb, June 2001. 29

[4] H. Blum. A Transformation for Extracting New Descriptors of Shape. In W. Whaten-Dunn, editor, *Symposium Models for the Perception of Speech and Visual Form*, pages 362–380. MIT Press, 1967. 28

[5] C. Boldak, Y. Rolland, and C. Toumoulin. An Improved Model-Based Vessel Tracking Algorithm with Application to Computed Tomography Angiography. *Biocybernetics and Biomedical Engineering*, 23:41–63, 2003. 24, 29

[6] C. Boldak, C. Toumoulin, and J. L. Coatrieux. 3D Segmentation and Characterization of Lower Limb Vessels in Multi-Slice Computed To-

mography. *25th Annual International Conference of the IEEE EMBS*, pages 580–583, September 2003. 27, 29

[7] B. Brooks. Intra-arterial Injection of Sodium Iodide. *Journal of the American Medical Association*, 82:1016–1019, 1924. 6

[8] K. Bühler, P. Felkel, and A. La Cruz. *Geometric Methods for Vessel Visualization and Quantification - A Survey*, pages 399–420. G. Brunnet, B. Hamann and H. Müller and L. Linsen (eds.). Kluwer Academic, 2003. 23, 24, 25, 26, 35

[9] J. Canny. A Computational Approach to Edge Detection. *IEEE Transactions Pattern Analysis Machine Intelligence*, 8(6):679–698, 1986. 39, 40, 45

[10] J. L. Coatrieux, J. Rong, and R. Collarec. A Framework for Automatic Analysis of the Dynamic Behavior of Coronary Angiograms. *International Journal Cardiac Imaging*, 8:1–10, 1992. 36

[11] J. D. Coffman and R. T. Eberhardt. *Peripheral Arterial Disease: Diagnosis and Treatment*. Humana Press Inc., 2003. 2, 4

[12] T. F. Cootes, A. Hill, C. J. Taylor, and J. Haslam. The Use of Active Shape Models for Locating Structures in Medical Images. In H.H. Barrett and A.F. Gmitro, editors, *13th International Conference on Information Processing in Medical Imaging*, pages 33–47, 1993. 24

[13] T.F. Cootes, D. Cooper, C.J. Taylor, and J. Graham. Active Shape Models - Their Training and Application. *Computer Vision and Image Understanding*, 61(1):38–59, January 1995. 24

[14] C. Q. Davis, Z. Z. Karu, and D. M. Freeman. Equivalence of Subpixel Motion Estimators Based on Optical Flow and Block Matching. In *International Symposium Computer Vision*, pages 7–12, 1995. 38

[15] T. Deschamps and L.D. Cohen. Fast Extraction of Tubular and Tree 3D Surfaces with Front Propagation Methods. In *16th International Conference on Pattern Recognition, ICPR'02.*, pages 731–734, August 2002. 26

[16] O. Lindenthal E. Haschek. A Contribution to the Practical use of Photography According to Röentgen. *Wien Chir Wochenschr*, 9:63–64, 1896. 6

[17] P. Felkel, R. Wegenkittl, and A. Kanitsar. Vessel Tracking in Peripheral CTA Datasets - An Overview. In *Spring Conference on Computer Graphics*, pages 232–239, April 2001. x, 13, 33

[18] J. Feng, H. S. Horace, and H. C. Shuk. A 3D Geometric Deformable Model for Tubular Structure Segmentation. In *Multimedia Modelling Conference (MMM'04)*, pages 174–180, January 2004. 27

[19] A. Fitzgibbon and R. Fisher. A Buyer's Guide to Conic Fitting. In *British Machine Vision Conference*, pages 513–522, 1995. 40

[20] D. Fleischmann, R.L. Hallet, and G.D. Rubin. CT Angiography of Peripheral Arterial Disease. *Journal of Vascular Intervention Radiology*, 17(1):3–26, January 2006. 10, 19

[21] D. Fleischmann, T. J. Hastie, F. C. Dannegger, D. S. Paik, M. Tillich, C. K. Zarins, and G. D. Rubin. Quantitative Determination of Age-Related Geometric Changes in the Normal Abdominal Aorta. *Journal of Vascular Surgery*, 33(1):97–105, May 2001. 2

[22] D. Fleischmann and G.D. Rubin. Quantification of Intravenously Administered Contrast Medium Transit Through the Peripheral Arteries: Implications for CT Angiography. *Radiology*, 236(3):1076–1082, September 2005. 14

[23] A. Frangi. *Three-Dimensional Model-Based Analysis of Vascular and Cardiac Images*. PhD thesis, University Medical Center Utrecht, The Netherlands, 2001. 28

[24] A.F. Frangi, W.J. Niessen, R.M. Hoogeveen, T. van Walsum, and M.A. Viergever. Model-Based Quantization of 3-D Magnetic Resonance Angiographic Images. *IEEE Transactions on Medical Imaging*, 18(10):946–956, October 1999. 28

[25] A.F. Frangi, W.J. Niessen, K.L. Vincken, and M.A. Viergever. Multi-scale Vessel Enhancement Filtering. In *Medical Image Computing and Computer-Assisted Intervention - MICCAI*, pages 130–137. Springer, 1998. 28, 30

[26] L. Gong, S.D. Pathak, D.R. Haynor, P.S. Cho, and Y. Kim. Parametric Shape Modeling Using Deformable Superellipses for Prostate Segmentation. *IEEE Transactions on Medical Imaging*, 23(3):304–349, March 2004. 26

[27] H.K. Hahn, B. Preim, D. Selle, and H.O. Peitgen. Visualization and Interaction Techniques for the Exploration of Vascular Structures. In *IEEE Visualization 2001*, pages 395–578, October 2001. 18

[28] M. Hernandez, A.F. Frangi, and R. Barrena. Pre-clinical Evaluation of Implicit Deformable Models for Three-Dimensional Segmentation of Brain Aneurysms from CTA Images. In *SPIE Medical Imaging, Image Processing*, volume 5032, pages 1264–74, 2003. 26

[29] C.-F. Ho, M.-H. Wu, H.-M. Wu, C.-Y. Chang, M. C.-M. Chen, and T.-Y. Chou. Comparison of Auto-moving Table Contrast-enhanced 3-D MRA and Iodinated Contrast-enhanced DSA for Evaluating the Lower-extremity Arteries. *Journal of the Chinese Medical Association*, 67(10):511–520, 2004. 8

[30] Q. Huang and C. Stockman. Generalized Tube Model: Recognizing 3D Elongated Objects from 2D Intensity Images. In *IEEE Conference on Computer Vision and Pattern Recognition, New York*, pages 104–109, June 1993. 30

[31] X. Jiang and D. Mojon. Adaptive Local Thresholding by Verification-Based Multithreshold probing with Application to Vessel Detection in Retinal Images. *IEEE Transaction on Patter Analysis and Machine Intelligence*, 25(1):131–137, 2003. 24

[32] S. Joshi, S. Pizer, P. Fletcher, P. Yushkevich, A. Thall, and J. Marron. Multiscale Deformable Model Segmentation and Statistical Shape Analysis using Medial Descriptions. In *IEEE Transactions on Medical Imaging*, pages 538–550, 2002. 28

[33] S.C. Joshi, S.M. Pizer, P.T. Fletcher, A. Thall, and G. Tracton. Multiscale 3-D Deformable Model Segmentation Based on Medial Description. In *International Conference on Information Processing in Medical Imaging, IPMI*, pages 64–77, London, UK, 2001. Springer-Verlag. 28

[34] R.E. Kalman. A New Approach to Linear Filtering and Prediction Problems. *Transaction of the ASME - Journal of Basic Engineering*, pages 35–45, March 1960. 31

[35] A. Kanitsar, D. Fleischmann, R. Wegenkittl, P. Felkel, and M. E. Gröller. CPR - Curved Planar Reformation. In *IEEE Visualization 2002*, pages 37–44, October 2002. 15, 16, 68

[36] A. Kanitsar, R. Wegenkittl, P. Felkel, D. Fleischmann, D. Sandner, and E. Gröller. Computed Tomography Angiography: A Case Study of Peripheral Vessel Investigation. In *IEEE Visualization*, pages 477–480, October 2001. x, 15, 36, 37, 44

[37] A. Kanitsar, R. Wegenkittl, P. Felkel, D. Fleischmann, D. Sandner, and E. Gröller. Computed Tomography Angiography: A Case Study of Peripheral Vessel Investigation. In *IEEE Visualization 2001*, pages 477–480, October 2001. 52, 60, 62

[38] E. Keogh. Exact Indexing of Dynamic Time Warping. In *28th International Conference on Very Large Data Bases, Proceedings*, pages 406–417. Endowment Inc., August 2002. xiv, 76

[39] C. Kirbas and F.K.H Quek. A Review of Vessel Extraction Techniques and Algorithms. *ACM Computing Surveys (CSUR) archive*, 36:81–121, June 2004. 23, 24, 25, 35

[40] A. Köchl, A. Kanitsar, F. Lomoschitz, E. Gröller, and D. Fleischmann. Comprehensive Assessment of Peripheral Arteries using Multi-path Curved Planar Reformation of CTA Datasets. In *European Radiology Conference - ECR, Vienna*, volume 13, pages 268–269, 2003. 15

[41] M. Kretowski, Y. Rolland, J. Bezy-Wendling, and J.-L. Coatrieux. Physiologically Based Modeling of 3-D Vascular Networks and CT Scan Angiography. *IEEE Transactions on Medical Imaging*, 22(2):248–257, February 2000. 32

[42] K. Krissian, G. Malandain, and N. Ayache. Model Based Multiscale Detection and Reconstruction of 3D Vessels. Technical Report 3442, INRIA Sophia Antipolis, June 1998. 25, 28

[43] K. Krissian, G. Malandain, N. Ayache, R. Vaillant, and Y. Trousset. Model-Based Multiscale Detection of 3D Vessels. In *IEEE Conference on Computer Vision and Pattern Recognition*, pages 722–727, Santa Barbara, June 1998. 25, 28

[44] K. Krissian, G. Malandain, N. Ayache, R. Vaillant, and Y. Trousset. Model Based Detection of Tubular Structures in 3D Images. *Computer Vision and Image Understanding*, 80(2):130–171, November 2000. 25, 27, 28

[45] A. La Cruz. Accuracy Evaluation of Different Centerline Approximations of Blood Vessels. In *Data Visualization 2004, Visualization Symposium*, pages 115–120. EUROGRAPHICS/IEEE TCVG, May 2004. 33, 60

[46] A. La Cruz, M. Straka, A. Köchl, M. Šrámek, E. Gröller, and D. Fleischmann. Non-linear Model Fitting to Parameterize Diseased Blood Vessels. In *IEEE Visualization 2004*, pages 393–400, October 2004. 52, 68, 85

[47] K. Levenberg. A Method for the Solution of Certain Nonlinear Problems in Least Squares. *Quart. Application Mathematic*, 2:164–168, 1944. 56

[48] S. Loncaric, M. Subasic, and E. Sorantin. 3-D Deformable Model for Aortic Aneurysm Segmentation from CT Images. In *Annual EMBS International Conference*, pages 398–401, Chicago IL., July 2000. 26

[49] L.M. Lorigo, O. Faugeras, W.E.L. Grimson, R. Keriven, R. Kikinis, A. Nabavi, and C.-F. Westin. Codimension-Two Geodesic Active Contours for the Segmentation of Tubular Structures. In *IEEE Conference on Computer Vision and Pattern Recognition*, pages 444–451, June 2000. 26

[50] R.A. MacLaughlin. Randomized Hough Transform: Improved Ellipse Detection with Comparison. In *Pattern Recognition Letters*, pages 299–305, 1998. 40, 41, 45

[51] D. W. Marquardt. An Algorithm for Least-Squares Estimation of Nonlinear Parameters. *Journal of the Society for Industrial and Applied Mathematics*, 11:431–441, 1963. 56

[52] J.S. Marques and A.J. Abrantes. A Class of Probabilistic Shape Models. In *IEEE Conference on Computer Vision and Pattern Recognition*, pages 1054–1059, June 1999. 26

[53] T. McInerney and D. Terzopoulos. Topology Adaptive Deformable Surfaces for Medical Image Volume Segmentation. *IEEE Transactions on Medical Imaging*, 18(10):840–850, 1999. 25, 26

[54] T.B. Möller and E. Reif. *Normal Findings in CT and MRI*. Theme Medical Publishers. Medical Publications, 2000. 2

[55] D. Nain, A. Yezzi, and G. Turk. Vessel Segmentation Using a Shape Driven Flow. In *Medical Image Computing and Computer-Assisted Intervention - MICCAI*, pages 51–59. Springer, September 2004. 32

[56] National Library of Medicine web site. Medline Plus. Medical Encyclopedia. Arteriosclerosis of the extremities. http://www.nlm.nih.gov/medlineplus/encyclopedia.html, 2005. x, 4

[57] N. Niki, Y. Kawata, H. Sato, and T. Kumazaki. 3D Imaging of Blood Vessels using X-ray Rotational Angiographic System. In *Medical Imaging Conference*, pages 1873–1877. IEEE, 1993. 36

[58] S. Oeltze and B. Preim. Visualization of Anatomic Tree Structures with Convolution Surfaces. In *Data Visualization 2004, Visualization Symposium*, pages 311–320. EUROGRAPHICS/IEEE TCVG, May 2004. 18

[59] S. Oeltze and B. Preim. Visualization of Vascular Structures: Method, Validation and Evaluation. *IEEE Transactions on Medical Imaging*, 24(4):540–548, April 2005. xi, 18, 19

[60] A. Ofer, S.S. Nitecki, and S. Linn. Multidetector CT Angiography of Peripheral Vascular Disease: A Prospective Comparison with Intraarterial Digital Substraction Angiography. *AJR Am R Roentgenol*, 180:719–724, 2003. 10

[61] S. Osher and J.A. Sethian. Fronts Propagating with Curvature-Dependent Speed: Algorithms Based on Hamilton-Jacobi Formulations. *Journal of Computational Physics*, pages 12–49, 1988. 26

[62] K. Ouriel. Endovascular Techniques in the Treatment of Acute Limb Ischemia: Thrombolytic Agents, Trials, and Percutaneous Mechanical Thrombectomy Techniques. In *Seminar Vascular Surgery*, volume 16, pages 270–279, 2003. 2

[63] M.E. Martínez P., A.D. Hughes, A.V. Stanton, S.A. Thom, N. Chapman, A.A. Bharath, and K.H. Parker. Geometrical and Morphological Analysis of Vascular Branches from fundus Retinal Images. In *Medical Image Computing and Computer-Assisted Intervention - MICCAI*, pages 756–765. Springer, October 2000. 24

[64] P. Paredos, M. Golob, and M. Jensterle. Interrelationship Between Peripheral Arterial Occlusive Disease, Carotid Atherosclerosis and Flow Mediated Dilation of the Brachial Artery. *International Angiology*, March 2003. 22(1):83-7. 2

[65] D.L. Pham, C. Xu, and J.L. Prince. A Survey of Current Methods in Medical Image Segmentation. In *Annual Review of Biomedical Engineering*, volume 2, pages 315–337. Annual Reviews, 2000. 30, 34

[66] W. Press and W. Vettering B. Flannery, S. Teukolsky. *Numerical Receipes in C*. Cambridge University press, Cambridge, 1992. 58

[67] A. Puig. Cerebral Blood Vessels Modelling. Technical Report LSI-98-21-R, Universidad Politècnica de Catalunya, 1998. 36

[68] O. Pujol and P. Radeva. Texture Segmentation by Statistic Deformable Models. *International Journal of Image and Graphics*, 4(3):433–452, July 2004. 26

[69] L.R. Rabiner, A.E. Rosenberg, and S.E. Levinson. Considerations In Dynamic Time Warping Algorithms For Discrete Word Recognition. *IEEE Transactions On Acoustics, Speech and Signal Processing*, ASSP-26(6), December 1978. 75

[70] D.A. Rajon and W.E. Bolch. Marching Cube Algorithm: Review and Trilinear Interpolation Adaptation for Image-Based Dosimetric Models. *Computerized Medical Imaging and Graphics*, 27(5):411–435, 2003. 14

[71] R. Raman, S. Napel, C.F. Beaulieua, E.S. Bain, R.B. Jeffrey, and G.D. Rubin. Automated Generation of Curved Planar Reformations from Volume Data: Method and Evaluation. *Radiology*, 223(1):275–280, 2002. 11

[72] W.C. Röntgen. Über eine nue Art von Strahlen [On a new kind of rays]. In *Sitzungsberichte der Wrzburger Phys-Med Ges. [Physical-Medical Society of Würzburg]*, pages 132–141, 1895. 6

[73] G.D. Rubin and D. Fleischmann. CT Angiography of the Lower Extremities. *The Use of Contrast in CT Angiography Applications. Online supplement to Applied Radiology*, pages 45–51, July 2004. 14

[74] J. Serra. *Image Analysis and Mathematical Morphology*. Academic Press, London, 1982. 24

[75] M. Straka, M. Červeňanský. A. La Cruz, A. Köchl, M. Šrámek, E. Gröller, and D. Fleischmann. The VesselGlyph: Focus & Context Visualization in CT-Angiography. In *IEEE Visualization 2004*, pages 385–392, October 2004. xi, 16, 17

[76] M. Subasic, S. Loncaric, and E. Sorantin. 3D Image Analysis of Abdominal Aortic Aneurysm. In *SPIE Medical Imaging, Image Processing*, volume 4684, pages 1681–1689, November 2002. 26

[77] E. Sueyoshi, I. Sakamoto, Y. Matsuoka, Y. Ogawa, H. Hayashi, R. Hashmi, and K. Hayashi. Aorto-iliac and Lower Extremity Arteries: Comparison of Three-dimensional Dynamic Contrast-enhanced Subtraction MR Angiography and Conventional Angiography. *Radiology*, 210(3):683–688, March 1999. x, 3

[78] J.S Suri, K. Liu, S. Singh, and S. Laxminarayan. Automatic Local Effect of Window/Level on 3D Scale-Space Ellipsoidal Filtering on Run-off-arteries from White Blood Magnetic Resonance Angiography. In *16th International Conference on Pattern Recognition*, pages 899–902. IEEE, August 2002. 28

[79] T. Tozaki, Y. Kawata, N. Niki, H. Ohmatsu, and N. Moriyama. An Approach for Detecting Blood Vessel Diseases from Cone-beam CT Images. In *IEEE Nuclear Science Symposium and Medical Imaging Conference*, pages 1470–1474, 1995. 36

[80] R. Truyen, T. Deschamps, and L.D. Cohen. Clinical Evaluation of an Automatic Path tracker for Virtual Colonoscopy. In *Medical Image Computing and Computer-Assisted Intervention - MICCAI*. Springer, October 2001. 75

[81] H.C van Assen, M. Egmont-Petersen, and J.H.C. Reiber. Accurate Object Localization in Gray Level Images Using the Center of Gravity Measure; Accuracy Versus Precision. *IEEE Transaction Imaging Processing*, 11(12):1379–1384, December 2002. 39

[82] M. Šrámek and A. Kaufman. Object Voxelization by Filtering. In *IEEE Symposium on Volume Visualization*, pages 111–118. North Carolina, 1998. 52

[83] K.C. Wang, R.W. Dutton, and C.A. Taylor. Improving Geometric Model Construction for Blood Flow Modeling. *Engineering in Medicine and Biology Magazine*, 18(6):33–39, Nov-Dec 1996. 26

[84] E. Weisstein. *CRC Concise Encyclopedia of Mathematics*. Boca Raton, FL: CRC Press, 1998. 54

[85] R.T. Whitaker and D.E. Breen. Level-Set Models for the Deformation of Solid Objects. In *Proceedings of Implicit Surfaces '98, Eurographics/Siggraph*, June 1998. 26, 27

[86] M.H. Wholey and J.A. Smith. Newer Atherectomy and Reperfusion Devices for the Peripheral Circulation. *Radiology: Diagnosis-Imaging-Intervention*, pages 1–12, 1991. 1

[87] O. Wink, W.J. Niessen, and M.A. Viergever. Fast Delineation and Visualization in 3D Angiographic Images. *IEEE Transactions on Medical Imaging*, 19(4):337–346, 2000. 25, 36, 37

[88] S. Wörz and K. Rohr. A New 3D Parametric Intensity Model for Accurate Segmentation and Quantification of Human Vessels. In *Medical Image Computing and Computer-Assisted Intervention - MICCAI*. Springer, September 2004. xi, 31, 32

[89] L. Xu, E. Oja, and P. Kultanen. A New Curve Detection Method: Randomized Hough Transform (RHT). In *Pattern Recognition Letters*, pages 331–338, 1990. 40

[90] P.J. Yim, J.R. Cebral, R. Mullick, H. Marcos, and P.L. Choyke. Vessel Surface Reconstruction With a Tubular Deformable Model. *IEEE Transactions on Medical Imaging*, 20(12):1411–1421, December 2001. 27

[91] P.J. Yim, P.L. Choyke, J.R. Cebral, and R.M. Summers. Gray-Scale Skeletonization of Small Vessels in Magnetic Resonance Angiography. *IEEE Transactions on Medical Imaging*, 19(6):568–576, June 2000. 27

[92] P.J. Yim, R. Mullick, R.M. Summers, H. Marcos, J.R. Cebral, R. Lohner, and P.L. Choyke. Measurement of Stenosis from Magnetic Resonance Angiography using Vessel Skeletons. In *SPIE Medical Imaging*, pages 3978–26. SPIE, 2000. 27

APPENDIX A

CURRICULUM VITAE

Alexandra La Cruz

Born in Caracas, Venezuela, in September of 1971. Second daughter of Juan de Mata La Cruz and Asunción Puente, sister of four boys and one girl. She loves to do sportive activities as well as scientific activities. The most she likes is go to conferences, travel and meet new people from different cultures.

Education

Since May 2002 - PhD student in Computer Graphics at the Institute of Computer Graphics and Algorithms at the Vienna University of Technology, Austria

Jan 1996–May 2000 Magister in Biomedical Engineering at the Simón Bolívar University in Caracas, Venezuela

Sep 1988–May 1995 Computer Engineering at the Simón Bolívar University in Caracas, Venezuela

Sep 1983–Jun 1987 High School at the Industrial Technique School "Rafael Vegas", in Caracas, Venezuela

Sep 1977–Jun 1983 Elementary School at the National School "Los Flores de Catia" in Caracas, Venezuela

Summary of Qualifications

- Research experience in the field of medical image processing, computer graphics, modeling, simulation and biomedical data analysis.

- Teaching experience in post-graduate level course "Image Processing".

- Teaching experience in graduate level course "Programming in C++".

- Clinical and research experience in medical image processing (Computed Tomography, Coronary Angiography)

Awards, Scholarship

- Scholarship of the Universidad Simón Bolívar 1988-1993.

- ORINOQUIA AWARD to the Applied Investigation. Period 1995-1996. ANIA: A tool for ANgiographic Image Analysis and study. Caracas, Venezuela.

- Excellence AWARD MARAVEN. Academic year 1996. Simón Bolívar University, Caracas, Venezuela.

- Mention Honorific by the theses work done for obtaining the Diploma of Computer Engineering. Feb 1995. Simón Bolívar University, Caracas, Venezuela.

- Scholarship of the Lateinamerika Institute, October 2004 until July 2005.

- Scholarship of the Lateinamerika Institute since October 2005.

- Third place of Eurographics 2005 Medical Prize, for "The Angio-Vis ToolBox". Authors: Matúš Straka, Miloš Šramek, Alexandra La Cruz, Eduard Gröller Arnold Köchl and Dominik Fleischmann. Competition to acknowledge the contribution that computer graphics is playing in the medical field, organized by the Eurographics Association.

Related Short Courses

- Fourth IEEE-EMBS International Summer School on Biomedical Imaging. June 17- 24, 2000, Ile de Berder, Bretagne, France. Co-Chairs: Christian Roux, Jean-Louis Coatrieux.

- Course on Medical Imaging. Bio-engineering and Applied Bio-physic Group. Simón Bolívar University. Caracas, Venezuela. 1995

Professional Experience

Jun 2004–Aug 2004 Research Assistant at the University of Medicine of Vienna, AUSTRIA

May 2002–May 2004 Research Assistant at the Institute of Computer Graphics and Algorithms, Vienna University of Technology, Vienna, Austria

May 1998–Abr 2002 Project Manager at Hipercom, System Department

Jan 1996–Dec 1997 Teaching Assistant at the Simón Bolívar University, Computer and Technology Department, Caracas, Venezuela

Jan 1995–Dec 1996 Research Assistant at Simón Bolívar University, Research and Development Department

Feb 1994–Dec 1995 Research Assistant at Bio-engineering and Applied Bio-physic Group, Simón Bolívar University, Caracas, Venezuela

Publication List

LS12004 **La Cruz A.**, Straka M., Köchl A., Šrámek M., Gröller E., Fleischmann D.: Non-linear Model Fitting to Parameterize Diseased Blood Vessels. In proceedings of IEEE Visualization 2004, Austin, USA. 10-15 October. pp. 393-400.

SCL2004 Straka M., Cervenanský M., **La Cruz A.**, Köchl A., Šrámek M., Gröller E., Fleischmann D.: The VesselGlyph: Focus & Context Visualization in CT-Angiography. In proceedings of IEEE Visualization 2004, Austin, USA. 10-15 October. pp. 385-392.

ALC2004   **La Cruz A.**: Accuracy Evaluation of Different Center-line Approximations of Blood Vessels. Data Visualiza-tion 2004, Eurographics/IEEE TCVG, Visualization Sym-posium Proceedings. In cooperation with ACM SIG-GRAPH. Konstanz, Germany, May 2004. pp. 115-120.

LS22004   **La Cruz A.**, Straka M., Köchl A., Šrámek M., Gröller E., and Fleischmann D.: Accuracy of Automated Centerline Approximation Algorithms for Lower Extremity Vessels in a CTA Phantom. Electronic Poster in ECR 2004, Aus-tria. March. Supplement 2, Volume 14, ECR. pp. 524.

AL12004   **La Cruz A.**, Straka M., Köchl A., Šrámek M., Gröller E., Fleischmann D.: Non-linear Model Fitting to Parame-terize Diseased Blood Vessels. Technical Report TR-186-2-04-05, Institute of Computer Graphics and Algorithms, Vienna University of Technology. May 2004.

AL12003   **La Cruz A.**: Accuracy Evaluation of Different Center-line Approximations of Blood Vessels. Technical Report TR-186-2-03-12, Institute of Computer Graphics and Al-gorithms, Vienna University of Technology. December 2003.

BFL2003   Bühler K., Felkel P., and **La Cruz A.**: Geometric Meth-ods for Vessel Visualization and Quantification - A Sur-vey. Geometric Modelling for Scientific Visualization. G. Brunnett, B. Hammann, H. Müller, and L. Linsen, editors. Springer. 2003. pp. 399-421.

SL12003   Straka M., **La Cruz A.**, Köchl A., Šrámek M., Gröller, E., Fleischmann D.: Bone Segmentation in CT-Angiography Data Using a Probabilistic Atlas. In proceedings of VMV 2003. November Münich, Germany. pp. 505-512.

SL22003   M. Straka, **La Cruz A.**, Köchl A., Šrámek M., Gröller E., Fleischmann D.: 3D Watershed Transform Combined with a Probabilistic Atlas for Medical Image Segmenta-tion. Journal of Medical Informatics and Technologies, Vol.6. November 2003, pp IT-69-IT-78.

NGG2000   Ng, F., Garcia, I., Gomis, P., **La Cruz, A.**, Passariello, G., Mora, F. Bayesian hierarchical model with wavelet transform coefficients of the ECG in obstructive sleep apnea screening; Computers in Cardiology 2000 , 24-27 September. pp. 275-278.

LW11998   **La Cruz A.**, Windyga P., Bevilacqua G., Mora F., Passariello G.: Angiographic Image Analysis and Study Tool ANIA: First Application. Devices, Circuits and Systems, 1998. Proceedings of the 1998 Second IEEE International Caracas Conference, 2-4 March. pp. 282-284.

LW21997   **La Cruz A.**, Windyga P., Bevilacqua G., Garreau M., Coatrieux J.L.: Analytic Description of the Estimated Ventricular Surface from Coronary Arteries. Engineering in Medicine and Biology society, 1997. Proceedings of the 19th Annual International Conference of the IEEE, Volume 2, 30 October - 2 November. pp. 845-847.

LLR1997   **La Cruz A.**, Lecuna M., Rodríguez N., Windyga P., Bevilacqua G.: Utilidad de la Rectificación de Imágenes en el Problema de la Reconstrucción Tridimensional (3D) de Arterias Coronarias a partir de Imágenes Angiográficas Biplano. Avances Recientes en Bioingeniería, Investigación y Tecnología Aplicada, 1997, Sociedad Venezolana de Métodos Numéricos en Ingeniería, Editores: Barrios V., Montilla G., Cerrolaza M., Valencia, Venezuela. pp. 29-36.

LDW1997   **La Cruz A.**, Dibe M., Windyga P., Bevilacqua G.: Descripción Analítica de la Superficie Ventricular Estimada a partir de las Arterias Coronarias. Avances Recientes en Bioingeniería, Investigación y Tecnología Aplicada, 1997, Sociedad Venezolana de Métodos Numéricos en Ingeniería, Editores: Barrios V., Montilla G., Cerrolaza M., Valencia-Venezuela. pp. 23-28.

LM11995   **La Cruz A.**, Morinelli G., Windyga P., Bevilacqua G., Silva J.: ANIA, A Tool for Angiographic Image Analysis

105

and Study. In proceedings of Annual Conference of Engineering in Medicine and Biology Society, 1995. IEEE. Volume 1, 20-23 September. pp. 381-382.

LM21995   **La Cruz A.**, Morinelli G., Windyga P.: ANIA, Herramienta para el Análisis de Imágenes Angiográficas. Acta Científica Venezolana, 1995, XLV Convención Anual de ASOVAC, Caracas, Venezuela. pp. 238.

Hobbys

Sportive activities in general, Volleyball, Biking, Climbing, Inline Skating, Swimming, Skiing, Cinema, Dance, Travel, Music, Dive lovely.

Language Knowledge

Spanish: native / **English:** fluently / **German:** fair / **French:** fair

Vienna, January 27, 2006